

Department of Neurology

Faculty2: Medicine Clinical Medicine

Saarland University Medical Center, Homburg/Saar

# **Microglial IKK $\beta$ Deficiency Ameliorates Alzheimer's Disease-Related Symptoms and Pathology**

*Dissertation for the degree of*

*Doctor of Medicine and Natural Sciences (MD/PhD)*

**Faculty of Medicine**

SAARLAND UNIVERSITY

2015

Submitted by Xu Liu

Born on July 15, 1984 in Jiangxi, P. R. China

Aus der Klinik für Neurologie

Klinische Medizin der Medizinischen Fakultät

Universitätsklinikum des Saarlandes (UKS), Homburg/Saar

# **Mikrogliale IKK $\beta$ Defizienz Mildert Symptome und Pathologie der Alzheimer-Krankheit**

*Dissertation zur Erlangung des Grades eines*

*Doktors der Medizin und der Naturwissenschaften (MD/PhD)*

**der Medizinischen Fakultät**

der UNIVERSITÄT DES SAARLANDES

2015

vorgelegt von Xu Liu

geb. am 15. Juli 1984 in Jiangxi, V. R. China

**To**

**My Parents**

**&**

**Chunmei Du**

## **Declaration**

I hereby declare that this thesis is my own original work and effort. All experiments, except for those specified, were exclusively performed by me. Except for the publications written by myself listed in the publication list, the data presented here have not been submitted anywhere else for any award. Where other sources of information and help have been used, they have been indicated and acknowledged.

Homburg/Saar, 25.02.2015

---

Xu Liu

## ABBREVIATIONS

A $\beta$	Amyloid $\beta$ -peptide
ACE	Angiotensin-converting enzyme
AD	Alzheimer's disease
ALK5	Activin-like kinase-5
AMPA	$\alpha$ -Amino-3-hydroxy-5-methyl-4-isoxazolepropionic acid
APP	Amyloid precursor protein
ARE	AU-rich element
$\alpha$ 7 nAChRs	$\alpha$ 7 nicotinic acetylcholine receptors
BACE	$\beta$ -site APP-cleaving enzyme
BMDM	Bone marrow derived macrophages
bp	Base pair
BSA	Bovine serum albumin
BLC10	B-cell lymphoma/leukemia 10
CARMA1	CARD-containing MAGUK protein 1
CCL-2	Chemokine (C-C motif) ligand 2
CCR-2	Chemokine (C-C motif) receptor 2
CD	Cluster of differentiation
cDNA	Complementary deoxyribonucleic acid
CHO	Chinese hamster ovary
CNS	Central nervous system
Ct	Threshold cycle
CTF	C-terminal fragment
Da	Dalton
DMEM	Dulbecco's Modified Eagle Medium
DMSO	Dimethyl sulfoxide
DNA	Deoxyribonucleic acid
dsDNA	Double-strand deoxyribonucleic acid
dsRNA	Double-stranded RNA
<i>e.g.</i>	<i>exempli gratia</i> , for example
ECE	Endothelin-converting enzyme
EDTA	Ethylene diamine tetraacetic acid
ELISA	Enzyme-linked immunosorbent assay
ERK	Extracellular-signal-regulated kinase
FACS	Fluorescence-activated cell sorting
FBS	Fetal bovine serum
FOXO3a	Forkhead box O3a
g	Gram
<i>g</i>	<i>Gravity</i>
GFP	Green fluorescence protein
Gua-HCl	Guanidine chloride buffer
H <sub>2</sub> O <sub>2</sub>	Hydrogen peroxide
Iba-1	Ionized calcium-binding adaptor molecule 1
IDE	Insulin-degrading enzyme

IgG	Immunoglobulin G
IL-10	Interleukin-10
IL-1 $\beta$	Interleukin-1 $\beta$
I- $\kappa$ B	NF-kappa-B inhibitor
IKK	I- $\kappa$ B kinase
iNOS	Inducible nitric oxide synthase
IP3R	Inositol trisphosphate receptor
IRAK	Interleukin-1 Receptor-Associated Kinase
IRS1	Insulin-receptor substrate-1
IS	Immunological synapse
kb	Kilo base pairs
kDa	Kilodalton
KO/ ko	knock out
KPI	Kunitz-type protease inhibitor
LAL	Limulus Amebocyte Lysate
LPS	Lipopolysaccharides
LTD	Long-term depression
LTP	Long-term potentiation
L-VGCC	L-type voltage-gated Ca <sup>2+</sup> channels
m	Micro
M	Molar
MAL	MyD88-adaptor-like
MALT1	Mucosa-associated lymphoid tissue lymphoma translocation protein 1
MAPKs	Mitogen Activated Protein (MAP) kinases
MEKK	MAP kinase kinase kinase
mFI	Mean fluorescence intensity
min	Minute
MMP	Matrix metalloproteinase
mTOR	The mammalian target of rapamycin
MUNC18-1	Mammalian uncoordinated18-1
MyD88	Myeloid Differentiation Factor 88
NC	Nitrocellulose
NEP	Neprilysin
NF- $\kappa$ B	Nuclear Factor kappa B
NLRP3	NOD-like receptor family, pyrin domain containing 3
NMDA	N-Methyl-D-aspartic acid
NO	Nitric oxide
NR2B	N-methyl D-aspartate receptor subtype 2B
NSAIDs	Nonsteroidal anti-inflammatory drugs
O.D.	Optical density
PBS	Phosphate-Buffered Saline
PCR	Polymerase chain reaction
PDK1	3-phosphoinositi dedependent kinase 1
PET	Positron emission tomography
PFA	Paraformaldehyde
PKC $\theta$	Protein kinase C $\theta$

PLC $\gamma$	Phosphoinositide phospholipase C $\gamma$
PPAR $\gamma$	Peroxisome proliferator-activated receptor $\gamma$
PSD-95	Postsynaptic density protein-95
PVDF	Polyvinylidene difluoride
RAGE	Receptor for advanced glycation end products
RIP1	Receptor-Interacting Protein kinase 1
RNA	Ribonucleic acid
RNase	Ribonuclease
ROS	Reactive oxygen species
rpm	Revolution(s) per minute
PrP	Prion Protein
RT-PCR	Reverse transcription PCR
SD	Standard deviation
SDS-PAGE	Sodium dodecyl sulfate-polyacrylamide gel electrophoresis
sec	Second
SEM	Standard error of the mean
SMADs	Sma and Mad related proteins
SR-A	Scavenger receptors, Class A
TAB	TAK binding protein
TAK	Transforming-growthfactor- $\beta$ -activated kinase
Taq	Thermus aquaticus
TBS	Tris buffer with salt
TCR	T-cell receptor
TEMED	Tetramethylethylenediamine
TFP	Tomato fluorescent protein
TGF $\beta$	Transforming-growth factor- $\beta$
TIRAP	TIR-associated protein
TLRs	Toll-like receptors
TNF- $\alpha$	Tumor necrosis factor- $\alpha$
TNFR	TNF- $\alpha$ receptor
TPL2	Tumor progression locus 2
TPP	Tristetraprolin
TRADD	TNF receptor type 1-associated death domain protein
TRAF	TNF receptor-associated factor
TRAM	TRIF-related adaptor molecule
TRIF	TIR-domain-containing adaptor inducing IFN- $\beta$
Tris	Tris-(hydroxymethyl)-aminomethane
TSC	Tuberous sclerosis
UV	Ultraviolet
V	Volt
WB	Western blot
WT/wt	Wild type
% (v/v)	Volume/volume percentage solution
% (w/v)	Weight/volume percentage solution

# CONTENT

<b>1</b>	<b>ABSTRACT.....</b>	<b>1</b>
<b>2</b>	<b>ZUSAMMENFASSUNG .....</b>	<b>2</b>
<b>3</b>	<b>INTRODUCTION.....</b>	<b>3</b>
3.1	Alzheimer's disease: overview.....	3
3.2	Pathology.....	4
3.2.1	Amyloid .....	4
3.2.2	Microglia.....	8
3.2.3	Microglia and A $\beta$ Pathogenesis .....	10
3.3	I $\kappa$ B kinases .....	11
3.3.1	NF- $\kappa$ B-dependent pathway .....	12
3.3.2	NF- $\kappa$ B-independent pathway.....	15
<b>4</b>	<b>AIM OF THIS WORK .....</b>	<b>17</b>
<b>5</b>	<b>MATERIALS AND METHODS .....</b>	<b>18</b>
5.1	Materials .....	18
5.1.1	Instruments.....	18
5.1.2	Experimental material .....	19
5.1.3	Chemicals.....	21
5.1.4	Kits.....	23
5.1.5	Oligonucleotides .....	23
5.1.6	Antibody .....	24
5.1.7	Buffer .....	25
5.1.8	Mice .....	28
5.2	Methods.....	29
5.2.1	Cell isolation and primary cell culture.....	29



5.2.2	Positive selection of CD11b-positive microglia in the adult mouse brain.....	29
5.2.3	Preparation of A $\beta$ peptides .....	31
5.2.4	Flow cytometric analysis of HiLyte Fluor™ 488-A $\beta$ 42 internalization in primary microglia and macrophages.....	32
5.2.5	Barnes maze test .....	32
5.2.6	Tissue collection for pathological analysis .....	33
5.2.7	Immunohistochemistry .....	34
5.2.8	Congo red staining .....	37
5.2.9	Immunofluorescent staining.....	38
5.2.10	Confocal microscopy .....	38
5.2.11	Brain homogenates.....	39
5.2.12	Bio-Rad Protein Assay.....	39
5.2.13	ELISA .....	40
5.2.14	Western blot analysis .....	41
5.2.15	Purification of membrane components and $\beta$ - and $\gamma$ -secretase activity assays	43
5.2.16	Reverse transcription and quantitative PCR for analysis of gene transcripts ...	44
5.2.17	Statistics .....	47
<b>6</b>	<b>RESULTS .....</b>	<b>49</b>
6.1	Establishment of APP-transgenic mice with IKK $\beta$ deficiency in myeloid cells, i.e., endogenous microglia in the brain.....	49
6.2	Deficiency of IKK $\beta$ in myeloid cells (microglia) rescues cognitive deficits in APP-transgenic mice .....	56
6.3	Deficiency of IKK $\beta$ in myeloid cells (microglia) reduces inflammatory activation in aged APP-transgenic mouse brains .....	58
6.4	Deficiency of IKK $\beta$ in myeloid cells (microglia) reduces A $\beta$ load in aged APP-transgenic mouse brains.....	62

6.5	Deficiency in IKK $\beta$ enhances microglial and macrophage recruitment toward A $\beta$ deposits and A $\beta$ internalization .....	64
6.6	Inhibition of TGF- $\beta$ –SMAD2/3 signaling could be involved in microglial A $\beta$ internalization enhanced by IKK $\beta$ deficiency .....	69
6.7	Deficiency in IKK $\beta$ in myeloid cells does not increase A $\beta$ clearance through brain-to-blood transportation .....	71
6.8	Deficiency in IKK $\beta$ in myeloid cells does not reduce amyloidogenic APP metabolism 73	
6.9	Deficiency in IKK $\beta$ in myeloid cells does not increase A $\beta$ clearance through endogenous degradation .....	73
<b>7</b>	<b>DISCUSSION .....</b>	<b>75</b>
7.1	IKK $\beta$ was specifically deleted in myeloid cells of APP-transgenic mice .....	75
7.2	Myeloid deficiency of IKK $\beta$ reduces neuroinflammation in the brain .....	77
7.3	Myeloid deficiency of IKK $\beta$ reduces A $\beta$ load in the brain .....	78
<b>8</b>	<b>APPENDIX.....</b>	<b>81</b>
<b>9</b>	<b>REFERENCES.....</b>	<b>92</b>
<b>10</b>	<b>LIST OF FIGURES AND COOPERATIONS.....</b>	<b>111</b>
<b>11</b>	<b>PUBLICATIONS AND PRESENTATIONS.....</b>	<b>113</b>
11.1	Publications .....	113
11.2	Poster presentations .....	113
<b>12</b>	<b>ACKNOWLEDGEMENTS .....</b>	<b>114</b>

## 1 ABSTRACT

Alzheimer's disease (AD) is characterized by extracellular amyloid- $\beta$  (A $\beta$ ) deposits, intracellular accumulation of tau filaments and microglia-dominated inflammatory activation. Innate immune signaling controls microglial inflammatory activities and A $\beta$  clearance. However, studies examining innate immunity in A $\beta$  pathology and neuronal degeneration have produced conflicting results.

In this thesis study, the pathogenic role of innate immunity in AD was investigated by ablating a key signaling molecule, IKK $\beta$ , specifically in the myeloid cells of TgCRND8 APP-transgenic mice. Firstly, deficiency of IKK $\beta$  in myeloid cells attenuated cognitive deficits and loss of synaptic structure proteins. Secondly, Microglial IKK $\beta$  deficiency simultaneously reduced inflammatory activation and A $\beta$  load in the brain. Thirdly, IKK $\beta$  deficiency enhanced microglial recruitment to A $\beta$  deposits and facilitated A $\beta$  internalization, perhaps by inhibiting TGF- $\beta$ -SMAD2/3 signaling, but did not affect A $\beta$  production and efflux. Therefore, inhibition of IKK $\beta$  signaling in myeloid cells improves cognitive functions in AD mice by reducing inflammatory activation and enhancing A $\beta$  clearance.

These results contribute to a better understanding of AD pathogenesis and could offer a new therapeutic option for delaying AD progression.

## 2 ZUSAMMENFASSUNG

Die Alzheimer-Krankheit (*Alzheimer's disease*, AD) wird durch Tau-Filamente und Mikroglia vermittelte Aktivierung der Inflammation charakterisiert. Die angeborene Immunantwort kontrolliert die mikrogliale inflammatorische Aktivität und den A $\beta$ - Abbau. Allerdings liefern Studien, welche die angeborene Immunantwort im Zusammenhang mit der A $\beta$ -Pathologie sowie der neuronalen Degeneration untersuchen, widersprüchliche Resultate.

In dieser Studie wurde durch eine spezifische Deletion eines Schlüssel-Signalmoleküls, dem IKK $\beta$ , in myeloiden Zellen von TgCRND8 APP-transgenen Mäusen die pathogene Rolle der angeborenen Immunreaktion in AD untersucht. Zunächst konnte gezeigt werden, dass eine IKK $\beta$ -Defizienz in myeloiden Zellen kognitive Defizite sowie den Verlust von synaptischen Strukturproteinen mildert. Darüber hinaus wurde gezeigt, dass eine mikrogliale IKK $\beta$ -Defizienz sowohl die inflammatorische Aktivität als auch den zerebralen A $\beta$ -Gehalt reduziert. Abschließend wurde unter einer IKK $\beta$ -Defizienz eine gesteigerte Rekrutierung der Mikrogliazellen zu den A $\beta$ -Ablagerungen und eine erleichterte A $\beta$ -Internalisierung, womöglich durch Inhibition der TGF- $\beta$ -SMAD2/3 Signalkaskade, jedoch ohne veränderte A $\beta$ -Produktion und Efflux nachgewiesen. Demzufolge verbessert eine Inhibition der IKK $\beta$  Signalkaskade in myeloiden Zellen kognitive Fähigkeiten in AD-Mäusen durch eine Reduktion der Inflammation und verstärkten A $\beta$ -Abbau.

Diese erzielten Resultate tragen zu einem besseren Verständnis der AD-Pathogenese bei und können eine neue therapeutische Option darstellen um die AD-Progression hinauszuzögern.

(Thank Miss Laura Schnöder for translating the English abstract to German)

### 3 INTRODUCTION

#### 3.1 Alzheimer's disease: overview

Alzheimer's disease (AD) is a type of a neurodegenerative disorder that causes problems with memory, thinking and behavior. Symptoms usually develop slowly and get worse over time, becoming severe enough to interfere with daily tasks. On 4 November 1906, the German psychiatrist and neuropathologist Alois Alzheimer (1864-1915) reported his lecture "A peculiar disease of the cerebral cortex" at the 37th Conference of the South German psychiatrist in Tübingen (O'Brien, 1996), which is one milestone in the research of dementia. Dr. Alzheimer firstly reported a novel case of his patient Auguste Deter who suffered with the increasing weakness of memory, impaired cognition and hallucinations (Alzheimer, 1907). Four and a half years after the onset of these symptoms, the patient died in age of 55 years at the consequences of this condition. During the brain autopsy, Dr. Alzheimer found many abnormal clumps (amyloid plaques) and tangled bundles of fibers (neurofibrillar tangles) (Alzheimer, 1907; Alzheimer, 1911). Today, this degenerative brain disorder bears his name, and when found during an autopsy, these plaques and tangles mean a definite diagnosis of AD.

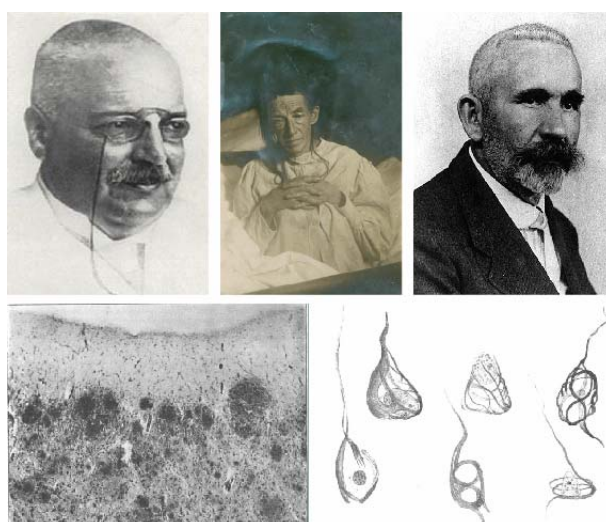


**Figure 1.1. History of Alzheimer's disease.** Above from left to right: Portrait of Alois Alzheimer, Auguste Deter and Emil Kraepelin. (The images come from Alzheimer's Disease International, International Kraepelin Society and the Frankfurter Allgemeine Zeitung). Below: pictures from the original article "On strange illness of later ages" by Alois Alzheimer, 1911.

Since its discovery more than a century ago, AD has been the most common form of dementia,

accounting for an estimated 50%-75% of cases and leading to death within 3-9 years after diagnosis (Xie et al., 2008; James et al., 2014; Querfurth and LaFerla, 2010). More than 36 million people worldwide -1.2 million in Germany- suffer this disease (Wimo et al., 2013). The principle risk factor for AD is advancing age. Most people with AD are diagnosed at age 65 or older (Ferri et al., 2005). In 2014, the 65-years-and-older population includes about 5 million people with AD, in whom 2 million people are 85-years-and-older in USA. By 2025, the number of AD patients at age 65 and older is estimated to reach 7.1 million. By 2050, the number of people age 65 and older with AD may nearly triple, from 5 million to a projected 13.8 million (Figure 1.2) (Alzheimer's association, 2014). Moreover, the cost for AD patients is huge. AD is estimated to have costed the world 604 billion in 2010 alone and more in future (Wimo et al., 2013; Alzheimer's association, 2014). Although research has revealed a great deal about AD, more should be discovered about how the disease can be prevented, slowed or stopped.

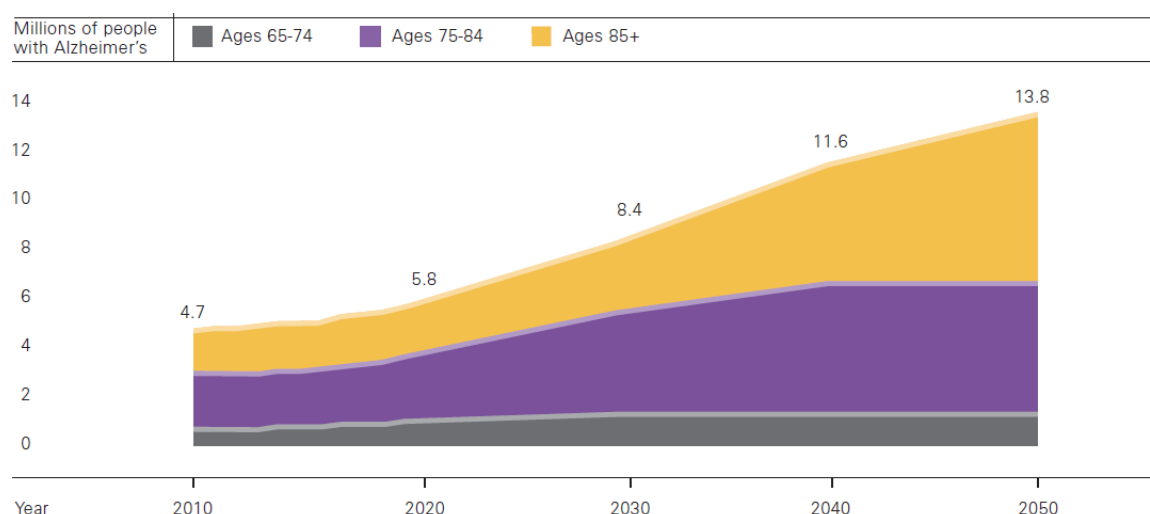


**Figure 1.2.** The projected number of people aged 65 years and older (total and by age group) in the U.S. population with Alzheimer's disease, 2010 to 2050 (Alzheimer's association, 2014).

## 3.2 Pathology

### 3.2.1 Amyloid $\beta$

Cerebral senile plaques with  $\beta$ -amyloid peptide ( $A\beta$ ) and dystrophic neurites as well as prominent neurofibrillary tangles formed by accumulation of abnormal filament tau are crucial

pathological features of AD. Loss of neurons, prominent neuroinflammation, and oxidative damage are also observed.

### **3.2.1.1 APP and Production of Amyloid $\beta$**

Amyloid precursor protein (APP) belongs to the family of type 1 transmembrane glycoproteins (Halim et al., 2011). Human APP mRNA undergoes alternatively splicing of exon 7 and 8, arising three main isoforms with 695, 751, and 770 residues. Their molecule weights are between 110 and 135kDa additionally due to post-translational modifications including N- and O-glycosylation, phosphorylation, and sulfation (Selkoe, 2008). 751 and 770-residue isoforms are widely expressed in cells throughout the body, whereas the 695-residue form is expressed more highly in neurons and occurs at very low abundance in other cells. The 751 and 770 isoforms contain a KPI (Kunitz-type protease inhibitor) domain (Figure 1.3) and are thus able to inhibit serine proteases such as trypsin and  $\alpha$ -chymotrypsin (Hook et al., 1999). APP exists lots of mutations that are named according to the geographic locations from which the affected family originated (Figure 1.3) (Hall and Roberson, 2012).

A $\beta$  is produced from APP via sequential cleavage by the secretases.  $\alpha$ -secretase is first identified as an important secretase which can proteolytically cleave APP. The APP is subjected to  $\alpha$ -secretase cleavage between amino acids toward the N-terminus from the transmembrane domain and produces a large soluble  $\alpha$ -APP peptide into the extracellular space, along with release of the 83-residue C-terminal fragment (CTF) in the membrane. Some APP molecules can be cleaved by  $\beta$ -secretase releasing the slightly smaller  $\beta$ -APP ectodomain derivative and retaining a 99-residue CTF (C99) in the residue of the membrane. The  $\beta$ -secretase cleavage can be followed by  $\gamma$ -secretase activity to produce A $\beta$ , or alternatively sequential action of  $\alpha$ - and  $\gamma$ - secretases (the latter acting on C83) produces the p3 peptide fragment. More specially, the presenilin/ $\gamma$ -secretase complex can cut the C-terminal end of A $\beta$  at other sites  $\epsilon$  and  $\zeta$  in the transmembrane domain to generate A $\beta$ 38, A $\beta$ 40, or A $\beta$ 42 (Hamley, 2012).

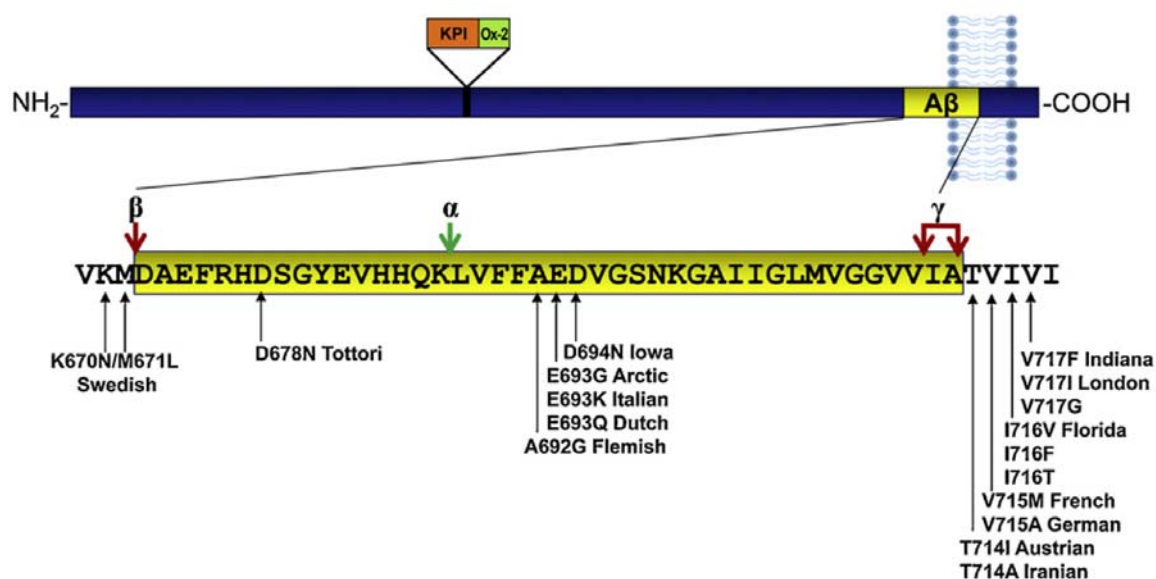


**Figure 1.3. APP processing and APP mutations (Hall and Roberson, 2012).** Aβ<sub>42</sub> is encoded by amino acids 672-713 of APP (numbered according to the longest isoform, APP770). Aβ is produced through sequential cleavage by β-secretase, then γ-secretase. γ-Secretase can cleave at alternate sites to produce Aβ<sub>40</sub> or Aβ<sub>42</sub>. Alternative APP processing by α-secretase prevents Aβ production. Common APP mutations include the Swedish mutation at the β-secretase cleavage site and multiple named and unnamed mutations at the γ-secretase cleavage site. Intra-Aβ mutations are also shown.

### 3.2.1.2 Degradation of Amyloid β

Aβ is degraded by lots of proteases with different characteristics. The most frequently investigated and best characterized Aβ degradation proteases are neprilysin (NEP) (Grimm et al., 2013) and insulin-degrading enzyme (IDE) (Haque and Nazir, 2014). Neprilysin, a member of M13 clan of zinc-metalloprotease, is capable of clearing Aβ monomers and oligomers (Turner et al., 2001). But mutated Aβ peptides show significantly resistance to neprilysin related proteolysis (Tsubuki et al., 2003). The importance of NEP for the degradation of Aβ is particularly proved by the fact that overexpression of NEP in neurons by eightfold result in dramatic decreases in monomeric Aβ levels and prevented all plaque formation and NEP deficiency causes to accumulation of Aβ in AD mouse model (Leissring et al., 2003; Iwata et al., 2001). In addition, in a study of post-mortem brain samples of AD patients demonstrated that the amount of NEP decreases with increasing age and that the NEP protein content with the Aβ level is negative correlation (Hellström-Lindahl et al., 2008).



IDE, a 110 kDa zinc-metalloprotease, is another well established A $\beta$ -degrading enzyme (Authier et al., 1996). Although the major part of this protein is present in the cytosol (Falkevall et al., 2006) and mitochondria (Leissring et al., 2004), IDE is also present in the extracellular spaces, both in secreted (Qiu et al., 1998) and cell-associated (Vekrellis et al., 2000) forms. In vitro study, genetic deletion of *ide* in primary culture neurons significantly decreases the degradation rate of physiological levels of exogenous monomer A $\beta$  (Farris et al., 2003). Using an *ide*-ko mouse model, Farris and Colleagues demonstrate that the degradation of A $\beta$  reduces more than 50% in the absence of the IDE (Farris et al., 2003). Conversely, overexpression of IDE inhibits formation of amyloid deposits (Leissring et al., 2003).

Other enzymes that can cleave in vitro A $\beta$  include endothelin-converting enzyme (ECE) -1 and 2, angiotensin-converting enzyme (ACE), plasmin and matrix metalloproteinases (MMPs),  $\beta$ -site APP-cleaving enzyme 1 and 2 gene (BACE1 and 2) and so on. Overexpression of intracellular zinc-metalloprotease ECE-1 and -2 in Chinese hamster ovary (CHO) cells decrease extracellular A $\beta$  by up to 90% (Eckman et al., 2001). ACE can cleave A $\beta$  40 and A $\beta$  42 in vitro; however, oral administration of ACE inhibitor to APP transgenic mice has no significant effect on A $\beta$  load in brains (Hu et al., 2001; Hemming et al., 2007). The serine protease plasmin can lead to A $\beta$  degradation and inhibit the aggregation of the A $\beta$  42 in vitro (Tucker et al., 2000; Exley et al., 2001). Multiple MMPs have involved in the degradation of A $\beta$ , including MMP2 (Roher et al., 1994), MMP9 (Yan et al., 2006) and MMP14 (Liao and Van Nostrand, 2010). However, compared with other A $\beta$  degrading proteases, MMPs are weaker in A $\beta$  degradation. For example, MMP2 or MMP9 deficiency in mice results in modest but statically significant increases of endogenous A $\beta$  in cortex and hippocampus (Yin et al., 2006).

### **3.2.1.3 Neurotoxicity of Amyloid $\beta$**

The accumulation of A $\beta$  pathology appears to be related to impairment of synaptic activity and neuronal network. A $\beta$  is believed to disrupt neuronal Ca<sup>2+</sup> homeostasis via altering the permeability of membrane Ca<sup>2+</sup>. There are three potential mechanisms involved in (Demuro et al., 2010). First of all, the correlation between A $\beta$  and endogenous plasmalemmal Ca<sup>2+</sup>-permeable ion channels, such as voltage-gated Ca<sup>2+</sup> channels (N, P, and Q-VGCC), nicotinic acetylcholine channels ( $\alpha$ 7 and  $\alpha$ 4 $\beta$ 2 nAChRs), glutamate receptors (AMPA and NMDA), dopamine receptors, serotonin receptors (5-hydroxytryptamine type 3), and intracellular inositol

trisphosphate receptors (IP3Rs), are observed. Secondly, the interaction of A $\beta$  with membrane lipids such as phosphoinositides (Decout et al., 1998), phosphatidylglycerol (Terzi et al., 1995), phosphatidylcholine (Avdulov et al., 1997), and gangliosides (McLaurin et al., 1998) damages membrane integrity. Third, the formation of A $\beta$  pores causes membrane leakage (Arispe et al., 1993; Quist et al., 2005; Inoue, 2008; Demuro et al., 2010). In synaptic plasticity, pathological A $\beta$  levels may indirectly lead to a partial block of NMDARs and shift long-term potentiation (LTP) to long-term depression (LTD) and synaptic loss (Kamenetz et al., 2003; Hsieh et al., 2006; Shankar et al., 2007). Receptor internalization (Snyder et al., 2005; Hsieh et al., 2006) or desensitization (Liu et al., 2004) and subsequent collapse of dendritic spines (Snyder et al., 2005; Hsieh et al., 2006) may involve in this process. In another way, soluble A $\beta$  oligomers may block neuronal glutamate uptake at synapses and lead to glutamate increase at the synaptic cleft (Li et al., 2009). The increased glutamate levels would initially activate synaptic NMDARs followed by desensitization of the receptors and enhancement of LTD, ultimately, synaptic depression.

A $\beta$  is also known to activate glial cells in the brain to release neurotoxic species, pro-inflammatory cytokines and reactive oxygen species. These mediators trigger neuronal apoptosis or necrosis (Akiyama et al., 2000; Glass et al., 2010; Meunier et al., 2014), as well as synaptic deficits (Medeiros et al., 2007; Schwalm et al., 2014). Although astrocytes were reported to release some neurotoxic mediators, such as TNF- $\alpha$ , IL-1 $\beta$ , ROS and NO (Schubert et al., 2009; Gong et al., 2014), microglia are responsible for most of A $\beta$ -induced inflammation in the central nervous system (CNS).

### **3.2.2 Microglia**

Microglia are the principal innate immune cells in the central nervous system (CNS) (Hickman and El Khoury, 2013). They constitute about 10% of all brain cells and distribute in all major brain regions (Lawson et al., 1990). For decades, microglia were reckoned as the same group with other neuroglia under the term mesoglia. They were described as “capable of acting as phagocytes” but were not considered as “taking part in the formative processes of repair in the central nervous system” (Hickman and El Khoury, 2013). It was amended that microglia was different special from other neuroglia after 1919, because Del Rio-Hortega found their phagocytic role “related to the elimination of substances resulting from metabolism of neuronal breakdown” and established their role in inflammatory and necrotizing processes, therefore

providing the foundation for modern studies of these cells (Rezaie and Male, 2002). The origin of resident microglia remains further investigation. Although it is clear that microglia are of myeloid origin and migrate into the CNS during early embryogenesis (Saijo and Glass, 2011), a major question has been whether peripheral monocytes contribute the population of microglia in CNS. Bone marrow transplantation (BMT) experiments done in the past two decades suggested that circulating peripheral blood monocytes can migrate into CNS and give rise to microglia (Priller et al., 2006). However, whether migration of monocytes into the brain in the absence of brain pathology is still under discussion, because body irradiation which is a required step for bone marrow ablation before transplantation of new marrow is observed to influence the extent to which these cells entered the CNS in chimeric mice (Mildner et al., 2007). Whether derived from monocytes or not, microglia perform almost the same functions in CNS as macrophage in periphery. They can express all known phagocytic receptors, such as scavenger receptor A (SRA), CD36, receptor for advanced glycation endproducts (RAGE) and CD47, and serve as the professional phagocytes for invading microorganisms and apoptotic cells in the CNS (Ribes et al., 2009; Takahashi et al., 2005). Microglia are antigen presenting cells (Beauvillain et al., 2008), and they respond to usual macrophage stimuli much as macrophages do with chemokine and cytokine production (El Khoury et al., 2003). In the physiological conditions, microglial processes are constantly scanning the microenvironment of CNS (Davalos et al., 2005; Nimmerjahn et al., 2005). Under pathological situations, such as neurodegenerative diseases, strokes, traumatic injuries and tumour invasions, microglia become activated, migrate to and surround damaged or dead cells, and subsequently clear cellular debris from the area, similarly to the phagocytic macrophages of the peripheral immune system (Fetler and Amigorena, 2005). Furthermore, microglial cells are capable of proliferating in response to several stimuli. Most immune receptors including the pattern recognition receptors, major histocompatibility complex molecules, and chemokine receptors, which are essential to the initiation and propagation of immune responses, are constitutively expressed at low levels in microglia. During microglial activation, the immunologically relevant molecules are upregulated and inflammatory mediators are produced (Walter et al., 2009).

### 3.2.3 Microglia and A $\beta$ Pathogenesis

Growing evidence suggests that inflammatory processes driven by microglia contribute to the AD pathogenesis (Wyss-Coray and Rogers, 2012). Increased expression of inflammatory mediators has been observed in postmortem AD brains (Eikelenboom and Stam, 1982; McGeer et al., 1988) and positron emission tomography studies have shown an association between microglial activation and disease progression in AD patients (Cagnin et al., 2001; Edison et al., 2008;). Moreover, epidemiological studies consistently link the use of non-steroidal anti-inflammatory drugs (NSAIDs) with reduced risk for later AD (in t' Veld et al., 2001) and there is evidence that the protective benefit of NSAIDs arises from their anti-inflammatory effects (Szekely et al., 2008), apart from their possible inhibitory effects on the A $\beta$  processing (Weggen et al., 2001). In the animal model of AD that over-expresses A $\beta$  precursor protein (APP), activation and recruitment of microglia can be visualized around A $\beta$  deposits even before neuronal damage occurs (Bolmont et al., 2008; Meyer-Luehmann et al., 2008), further arguing for a role of neuroinflammation in progressive neurodegeneration in AD.

Recent studies, however, challenge the view that microglia play a solely detrimental role in AD. Paradoxically, microglia also exert beneficial effects in AD pathophysiology. Microglia, especially the bone marrow-derived microglia, can clear A $\beta$  plaques via phagocytosis (Simard et al., 2006; Prokop et al., 2013; Matsumura et al., 2014). In APP transgenic mice, deficiency of chemokine receptor CCR2 reduces accumulation of microglia in the brain, which leads to development of early visible A $\beta$  deposits (El Khoury et al., 2007). On the contrary, enhancement of microglial recruitment from the blood into the brain by blocking transforming growth factor- $\beta$  signaling decreased A $\beta$  deposition in the AD mice (Town et al., 2008). Moreover, increased microglial activation by over-expressing IL-1 $\beta$  or IL-6 in the brain, or by vaccinating mice with Th2 immunity-driven antigens, such as glatiramer acetate, can also ameliorate AD-like plaque pathology (Frenkel et al., 2005; Butovsky et al., 2006; Shaftel et al., 2007; Chakrabarty et al., 2010). However, it should be noted that the pro-inflammatory activation itself could damage neuronal function and impair cognitive activity (Patterson, 2014).

Thus, microglia act as a double-edged sword in AD pathogenesis. The relationship between these two controversial behaviors is under debate. Although inflammatory activation reduced cerebral

A $\beta$  plaques (Shaftel et al., 2007; Chakrabarty et al., 2010), it is yet considered that A $\beta$  clearance is decreased in both AD patients and aged APP transgenic mice in correlation with higher cytokine production (Fiala et al., 2005 and 2007; Hickman et al., 2008). Pro-inflammatory activation was reported to inhibit phagocytosis in mononuclear phagocytes (Koenigsknecht-Talboo and Landreth, 2005; Zelcer et al., 2007; Hickman et al., 2008). In our group study, we observed that creating a pool of MyD88-deficient bone marrow-derived brain macrophages (Hao et al., 2011) or genetically blocking of NF- $\kappa$ B activation, downstream to MyD88 signaling in microglia (Liu et al., 2014), reduces both inflammatory activation and A $\beta$  load in the brain. Thus, our study supported the anti-inflammatory therapy for AD patients.

### **3.3 I $\kappa$ B kinases**

NF- $\kappa$ B represents a family of transcription factors that exists in a latent form in the cytoplasm bound by its inhibitors of NF- $\kappa$ B (I $\kappa$ B) molecules (Tong et al., 2015). Upon activation, I $\kappa$ Bs are phosphorylated by the I $\kappa$ B kinase (IKK) complex, which consists of three core units- two related catalytic subunits IKK $\alpha$  and IKK $\beta$  (also known as IKK1 and IKK2) (Chen et al., 1996; Didonato et al., 1997) and several copies of a regulatory subunit called the NF- $\kappa$ B essential modulator (NEMO, also known as IKK $\gamma$ ) (Yamaoka et al., 1998). Phosphorylation of I $\kappa$ Bs triggers a cascade of events, involving the polyubiquitination and proteasome-mediated degradation of I $\kappa$ B proteins, resulting in the exposure of the DNA-binding domain and nuclear localization sequence on NF- $\kappa$ B, which permits stable translocation of NF- $\kappa$ B to the nucleus and initiates the downstream transcription of target genes (Perkins, 2007). Without two IKKs or NEMO in mouse embryonic fibroblasts (MEFs), NF- $\kappa$ B activation is completely blocked after induction with various stimuli (Li et al., 2000; Rudolph et al., 2000). Therefore, the 700–900 kDa IKK complex is converging point for the activation for NF- $\kappa$ B signal pathways. In recent years, many NF- $\kappa$ B -independent functions of IKK complex members have been identified, some of which require the kinase activities, while others do not. These functions encompass tumor suppression, immune functions, cell proliferation, and chromatin remodeling and so on. They provide a bridge for crosstalk between NF- $\kappa$ B pathways with other important pathways such as p53 and mitogen-activated protein kinase (MAPK) (Perkins, 2007).

### 3.3.1 NF- $\kappa$ B-dependent pathway

A series of studies suggest that IKK $\beta$  is involved in three classical NF- $\kappa$ B signaling pathways (Figure 1.4) (Li and Verma, 2002; Vallabhapurapu and Karin, 2009). First of all, ligand binding by toll like receptors (TLRs) results in the recruitment of receptor-specific adapters and induces activation of NF- $\kappa$ B. In the case of TLR4, lipopolysaccharide (LPS) binding results in NF- $\kappa$ B activation via both TRIF- and MyD88-dependent pathways. MyD88 and TRIF are recruited via two bridge protein TIRAP (also known as MAL) and TRAM, respectively (Kawai and Akira, 2007). MyD88 recruits TRAF6 and IL-1R associated kinase (IRAK) family members, leading to oligomerization and self-ubiquitination of TRAF6. In addition, TRAF6 recruits TAK binding protein 2/3 (TAB2/3), which in turn activate TAK1 (Cao et al., 1996; Takatsuna et al., 2003; Takaesu et al., 2000; Qian et al., 2001). Activated TAK1 may then directly phosphorylate IKK $\beta$  to activate the IKK complex (Wang et al., 2001), resulting in I $\kappa$ B $\alpha$  degradation and NF- $\kappa$ B activation. Similar to MyD88-dependent pathway, TRIF also recruits TRAF6 by direct interaction (Kawai and Akira, 2007). TRAF6 then activates TAK1, culminating in IKK and NF- $\kappa$ B activation. In addition to recruiting TRAF6, RIP1 is also recruited by TRIF and associate with TRAF6 to facilitate TAK1 activation (Kopp and Medzhitov, 2003). Secondly, activation of classical NF- $\kappa$ B signaling is triggered by TNF- $\alpha$ . Ligation of TNFR1 results in TRADD-dependent TRAF2/TRAF5 and RIP1 recruitment. TRAF2 leads to K63-linked ubiquitination of RIP1 and also recruits IKK to the receptor complex (Wu et al., 2006; Ea et al., 2006). Binding of IKK $\gamma$  to ubiquitinated RIP1 stabilizes IKK complex interaction with the receptor complex, which causes a conformational change of the IKK complex and results in its activation by autophosphorylation (Rothwarf and Karin, 1999). Alternatively, MEKK3 and TAK1, which are brought near the receptor complex presumably by RIP1 may also phosphorylate and activate IKK complex (Blonska et al., 2004; Wang et al., 2001; Kanayama et al., 2004). Activated IKK phosphorylates I $\kappa$ B $\alpha$  at serine 32 and 36, leading to the proteasome-mediated degradation of the latter. Degradation of I $\kappa$ B $\alpha$  releases the NF- $\kappa$ B heterodimers, which then migrate to the nucleus and regulate gene expression. Thirdly, the T-cell receptor (TCR) recruits and activates the Src (Lck and Fyn) and Syk (ZAP70) family kinases after stimulation (Weil and Israel, 2006). ZAP70 then phosphorylates adapter proteins LAT and SLP-76, resulting in formation of a multimolecular complex containing PLC $\gamma$ 1 and nucleotide exchange factor Vav1 (Weil and

Israel, 2006). Activation of PLC $\gamma$ 1 results in generation of IP3 and Ca<sup>2+</sup>, as well as DAG, which in turn stimulates PKC $\theta$ . Costimulatory signals from TCR and CD28 activate PI3K, which induces recruitment of PDK1 and AKT. PDK1 can phosphorylate PKC $\theta$  and mediate its translocation to the immunological synapse (IS) (Herndon et al., 2001; Villalba et al., 2002; Lee et al., 2005). Upon translocation to IS, PKC $\theta$  might control the recruitment of IKK and CARMA1 into the signaling complex. Phosphorylation of CARMA1 by PKC $\theta$  results in the recruitment of BCL10 and MALT1, thus leading to formation of a stable CBM complex (Schulze-Luehrmann and Ghosh, 2006). IKK activation is induced by CBM complex through an ill-defined mechanism, which may involve IKK *trans*-autophosphorylation (Schulze-Luehrmann and Ghosh, 2006). The activation of IKK complex, which phosphorylates I $\kappa$ B $\alpha$ , leads to its degradation and activation of NF- $\kappa$ B.

In myeloid cells, IKK $\beta$  and IKK $\gamma$  are essential for NF- $\kappa$ B activation via the canonical pathway, which is induced by proinflammatory stimuli such as TNF- $\alpha$ , IL-1 $\beta$  and lipopolysaccharide (Pasparakis et al., 2006). In AD, aggregated A $\beta$  has been clearly demonstrated to activate NF- $\kappa$ B in microglia and astrocytes through CD14, TLR2 and TLR4 (Akama et al., 1998; Fassbender et al., 2004; Walter et al., 2007; Richard et al., 2008; Reed-Geaghan et al., 2009). Inhibition of NF- $\kappa$ B activation could reduce microglia-dependent A $\beta$ -induced neurotoxicity (Chen et al., 2005). NSAIDs are considered to target NF- $\kappa$ B and suppress inflammatory activation (Yamamoto and Gaynor, 2001). Interestingly, IKK $\beta$ -mediated NF- $\kappa$ B activation is reported to protect macrophages from TLR4 signaling-induced apoptosis, thus NF- $\kappa$ B not only initiates inflammation, but also inhibits inflammatory resolution (Park et al., 2005).

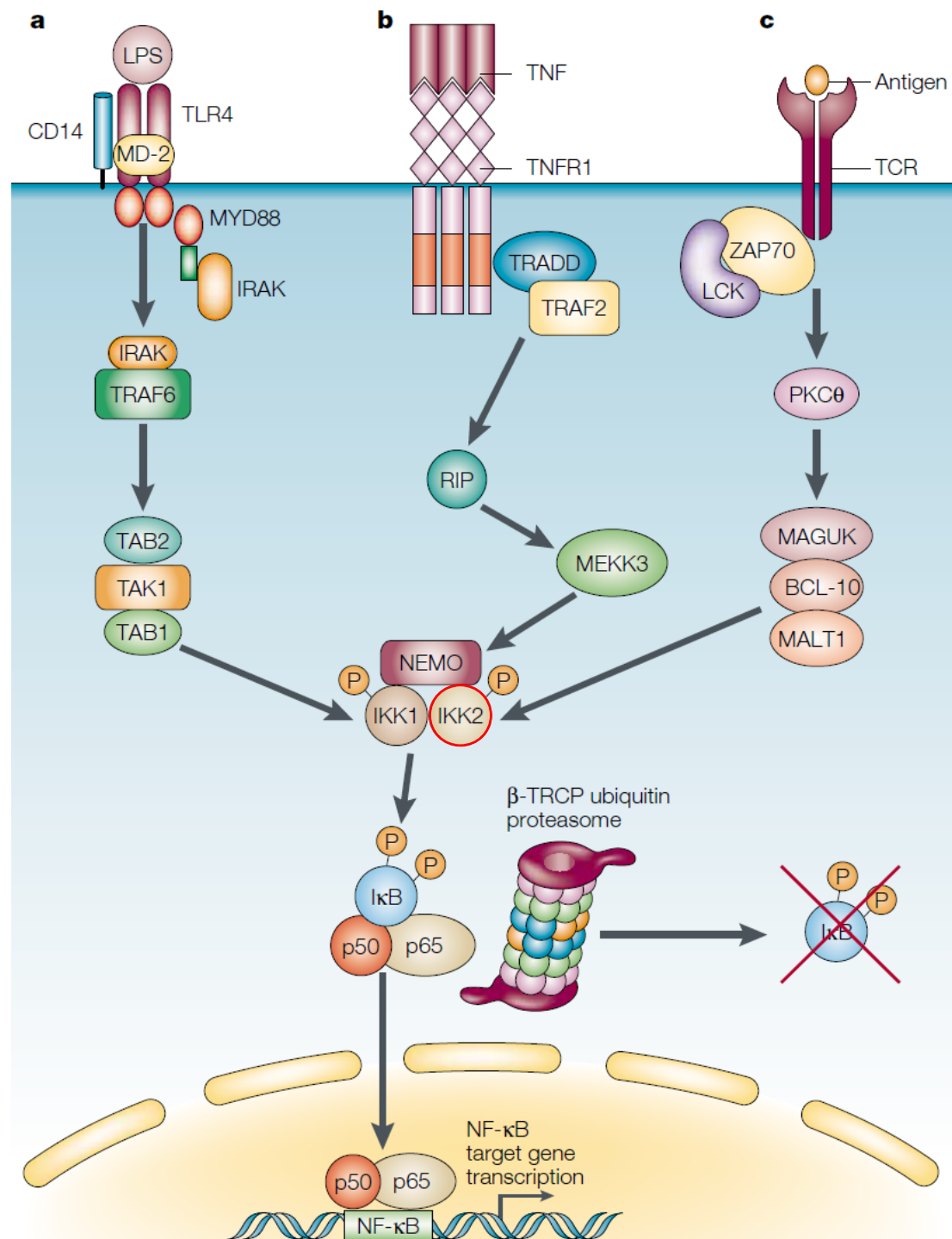


Figure 1.4. IKKs-NF-κB activation pathways (Li and Verma, 2002). Nuclear factor-κB (NF-κB) activity is stimulated by many pathways, including toll like receptor (TLR), tumour-necrosis factor (TNF) and T-cell receptor (TCR) signalling. IKKβ (IKK2) is essential for NF-κB activation via the canonical pathways.



### 3.3.2 NF- $\kappa$ B-independent pathway

In addition to their role in the NF- $\kappa$ B signaling pathway, IKK $\beta$  has been reported to phosphorylate abundant substrates and programme the cellular response to a variety of stimuli (Figure 1.5) (Perkins, 2007).

IKK $\beta$  has been shown to phosphorylate several tumor suppressor proteins, including the complex of p53, FOXO3a and TSC1/2 complex which is suppressor upstream of mTOR. IKK $\beta$  phosphorylates p53 at S362 and S366 resulting in  $\beta$ -TrCP-mediated ubiquitination and proteasomal degradation (Xia et al., 2009). Phosphorylation of TSC1 by IKK $\beta$  at S487 and S511 leads to the inhibition of TSC1/2 complex and induces tumorigenesis due to mTOR activation (Lee et al., 2007). IKK $\beta$  might regulate another tumour suppressor FOXO3a to promote cell survival (Hu et al., 2004). In some inactivated cells, IKK $\beta$  phosphorylates p105 NF- $\kappa$ B subunit that interacts with extracellular signal-regulated kinase (ERK) kinase TPL2 (also known as COT) as a complex and leads to its degradation. The damage of the complex releases TPL2 resulting in activation of the pro-proliferative ERK signaling pathway (Beinke et al., 2004). By contrast, phosphorylation of the adaptor protein DOK1 by IKK $\beta$  has been shown to block MAP kinase signalling and cell proliferation (Lee, et al., 2004). IKK $\beta$  phosphorylates and inhibits the 14-3-3 $\beta$  protein when complexed with tristetraprolin (TPP), an AU-rich element (ARE) binding protein that regulates mRNA stability. IKK $\beta$  phosphorylation inhibits TPP–14-3-3 $\beta$  ARE binding and might therefore stabilize cytokine, chemokine and growth factor transcripts (Gringhuis et al., 2005). Insulin signal is also controlled by IKK $\beta$  through phosphorylating insulin-receptor substrate-1 (IRS1) (Gao et al., 2002). Phosphorylation of BCL10 by IKK $\beta$  inhibits the BCL10–MALT1 interaction as CMB complex, thereby decreasing T-cell signaling (Wegener et al., 2006). Thus, BCL10 phosphorylation can be considered as a negative feedback loop compared to TCR–NF- $\kappa$ B pathway.

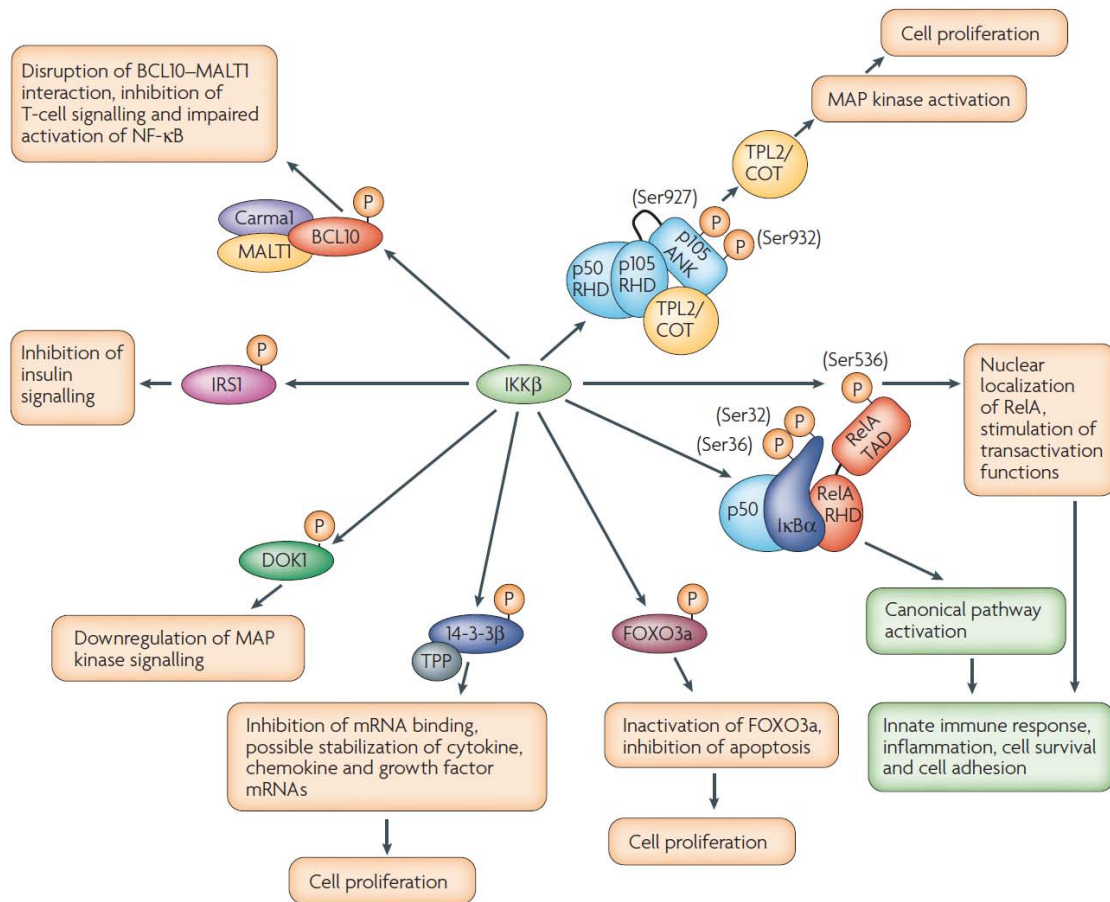


**Figure 1.5. The consequences of IKK $\beta$  activation (Perkins, 2007).** Activation of IKK $\beta$  stimulates anti-apoptotic, pro-inflammatory and proliferative pathways.

## 4 AIM OF THIS WORK

Growing evidence has shown that microglia act as a double-edged sword in AD pathogenesis: on one side, they contribute to neuronal death by secreting inflammatory mediators; on the other side, they clear neurotoxic A $\beta$  to prevent AD progression. Thus, the net effect of microglial activation in AD is still unclear. The mechanism switching between detrimental and beneficial effects need to be understood.

Recently, our group and others have observed that innate immune receptors, e.g. CD14, toll-like receptor 2 (TLR2) and TLR4, mediate A $\beta$ -induced microglial inflammatory activation and neurotoxicity (Fassbender et al., 2004; Walter et al., 2007; Reed-Geaghan et al., 2009; Hao et al., 2011; Liu et al., 2012). Genetic deletion of MyD88 or IRAK4, the common signaling molecules down-stream to TLRs, in brain macrophages or microglia reduces pro-inflammatory and cerebral A $\beta$  load and improved neural function (Hao et al., 2011; Cameron et al., 2012; Liu et al., 2012). Therefore, this study aims to investigate the pathogenic role of IKK $\beta$ , the key signaling molecules downstream of TLRs-MyD88-IRAK4, in the AD mouse model.

In detail, the special aims of this study are:

1. To investigate the role of microglial IKK $\beta$  in the neuroinflammatory activation, cerebral A $\beta$  load and neuronal function in APP-transgenic mice.
2. To investigate effects of IKK $\beta$  on A $\beta$ -induced inflammatory activation and A $\beta$  endocytosis in primary microglia.

## 5 MATERIALS AND METHODS

### 5.1 Materials

#### 5.1.1 Instruments

Instruments	Company
7500 Fast Real-Time PCR System	Applied Biosystems (Darmstadt, Germany)
Accu jet Pipettes Control	BrandTech Scientific (Essex, CT, USA)
Autoclave 3870 ELV	Systec (Wettenberg, Germany)
Autoclave V-150	Systec (Wettenberg, Germany)
Axiovert 25 inverted Microscope	Carl Zeiss Microscopy (Jena, Germany)
Axiovert 40 CFL Microscope	Carl Zeiss Microscopy (Jena, Germany)
Barnes Maze	Noldus Information Technology (Oberreifenberg, Germany)
Biofuge 13 Centrifuge	Heraeus (Hanau, Germany)
Biowizard KR-200 Bench	Kojair Tech Oy (Vilppula, Finland)
Coolbox KB 1001	Liebherr (Lindau, Germany)
Drying cabinet	Heraeus (Hanau, Germany)
Eclipse TS100 Inverted Microscope	Nikon Instruments (Melville, NY, USA)
Eclipse E600 Fluorescence Microscopy	Nikon Instruments (Melville, NY, USA)
FACSCanto II Flow Cytometer	BD Biosciences (Heidelberg, Germany)
Freezer Premium no frost	Liebherr (Lindau, Germany)
Freezer UF75-110 T	Colora (Frankfurt, Germany)
General Rotator STR4	Stuart Scientific (Staffordshire, UK)
HERAcell CO <sub>2</sub> Incubators	Heraeus (Hanau, Germany)
HERAcell 150i CO <sub>2</sub> Incubators	Thermo Scientific (Langenselbold, Germany)
HERAsafe HS 12 biological safety cabinet	Heraeus (Hanau, Germany)
Ice Machine	Eurfrigor Ice Makers Srl (Lainate, Italy)
Incubations hood TH-30	Edmund Bühler GmbH (Hechingen, Germany)
InoLab pH 720 pH-meter	WTW (Weilheim, Germany)
Jouan B4i Centrifuge	Thermo Scientific (Langenselbold, Germany)
Laboshaker	Gerhardt Analytical Systems (Königswinter, Germany)
Liquid Nitrogen Container	KGW-Isotherm (Karlsruhe, Germany)
Microwelle HF 26521	Siemens (München, Germany)
Mini-PROTEAN 3 Electrophoresis system	Bio-Rad Laboratories (München, Germany)
Mini Trans-Blot Cell	Bio-Rad Laboratories (München, Germany)
Multipette Plus	Eppendorf (Hamburg, Germany)
Nalgene Mr. Frosty Freezing Container	A. Hartenstein (Würzburg, Germany)
Nanodrop ND-1000 Spectrophotometer	PEQLAB Biotechnologie (Erlangen, Germany)

Optima Max Ultracentrifuge	Beckman Coulter (Krefeld, Germany)
Perfection V700 Photoscanner	Epson (Meerbusch, Germany)
Pipette PIPETMAN	Gilson (Middleton, WI, USA)
Pipette Single-Channel	Eppendorf (Hamburg, Germany)
Pipette Pipetus	Hirschmann (Eberstadt, Germany)
PowerPac 200 Power Supply	Bio-Rad Laboratories (München, Germany)
Precision Balance scale 770	Kern & Sohn (Balingen, Germany)
Precision Balance scale CP 42023	Sartorius (Göttingen, Germany)
PS250 Power Supply	Hybaid (Heidelberg, Germany)
PTC 200 DNA Engine Thermal Cycler	MJ Research (St. Bruno, Canada)
PURELAB Ultra Water Purification system	Elga (Celle, Germany)
QuadroMACS™ Separator	Miltenyi Biotec (Bergisch Gladbach, Germany)
Refrigerated Laboratory Centrifuge	Eppendorf (Hamburg, Germany)
Refrigerator KG39VVI30	Siemens (München, Germany)
Refrigerator Premium	Liebherr (Lindau, Germany)
Refrigerator V.I.P. Series -86 °C Freezer	Sanyo (Wood Dale, IL, USA)
Rocky 3D	Labortechnik Frübel (Lindau, Germany)
Savant SpeedVac DNA 110	Thermo Scientific (Langenselbold, Germany)
Shakers SM-30	Edmund Bühler (Hechingen, Germany)
SmartSpec 3000 Spectralphotometer	Bio-Rad Laboratories (München, Germany)
Sunrise Microtiter plate reader	Tecan (Männedorf, Schweiz)
Tabletop Centrifuge 4K10	Sigma Laborzentrifugen (Osterode am Harz, Germany)
Tabletop Centrifuge 4K15C	Sigma Laborzentrifugen (Osterode am Harz, Germany)
Thermoblock TDB-120	BioSan (Riga, Latvia)
Thermomixer comfort	Eppendorf (Hamburg, Germany)
TLA-55 Rotor Package, Fixed Angle	Beckman Coulter (Krefeld, Germany)
Transsonic Ultrasonic Cleaning Units	Elma (Singen, Germany)
Ultrospec 3100 pro Spectralphotometer	Amersham Biosciences (München, Germany)
Vortex Genie 2	Scientific Industries (Bohemia, NY, USA)
Vortex Shaker REAX 2000	Heidolph (Schwabach, Germany)
Water bath	Köttermann (Hänigsen, Germany)
XCell SureLock Mini-Cell Electrophoresis system	Invitrogen (Darmstadt, Germany)

### 5.1.2 Experimental material

Experimental materials	Company
Amersham Hyperfilm ECL	GE Healthcare (Buckinghamshire, UK)
Beackers	VWR (Darmstadt, Germany)

## MATERIALS AND METHODS

Biosphere Filter Tips (10 µl, 200 µl, 1000 µl)	Sarstedt (Nümbrecht, Germany)
Blotting Paper Grade GB003	Whatman (Dassel, Germany)
Cell Scrapers	TPP (Trasadingen, Schweiz)
Centrifugentubes (15 ml, 50 ml)	Sarstedt (Nümbrecht, Germany)
Combitips Plus (5 ml, 10 ml)	Eppendorf (Hamburg, Germany)
CryoPure tubes 1.8 ml	Sarstedt (Nümbrecht, Germany)
Cuvettes	Sarstedt (Nümbrecht, Germany)
Erlenmeyer Flasks	Schott (Mainz, Germany)
Falcon Multiwell Cell Culture Plates	BD Biosciences (Heidelberg, Germany)
Falcon Round bottom test tubes 5 ml	BD Biosciences (Heidelberg, Germany)
Filtropur Cell Strainer	Sarstedt (Nümbrecht, Germany)
Filtropur Syringe Filter	Sarstedt (Nümbrecht, Germany)
Glass Bottles	Fisher Scientific (Schwerte, Germany)
Gloves, Latex	VWR (Darmstadt, Germany)
Gloves, Nitril	VWR (Darmstadt, Germany)
Hemocytometer	Brand (Wertheim, Germany)
LS Columns	Miltenyi Biotec (Bergisch Gladbach, Germany)
MicroAmp Optical 96-Well Reaction Plate	Applied Biosystems (Darmstadt, Germany)
MicroAmp Optical Adhesive Film	Applied Biosystems (Darmstadt, Germany)
Microlance™ needles	BD Biosciences (Heidelberg, Germany)
Microlon 600 96-Well Microplate	Greiner Bio-One (Frickenhäusen, Germany)
Microscopic cover glasses 12x12 mm	R. Langenbrinck (Emmendingen, Germany)
Microtestplate 96-Well	Sarstedt (Nümbrecht, Germany)
Mini-PROTEAN 3 Short Plates	Bio-Rad Laboratories (München, Germany)
Mini-PROTEAN 3 Spacer Plates 1,5 mm	Bio-Rad Laboratories (München, Germany)
Mini-PROTEAN Comb (15 Wells, 1,5 mm)	Bio-Rad Laboratories (München, Germany)
Myelin Removal Beads II	Miltenyi Biotec (Bergisch Gladbach, Germany)
Nunc MaxiSorp 96-Well Plate, black	Thermo Scientific (Langenselbold, Germany)
Overhead Transparencies	R. Langenbrinck (Emmendingen, Germany)
Pasteur Pipettes	VWR (Darmstadt, Germany)
PCR Soft Tube 0.2 ml	Biozym Scientific (Oldendorf, Germany)
Pipette Tips (10 µl, 200 µl, 1000 µl)	Sarstedt (Nümbrecht, Germany)
Polyallomer Tube, 1.5 ml, Snap-On Cap	Beckman Coulter (Krefeld, Germany)
Precision Wipes Kimtech Science	Kimberly-Clark (Koblenz, Germany)
Pro-Gel 10-20% Tris-Tricin-Gel	Anamed Elektrophorese (Groß-Bieberau/Rodau, Germany)
Protran Nitrocellulose Transfermembranes	Whatman (Dassel, Germany)
PVDF Western Blotting Membranes	Roche (Mannheim, Germany)
Safe-Lock Tubes (0.5 ml, 1 ml, 2 ml)	Eppendorf (Hamburg, Germany)
Scalpel Blades	B. Braun (Melsungen, Germany)
Serological Pipettes (5 ml, 10 ml, 25 ml)	Sarstedt (Nümbrecht, Germany)

Slide Box	neoLab (Heidelberg, Germany)
Standing Cylinders	VWR (Darmstadt, Germany)
Syringes	B. Braun (Melsungen, Germany)
Tissue Culture Dish	Sarstedt (Nümbrecht, Germany)
Tissue Culture Flask	Sarstedt (Nümbrecht, Germany)
UV Quartz cuvette 10 mm	Hellma (Müllheim, Germany)

### 5.1.3 Chemicals

Chemicals	Company
0.05% Trypsin/EDTA (1x)	Invitrogen (Darmstadt, Germany)
(3-Aminopropyl) triethoxysilane	Sigma Aldrich (Taufkirchen, Germany)
$\beta$ -Mercaptoethanol	Sigma Aldrich (Taufkirchen, Germany)
$\beta$ -Secretase Substrate IV, Fluorogenic	Merck (Darmstadt, Germany)
$\gamma$ -Secretase Substrate , Fluorogenic	Merck (Darmstadt, Germany)
Agarose	Biozym (Oldendorf, Germany)
Ammoniumpersulfat (APS)	Sigma Aldrich (Taufkirchen, Germany)
Antibiotic-Antimycotic 100x	Invitrogen (Darmstadt, Germany)
Bovine Serum Albumin (BSA)	Sigma Aldrich (Taufkirchen, Germany)
Borat	VWR (Darmstadt, Germany)
Bromphenol blue	Sigma Aldrich (Taufkirchen, Germany)
Casein	Fluka (Buchs, Switzerland)
Chloroform	Applichem (Darmstadt, Germany)
Citrate acid	Serva (Heidelberg, Germany)
Congo red	Sigma Aldrich (Taufkirchen, Germany)
Dimethylsulfoxid (DMSO)	Sigma Aldrich (Taufkirchen, Germany)
Diaminobenzidin-Hydrochlorid (DAB)	Sigma Aldrich (Taufkirchen, Germany)
DNA Ladder (100 bp, 1 kb)	New England Biolabs (Frankfurt am Main, Germany)
dNTP Mix	Roche (Mannheim, Germany)
Dithiothreitol (DTT)	Sigma Aldrich (Taufkirchen, Germany)
Dulbecco's Modified Eagle Medium (DMEM)	Invitrogen (Darmstadt, Germany)
Entellan®mounting media	VWR (Darmstadt, Germany)
Ethidiumbromid	Carl Roth (Karlsruhe, Germany)
Ethanol	Sigma Aldrich (Taufkirchen, Germany)
Ethylendiaminetetraacetat acid (EDTA)	Sigma Aldrich (Taufkirchen, Germany)
Ethylene glycol tetraacetic acid (EGTA)	Sigma Aldrich (Taufkirchen, Germany)
Fetal Bovine Serum (FBS)	Invitrogen (Darmstadt, Germany)
Glycine	Carl Roth (Karlsruhe, Germany)
Glycerol	Sigma Aldrich (Taufkirchen, Germany)
Guanidine Hydrochloride	Sigma Aldrich (Taufkirchen, Germany)

H <sub>2</sub> O <sub>2</sub>	Otto Fishar (Saarbrücken, Germany)
H <sub>2</sub> SO <sub>4</sub>	Fluka (Buchs, Switzerland)
HCl	Sigma Aldrich (Taufkirchen, Germany)
Ham's F-12 Medium	Invitrogen (Darmstadt, Germany)
Hank's Buffered Salt Solution (HBSS)	Sigma Aldrich (Taufkirchen, Germany)
Hexamer Random Primer	Invitrogen (Darmstadt, Germany)
HiLyte Fluor™ 488-conjugated Aβ42	AnaSpec (Fremont, USA)
Isoflurane	Baxter (Unterschleißheim, Germany)
Isopropanol	Carl Roth (Karlsruhe, Germany)
KHCO <sub>3</sub>	Merck (Darmstadt, Germany)
KCl	Merck (Darmstadt, Germany)
Lipopolysaccharide (LPS)	Axxora (Lörrach, Germany)
MgCl <sub>2</sub>	Fluka (Buchs, Switzerland)
MgSO <sub>4</sub>	Fluka (Buchs, Switzerland)
Mayer's Hematoxylin	VWR (Darmstadt, Germany)
Methanol	Sigma Aldrich (Taufkirchen, Germany)
Milk powder	Carl Roth (Karlsruhe, Germany)
NaCl	Merck (Darmstadt, Germany)
NaF	Merck (Darmstadt, Germany)
Na <sub>2</sub> HPO <sub>4</sub>	Carl Roth (Karlsruhe, Germany)
NaH <sub>2</sub> PO <sub>4</sub> x H <sub>2</sub> O	Merck (Darmstadt, Germany)
Na <sub>4</sub> P <sub>2</sub> O <sub>7</sub>	Sigma Aldrich (Taufkirchen, Germany)
Na <sub>3</sub> VO <sub>4</sub>	Sigma Aldrich (Taufkirchen, Germany)
NH <sub>4</sub> Cl	Sigma Aldrich (Taufkirchen, Germany)
Okadic acid	Sigma Aldrich (Taufkirchen, Germany)
Orange G	Merck (Darmstadt, Germany)
PageRuler Prestained Protein Ladder	Invitrogen (Darmstadt, Germany)
Pam3CSK4	Invivogen (San Diego, CA, USA)
Paraformaldehyd (PFA)	Merck (Darmstadt, Germany)
Protease inhibitor Cocktail	Roche (Mannheim, Germany)
Rotiphorese Gel 30	Carl Roth (Karlsruhe, Germany)
RPMI 1640	Invitrogen (Darmstadt, Germany)
Sodium acetate	Merck (Darmstadt, Germany)
Sodium dodecylsulfat (SDS)	Carl Roth (Karlsruhe, Germany)
Sucrose	VWR (Darmstadt, Germany)
Tetramethylethyldiamin (TEMED)	Serva (Heidelberg, Germany)
Tricine	Carl Roth (Karlsruhe, Germany)
Trizma®base	Sigma Aldrich (Taufkirchen, Germany)
Triton X-100	Sigma Aldrich (Taufkirchen, Germany)
TRizol	Sigma Aldrich (Taufkirchen, Germany)



Tween 20	Sigma Aldrich (Taufkirchen, Germany)
Western Lightning ECL Substrate	Perkin Elmer (Rodgau, Germany)
Xylene	Otto Fischar (Saarbrücken, Germany)
Xylene cyanol	Molekula (München, Germany)

### 5.1.4 Kits

Title	Company
A $\beta$ 40 Human ELISA Kit	Invitrogen (Darmstadt, Germany)
A $\beta$ 42 Human ELISA Kit	Invitrogen (Darmstadt, Germany)
Bio-Rad Protein Assay	Bio-Rad Laboratories (München, Germany)
DyNAmo <sup>TM</sup> Flash probe qPCR Kit	Thermo Scientific (Bonn, Germany)
DyNAmo <sup>TM</sup> Flash SYBR Green qPCR Kit	Thermo Scientific (Bonn, Germany)
Mouse TNF alpha ELISA Ready-SET-Go!	eBioscience (San Diego, CA, USA)
Neural Tissue Dis. Kit (p)	Miltenyi Biotec (Bergisch Gladbach, Germany)
OptEIA <sup>TM</sup> TMB Substrate Reagent Set	BD Bioscience (Heidelberg, Germany)
RNeasy <sup>®</sup> Plus Mini Kit	Qiagen (Hilden, Germany)
RQ1 RNase-free DNase	Promega (Mannheim, Germany)
SuperScript <sup>®</sup> II Reverse Transcriptase	Invitrogen (Darmstadt, Germany)
VECTOR Blue Alkaline Phosphatase Substrate kit	Vector Laboratorie (Burlingame, USA)
VectaStain Elite ABC kit	Vector Laboratorie (Burlingame, USA)
VectaStain Elite ABC-AP kit	Vector Laboratorie (Burlingame, USA)

### 5.1.5 Oligonucleotides

**Table 3.1 Primers for the Real-Time-quantitative-PCR (SYBR<sup>®</sup> Green method)**

Gen	Primer forward 5' - 3'	Primer reverse 5' - 3'
<i>mouse ccl-2</i>	AAGAGATCAGGGAGTTTGCT	CTGCCTCCATCAACCACTTT
<i>mouse gapdh</i>	ACAACCTTTGGCATTGTGGAA	GATGCACGGATGATGTTCTG
<i>mouse il-1<math>\beta</math></i>	GAAGAAGAGCCCATCCTCTG	TCATCTCGGAGCCTGTAGTG
<i>mouse il-10</i>	AGGCGCTGTCATCGATTCTC	TGCTCCACTGCCTTGCTCTTA

<i>mouse inos</i>	ACCTTGTTTCAGCTACGCCTT	CATTCCCAAATGTGCTTGTC
<i>mouse tnfr-<math>\alpha</math></i>	ATGAGAAGTTCCCAAATGGC	CTCCACTTGGTGGTTTGCTA

### 5.1.6 Antibody

**Table 3.2 Antibodies used in this work**

<b>Antibody</b>	<b>Company</b>
<i>mouse monoclonal anti <math>\alpha</math>-tubulin</i> <i>Clone, DM1A</i>	Abcam (Cambridge, UK)
<i>rabbit polyclonal anti <math>\beta</math>-actin</i>	Cell Signaling (Beverly, MA, USA)
<i>mouse monoclonal anti Amyloid <math>\beta</math></i> <i>Clone, WO2</i>	Millipore (Schwalbach, Germany)
<i>mouse monoclonal anti Amyloid <math>\beta</math></i> <i>Clone, 6F/3D</i>	Dako (Hamburg, Germany)
<i>rat monoclonal anti CD16/CD32</i> <i>Clone, 2.4G2</i>	BD Pharmingen (NJ, USA)
<i>rat monoclonal anti CD45</i> <i>Clone, 69/CD45</i>	BD Pharmingen (NJ, USA)
<i>rabbit polyclonal anti Collagen type IV</i>	Abcam (Cambridge, UK)
<i>chicken polyclonal anti GFP</i>	Abcam (Cambridge, UK)
<i>mouse monoclonal anti Iba1</i> <i>Clone, 20A12.1</i>	Millipore (Schwalbach, Germany)
<i>rabbit polyclonal anti Iba1</i>	Wako (Neuss, Germany)
<i>rabbit monoclonal anti IKK<math>\beta</math></i> <i>Clone, Y466</i>	Abcam (Cambridge, UK)
<i>rabbit polyclonal anti IKK<math>\beta</math></i>	Novus Biologicals (Littleton, USA)
<i>rabbit monoclonal anti Ki67</i> <i>Clone, SP6</i>	Abcam (Cambridge, UK)
<i>rabbit polyclonal anti Munc18-1</i>	Cell Signaling (Beverly, MA, USA)
<i>mouse monoclonal anti NeuN</i> <i>Clone, A60</i>	Millipore (Schwalbach, Germany)
<i>rabbit monoclonal anti phosho-p65</i> <i>Clone, 93H1</i>	Cell Signaling (Beverly, MA, USA)
<i>rabbit monoclonal anti p65</i> <i>Clone, D14E12</i>	Cell Signaling (Beverly, MA, USA)

<i>mouse monoclonal anti PSD95</i> <i>Clone, 6G6-1C9</i>	Abcam (Cambridge, UK)
<i>rabbit polyclonal anti RFP</i>	Rockland (Gilbertsville, USA)
<i>mouse monoclonal anti S100</i> <i>Clone, 4C4.9</i>	Abcam (Cambridge, UK)
<i>rabbit monoclonal anti phosho-SMAD2</i> <i>Clone, 138D4</i>	Cell Signaling (Beverly, MA, USA)
<i>rabbit monoclonal anti SMAD2</i> <i>Clone, D43B4</i>	Cell Signaling (Beverly, MA, USA)
<i>rabbit monoclonal anti phosho-SMAD5</i> <i>Clone, 41D10</i>	Cell Signaling (Beverly, MA, USA)
<i>rabbit monoclonal anti SMAD5</i> <i>Clone, D4G2</i>	Cell Signaling (Beverly, MA, USA)
<i>goat anti chicken Alexa 488 Conjugate</i>	Invitrogen (Darmstadt, Germany)
<i>goat anti rabbit Alexa 488 Conjugate</i>	Invitrogen (Darmstadt, Germany)
<i>goat anti mouse Alexa 546 Conjugate</i>	Invitrogen (Darmstadt, Germany)
<i>goat anti rabbit biotin Conjugate</i>	Vector Laboratorie (Burlingame, USA)
<i>goat anti rat biotin Conjugate</i>	Vector Laboratorie (Burlingame, USA)
<i>goat anti mouse HRP Conjugate</i>	Dako (Hamburg, Germany)
<i>goat anti rabbit HRP Conjugate</i>	Promega (Mannheim, Germany)

### 5.1.7 Buffer

**Table 3.3 Recipe of solution**

Recipe	Chemicals	Amount	Concentration
<b>10x Citric buffer</b>	Citric acid	2.014g	10mM
		Up to 1 Liter	
<b>10x PBS</b>	NaCl	400 g	1.37 M
	KCl	10 g	27 mM
	Na <sub>2</sub> HPO <sub>4</sub>	71 g	100 mM
	NaH <sub>2</sub> PO <sub>4</sub> x H <sub>2</sub> O	69 g	100 mM

## MATERIALS AND METHODS

	dest. H <sub>2</sub> O	Up to 5 Liter	
	Adjust to pH 7.4		
<b>10x TBS</b>	Tris	302.5 g	500 mM
	NaCl	425 g	1.45 M
	dest. H <sub>2</sub> O	Up to 5 Liter	
	Adjust to pH 7.4		
<b>5x DNA-Laoding buffer</b>	Bromphenol blue	1 mg	0.1%
	Xylene cyanol	2 mg	0.2%
	Orange G	2 mg	0.2%
	Sucrose	500 mg	50%
	0.5 M EDTA [pH 8.0]	2 µl	1 mM
	dest. H <sub>2</sub> O	Up to 1 ml	
<b>5x TBE</b>	Tris	270 g	446 mM
	Borat	137.5 g	446 mM
	0.5 M EDTA [pH 8.0]	100 ml	10 mM
	dest. H <sub>2</sub> O	Up to 5 Liter	
<b>3x SDS-Page Laoding buffer</b>	1 M Tris/HCl [pH 6.8]	187.5 µl	187.5 mM
	20% SDS	300 µl	6%
	Glycerol	300 µl	30%
	β-Mercaptoethanol	150 µl	15%
	3% Bromphenol blue (w/v)	10 µl	0.03%
	dest. H <sub>2</sub> O	Up to 1 ml	
<b>10x SDS-Tris-Glycine Running buffer</b>	Tris	151.5 g	250 mM
	Glycine	720.5 g	1.92 M
	SDS	50 g	1% (w/v)
	dest. H <sub>2</sub> O	Up to 5 Liter	

## MATERIALS AND METHODS

<b>10x SDS-Tris-Tricine running buffer</b>	Tris	121 g	1 M
	Tricine	171 g	1 M
	SDS	10 g	1% (w/v)
	dest. H <sub>2</sub> O	Up to 1 Liter	
<b>10x Transfer buffer</b>	Tris	30 g	248 mM
	Glycine	138 g	1.84 M
	dest. H <sub>2</sub> O	Up to 1 Liter	
* for use mix 100 mL 10X Transfer buffer with 200 mL methanol and 700 mL dest. H <sub>2</sub> O			
<b>Blocking buffer</b>	Nonfatty milk	5g	10%
	1x PBS	Up to 50 ml	
<b>DMEM media</b>	Dulbecco's Modified Eagle Medium (DMEM)(High Glucose)	445 ml	89%
	Fetal bovine serum	50 ml	10%
	Antibiotic-antimycotic(100x )	5 m	1%
* Fetal bovine serum should be inactivated in 56°C water bath for 30 min.			
<b>RPMI media</b>	RPMI 1640 Medium	445 ml	89%
	Fetal bovine serum	50 ml	10%
	Antibiotic-antimycotic(100x )	5 ml	1%
* Fetal bovine serum should be inactivated in 56°C water bath for 30 min.			
<b>SDS-Cell lysis buffer</b>	1 M Tris/HCl [pH 7.5]	2.5 ml	50 mM
	0.5 M EDTA [pH 8.0]	200 µl	2 mM
	0.5 M EGTA [pH 8.0]	200 µl	2 mM
	Protease inhibitor Cocktail	1 Tablet	1x
	20 µM Okadic acid	125 µl	50 mM
	0.25 M Na <sub>4</sub> P <sub>2</sub> O <sub>7</sub>	1 ml	5 mM
	1 M Na <sub>3</sub> VO <sub>4</sub>	100 µl	100 µM

	1 M DTT	50 $\mu$ l	1 mM
	1 M NaF	2.5 ml	50 mM
	20% SDS	5 ml	2%
	dest. H <sub>2</sub> O	Up to 50 ml	

### 5.1.8 Mice

TgCRND8 APP-transgenic mice (*app<sup>tg</sup>*) on a 129 background (continuously interbred for more than 9 generations to reach the genetic cognate) expressing a transgene incorporating both the Indiana mutation (V717F) and the Swedish mutations (K670N/M671L) in the human *app* gene under the control of hamster prion protein (PrP) promoter were kindly provided by D. Westaway (University of Toronto). In this mouse strain, the A $\beta$  load does not differ between male and female mice (Chishti et al., 2001). *Ikkb<sup>fl/fl</sup>* mice carrying loxP site-flanked *ikkbk* alleles on a C57BL6/N genetic background were kindly provided by M. Pasparakis (University of Cologne; Pasparakis et al., 2002). *Ikkb<sup>fl/fl</sup>* mice express normal levels of IKK $\beta$ . LysM-Cre knock-in mice (*LysM-Cre<sup>+/+</sup>*) expressing Cre from the endogenous *lysozyme 2* gene locus were obtained from Jackson Laboratory (Bar Harbor, ME, USA; Stock Number 004781; Clausen et al., 1999) and were back-crossed to C57BL6/J mice for more than 6 generations. Thus, myeloid cell type (e.g., microglia and macrophages)-specific IKK $\beta$ -deficient (*ikkbk<sup>fl/fl</sup>Cre<sup>+/-</sup>*) mice were generated by breeding *ikkbk<sup>fl/fl</sup>* mice and LysM-Cre knock-in mice. APP-transgenic mice deficient in IKK $\beta$  specifically in myeloid cells (*app<sup>tg</sup>ikkbk<sup>fl/fl</sup>Cre<sup>+/-</sup>*) were then established by cross-breeding APP-transgenic mice with *ikkbk<sup>fl/fl</sup>* and LysM-Cre mice on a constant C57BL6/129 (1:1) genetic background. All mice from the same litter were used for the study without any exclusion so that the phenotype of APP-transgenic mice with or without IKK $\beta$  ablation in myeloid cells was compared only between siblings.

To demonstrate the cell-specific expression of Cre recombinase, we cross-bred LysM-Cre mice to ROSA<sup>mT/mG</sup> Cre report mice (Jackson Laboratory; Stock Number 007676), which express cell membrane-targeted tomato fluorescent protein (TFP) before Cre exposure and express cell membrane-targeted GFP in Cre-expressing cells. To track microglia and brain macrophages with deficiency of IKK $\beta$  in the AD mice, *app<sup>tg</sup>ikkbk<sup>fl/fl</sup>Cre<sup>+/-</sup>* mice were further mated to ROSA<sup>mT/mG</sup> mice to obtain *app<sup>tg</sup>ikkbk<sup>fl/fl</sup>ROSA<sup>mT/mG</sup>Cre<sup>+/-</sup>* mice.

To demonstrate the chemokine (C-C motif) receptor 2 (CCR2)-positive cells in the AD mice, we cross-bred TgCRND8 APP-transgenic mice to CCR2-RFP mice (Jackson Laboratory; Stock Number 017586), in which the CCR2 coding sequence has been replaced with an RFP encoding sequence. All animal experiments were approved by the regional ethical committee of the regional council in Saarland, Germany.

## 5.2 Methods

### 5.2.1 Cell isolation and primary cell culture

Primary microglia were isolated from brains of newborn C57BL6 mice and cultured as previously described (Liu et al., 2005). Briefly, the meninges from the forebrains of newborn mice were mechanically removed. The cells were seeded into poly-lysine-coated flasks and cultured in DMEM medium supplemented with 10% FBS under a humidified atmosphere of 10% CO<sub>2</sub> at 37°C for at least 14 days (Ishii K, 2000). Microglial cells were then collected from the microglia-astrocyte co-cultures by shaking with a rotary shaker (220 rpm, 15min).

Bone marrow cells were isolated from medullar cavities of the tibia and femur of 8-week-old littermate mice resulting from crosses of *ikbbk<sup>fl/fl</sup>* and LyzM-Cre knock-in mice (*ikbbk<sup>fl/fl</sup>Cre<sup>-/-</sup>* and *ikbbk<sup>fl/fl</sup>Cre<sup>+/-</sup>* mice). Bone marrow-derived macrophages (BMDM) were cultured in Dulbecco's modified Eagle medium (Life Technologies, Karlsruhe, Germany) supplemented with 10% fetal bovine serum (FBS, PAN Biotech, Aidenbach, Germany) and 20% L929 cell-conditioned medium (DSMZ, Braunschweig, Germany) in  $\Phi$ 10 cm dishes (BD, Heidelberg, Germany) according to a published protocol (Hao et al., 2011). As shown in flow cytometry, >98% BMDM cells were CD11b-positive.

### 5.2.2 Positive selection of CD11b-positive microglia in the adult mouse brain

In order to determine the ablating efficiency of floxed *ikbbk* gene by LyzM-Cre and the microglial inflammatory activation, the whole cerebrum harvested from 3 or 6-month-old APP-transgenic mice with and without deficiency of myeloid IKK $\beta$  (*ikbbk<sup>fl/fl</sup>Cre<sup>-/-</sup>* or *ikbbk<sup>fl/fl</sup>Cre<sup>+/-</sup>*) was carefully dissected to prepare a single cell suspension using Neural Tissue Dissociation Kit (papain) with the removal of myelin using Myelin Removal Beads II (both from Miltenyi Biotec

GmbH, Bergisch Gladbach, Germany) according to the protocols provided by the company (Liu et al., 2014). Procedure is as follows:

1. Prepare 1950 µl enzyme mix 1 for up to 400 mg tissue and vortex. Pre-heat the mixture at 37 °C for 10 minutes before use.
2. Remove the mouse brain. Determine the weight of tissue in 1 ml of cold HBSS to make sure the 400 mg limit per digestion is not exceeded.
3. Place the brain on the lid of a 100 mm diameter petri dish, remove the meninges, and cut brain into small pieces using a scalpel.
4. Using a 5 ml pipette, add 5 ml of HBSS (w/o) and pipette pieces back into an appropriate-sized tube. Rinse with HBSS (w/o).
5. Centrifuge at 300 g for 7 minutes at room temperature and aspirate the supernatant carefully.
6. Add 1950 µl of pre-heated enzyme mix 1 (Solutions 1 and 2) per up to 400 mg tissue.
7. Incubate in closed tubes for 15 minutes at 37 °C under slow, continuous rotation.
8. Prepare 30 µl enzyme mix 2 per tissue sample by adding 20 µl of Solution 3 to 10 µl of Solution 4. Then add to samples.
9. Invert gently to mix. Do not vortex.
10. Dissociate tissue mechanically using the 17G needles by pipetting up and down 8 times slowly. Avoid forming air bubbles.
11. Incubate at 37 °C for 10 minutes.
12. Dissociate tissue mechanically using the 22G needles. Pipette slowly up and down 5 times with each pipette, or as long as tissue pieces are still observable. Be careful to avoid the formation of air bubbles.
13. Incubate at 37 °C for 10 minutes.
14. Apply the cell suspension to a 70µm cell strainer, placed on a 50 ml tube.
15. Discard cell strainer and centrifuge cell suspension at 300 g for 10 minutes at room temperature. Aspirate supernatant completely.
16. Suspend cells with buffer to the required volume for further applications.

After pelleting cells by centrifugation, 80µl of blocking buffer containing 25µg/ml rat anti-mouse CD16/CD32 antibody (2.4G2, BD), 10% FBS was added to prevent non-specific binding. Thirty minutes after blocking at 4 °C, 20µl MicroBeads-conjugated CD11b antibody (Miltenyi



Biotec GmbH) was directly added to the cells. After 1 more hour of incubation at 4°C, cells were washed with buffer and loaded onto MACS LS Column (Miltenyi Biotec GmbH) to separate CD11b-positive and negative cells. Lysis buffer was immediately added to both the CD11b-positive and the CD11b-negative cells for isolation of total RNA using RNeasy Plus Mini Kit (Qiagen GmbH). alternatively, CD11b<sup>+</sup> cells were used for flow cytometric analysis after cells were stained with fluorescence-labeled anti-CD45 antibody (clone 30-F11, eBioscience, San Diego, CA, USA); or CD11b<sup>+</sup> cells were used for Western blot detection of IKK $\beta$  after cells were lysed in buffer (50 mM Tris/HCl [pH 7.4], 145 mM NaCl, 1% Triton-100, and protease inhibitor cocktail; Roche Applied Science) and the rabbit monoclonal antibody against IKK $\beta$  (clone Y466; Abcam, Cambridge, UK) was used to blot the membrane.

### **5.2.3 Preparation of A $\beta$ peptides**

The 42-amino acid form of human A $\beta$  (A $\beta$ 42) was kindly provided by Dr. L. Fülöp (Albert Szent Gyorgyi Medical University, Hungary). The oligomeric and fibrillar A $\beta$  were prepared according to the published protocol with minor modification (Dahlgren et al., 2002).

The A $\beta$  (1–42) peptide was initially dissolved to 1 mM in hexafluoroisopropanol (Sigma) and separated into aliquots in sterile microcentrifuge tubes. Hexafluoroisopropanol was removed under vacuum in a Speed Vac, and the peptide film was stored dessicated at -20 °C. For the aggregation protocols, the peptide was first resuspended in dry dimethyl sulfoxide (Me<sub>2</sub>SO, Sigma) to a concentration of 5 mM. For oligomeric conditions, Ham's F-12 (phenol red-free, BioSource, Camarillo, CA) was added to bring the peptide to a final concentration of 100  $\mu$ M and incubated at 37 °C for 48 h. For fibrillar conditions, 10 mM HCl was added to bring the peptide to a final concentration of 100  $\mu$ M and incubated for 48 h at 37 °C. After these solubilization and aggregation protocols, no major differences were observed in the preparation and structural characterization of synthetic and recombinant peptide. Fluorescent A $\beta$  was prepared by mixing HiLyte Fluor™ 488-conjugated A $\beta$ 42 (AnaSpec, Fremont, USA) and unlabeled A $\beta$  at the ratio of 1:10. Endotoxin concentrations of peptide samples were <0.01 EU/ml as determined by the LAL assay (Lonza, Basel, Switzerland). Western blot analysis confirmed that HiLyte Fluor™ 488-conjugated and non-conjugated forms of A $\beta$ 42 peptides had similar oligomeric conformation.

### 5.2.4 Flow cytometric analysis of HiLyte Fluor™ 488-A $\beta$ 42 internalization in primary microglia and macrophages

In order to investigate the different internalization of A $\beta$  oligomers and fibrils by microglia and macrophages, and effects of IKK $\beta$  on A $\beta$  internalization, microglia cells cultured in a 24-well plate (BD) at a density of  $2 \times 10^5$  cells/well were treated with 0.2 and 1  $\mu$ M HiLyte Fluor™ 488–conjugated A $\beta$ 42 aggregates for different time durations as indicated in the results. As controls, cells were challenged with 10 and 100  $\mu$ g/ml pHrodo™ Green-conjugated E. coli BioParticles (Life Technologies) and 1  $\mu$ l/ml FluoSpheres fluorescent microspheres ( $1 \times 10^7$  polystyrene microspheres/ml, 1  $\mu$ m diameter; Life Technologies) (Liu et al., 2006; Hao et al., 2011). To investigate effects of blocking TGF- $\beta$ –SMAD2/3 signalling on A $\beta$  internalization, wild-type microglia were pre-treated with activin-like kinase-5 (ALK5) inhibitors, SB-505124 and SB-431542 at 0, 0.004, 0.02, 0.1, 0.5 or 1.0  $\mu$ M for 1 hour, which was followed by the incubation with 1.0  $\mu$ M fluorescent oligomeric A $\beta$ 42 aggregates for 6 hours in the presence of pre-treated inhibitors. Thereafter, macrophages or microglia were washed with  $1 \times$  phosphate buffered saline (PBS) and detached from the plate with trypsin-ethylenediaminetetraacetic acid (EDTA) (Life Technologies). The mean fluorescence intensity (mFI) of internalized fluorophore-conjugated A $\beta$ 42, E. coli or beads and percentages of positive cell with intracellular proteins or particles were immediately determined by BD FACSCanto II flow cytometry (Franklin Lakes, USA). To examine the surface binding of A $\beta$ , cells were incubated with HiLyte Fluor™ 488-conjugated 1  $\mu$ M A $\beta$ 42 aggregates for 6 hours on ice and then analyzed for mFI.

### 5.2.5 Barnes maze test

The Barnes maze test was used to assess the cognitive function of different APPtransgenic and wild-type littermate mice, using the established protocol (Hao et al., 2011; Liu et al., 2012). The test involved five days of acquisition training with two trials per day. For each trial, latency to enter the escape chamber and distance travelled were recorded by EthoVision® XT (V7.0) tracking software (Noldus Information Technology, Wageningen, The Netherlands), and the latency and total distance were averaged from the two trials per day. Twenty-four hours after the last training day, a probe trial was performed, in which: i) the escape chamber was removed; ii)

mice were placed in the center of the maze as same as in the acquisition training; iii) Each mouse was given 5 minutes to explore the maze. During the probe phase, the time mice spent in the target zone which is adjacent to the escape hole and its two neighboring holes and the frequency mice visited the target zone and non-targeting zone surrounding other holes far from the escape hole (see Figure. 4.6) were recorded. The experimenter was kept blind to the mouse genotypes during the whole test.

### 5.2.6 Tissue collection for pathological analysis

Animals were euthanized at 6 months of age by inhalation of isoflurane (Abbott, Wiesbaden, Germany). Whole blood was collected via intracardial puncture and kept in EDTA-containing Eppendorf tubes. Mice were then rapidly perfused transcardially with ice-cold PBS and the brain removed and divided. The left hemi-brain was immediately fixed in 4% paraformaldehyde (PFA, Sigma) for immunohistochemistry. A 0.5mm thick piece of tissue was sagittally cut from the right hemi-brain. The cortex and hippocampus were carefully separated and homogenized in Trizol (Life Technologies) for RNA isolation. The remainder of the right hemi-brain was snap frozen in liquid nitrogen for biochemical analysis (Figure 3.1) (Hao et al., 2011; Liu et al., 2012; Xie et al., 2013).

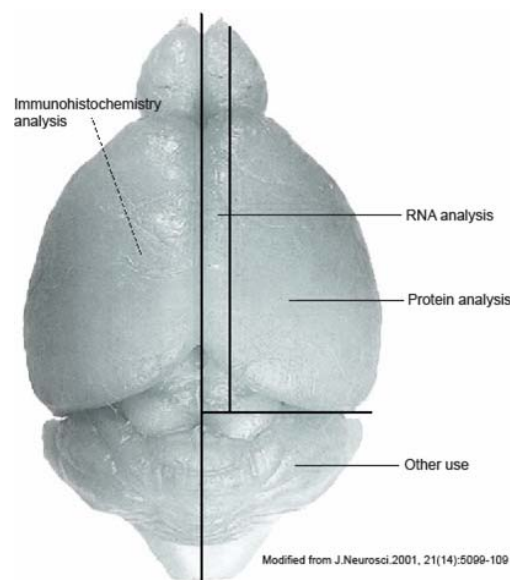


**Figure 3.1 Schematic figure of brain sample sections preparation.** The brain was divided into 4 parts. The left hemi-brain was immediately fixed in 4% PFA and stored at 4 °C for immunohistochemistry process. A 0.5 mm-thick piece of cerebral tissue was sagittally cut from the right hemi-brain, homogenized in TRIzol for RNA isolation. The rest of right hemi-cerebral was snap frozen in liquid nitrogen for biochemical analysis. The remained part was frozen in liquid nitrogen as well.

### 5.2.7 Immunohistochemistry

#### 5.2.7.1 Iba-1 and Ki67 Staining

In order to evaluate neuroinflammatory activation, 4% PFA-fixed left hemispheres were embedded in paraffin and serial 40µm thick sagittal sections were cut and mounted on glass slides. Immunohistochemical staining with the primary antibody, rabbit anti-Iba-1 (1:500, Wako Chemicals, Neuss, Germany), was performed on these sections (Liu et al., 2013). Detailed procedures are as follows:

1. The slides were serially deparaffinized in the solutions (2 x 5 min Xylene, 2 x 5 min 100% ethanol, 5 min 96% ethanol, 5 min 70% ethanol, and 5 min 50% ethanol).
2. Antigen retrieval by cooking the sections in 1× citrate buffer (10 mM, pH 6.0) in a microwave oven, 560 watts, 3 min × 5 times. Refill with buffer between each cooking. Cool down slowly by leaving on the bench for >30 min after cook.
3. The endogenous peroxidase of the tissue was inactivated via incubating the slides in the mixture of H<sub>2</sub>O<sub>2</sub>/Methanol/dH<sub>2</sub>O buffer, RT, 30min.
4. Wash slides with TBS, 5 min × 2 times and then with TBS-T, 5 min, once.
5. Block with blocking buffer (0.2% Casein (w/v) + 0.1% Tween 20 + 0.1% Triton X-100 in PBS), RT, 1h.
6. 1<sup>st</sup> Antibody reaction: with 1:500 dilution of the polyclonal rabbit-anti mouse-Iba-1 (Wako) in dilution buffer (0.02% Casein (w/v) + 0.01% Tween 20 + 0.01% Triton X-100 in PBS), incubate at 4 °C, overnight.
7. Wash as step 4.
8. 2<sup>nd</sup> Antibody reaction: with the 1:500 diluted HRP labeled goat-anti-rabbit (Promega) in dilution buffer, RT, 1h.
9. Wash as step 4.
10. Develop with DAB, 120 sec, and then wash with dH<sub>2</sub>O, 3 times.
11. Counterstaining with Hematoxylin, 10 sec, forward to dH<sub>2</sub>O wash 3 times. Then develop in running tap water for 5 min, and then change back to dH<sub>2</sub>O.
12. Dehydration: serially treat the slides in the following solutions: water, 3 min, 50% ethanol, 3 min 70% ethanol, 3 min 96% ethanol, 2 x 3 min 100% ethanol, 2 x 5 min Xylene.

13. Mount the slides with Entellan® Neu (Merck), and then cover the tissue with cover glass.

To detect proliferating microglia, the rabbit monoclonal antibody (clone SP6, Abcam) directed against Ki67 was added to sections after stained with Iba-1 antibodies, but before haematoxylin counterstaining. Thereafter, VectaStain ABC-AP kit and VECTOR Blue Alkaline Phosphatase Substrate kit were used, without haematoxylin counterstaining. Ki67 staining was visualized in blue. Detailed procedures are as follows:

14. After step 10, adds 1st Antibody: 1:200 dilution of anti Ki67 monoclonal antibody (Abcam) in dilution buffer (0.02% Casein (w/v) + 0.01% Tween 20 +0.01% Triton X-100 in PBS), incubate at 4 °C, overnight.
15. Wash as step 4.
16. 2nd Antibody reaction: with the 1:200 diluted biotin labeled goat-anti-rabbit (Vector Laboratories) in dilution buffer, RT, 1h.
17. Preparation of ABC-AP reagent: Add 10 µl Reagent A, 10 µl Reagent B to 1 ml PBS/T. Incubate in dark for at least 30 min before use.
18. Wash the slides as step 4.
19. Incubate the slides with ABC-AP reagent, RT, 30 min.
20. Wash as step 4.
21. Develop with Alkaline Phosphatase Substrate, 10min, at 37 °C and then wash with dH<sub>2</sub>O, 3 times.
22. Dehydration: serially treat the slides in the following solutions: water, 3 min, 50% ethanol, 3 min 70% ethanol, 3 min 96% ethanol, 2 x 3 min 100% ethanol, 2 x 5 min Histo-clear.
23. Mount the slides with VectaMount™ (Vector Laboratories), and then cover the tissue with cover glass.

#### 5.2.7.2 Aβ staining

In order to evaluate Aβ load, the sections throughout the entire hippocampus were randomly selected according to the random sampling method described in the last section. Volumes of Aβ, congo red staining and brain tissues (hippocampus and cortex) were estimated with the *Cavalieri* probe (Gundersen and Jensen, 1987) with 20µm of a grid size, which provided CE estimates

<0.04. The A $\beta$  load was demonstrated as the ratio of A $\beta$  volume to relevant brain tissue volume.

Detailed procedures are as follows:

1. The slides were serially deparaffinized in the solutions (2 x 5 min Xylene, 2 x 5 min 100% ethanol, 5 min 96% ethanol, 5 min 70% ethanol, and 5 min 50% ethanol).
2. Antigen retrieval by cooking the sections in HCl solution (2 mM) in a microwave oven, 560 watts, 3 min  $\times$  5 times. Refill with solution between each cooking. Cool down with distill water after cook and incubate in formic acid for 1 min.
3. Wash slides with TBS, 5 min  $\times$  2 times and then with TBS-T, 5 min, once.
4. Block with blocking buffer (0.2% casein + 0.1% Tween 20 +0.01% Triton X-100 in PBS), RT, 1h.
5. 1<sup>st</sup> Antibody reaction: with 1:50 dilution of the mouse monoclonal anti-human A $\beta$  antibody (clone 6F/3D, Dako, Hamburg, Germany) in dilution buffer (0.02% casein + 0.01% Tween 20 +0.01% Triton X-100 in PBS), incubate at 4 °C, overnight.
6. Wash as step 3.
7. 2<sup>nd</sup> Antibody reaction: with the 1:200 diluted HRP-conjugated goat anti-mouse IgG (Dako) in dilution buffer, RT, 1h.
8. Wash as step 3.
9. Develop with DAB, 120 sec, and then wash with dH<sub>2</sub>O, 3 times.
10. Dehydration: serially treat the slides in the following solutions: water, 3 min, 50% ethanol, 3 min 70% ethanol, 3 min 96% ethanol, 2 x 3 min 100% ethanol, 2 x 5 min Xylene
11. Mount the slides with Entellan® Neu (Merck), and then cover the tissue with cover glass.

All images were acquired by Zeiss AxioImager.Z2 microscope (Carl Zeiss, Göttingen, Germany) equipped with a Stereo Investigator system (MicroBrightField, Williston, USA). The stereological technique was used to count the number of microglia. Briefly, after systematic random sampling of every 10<sup>th</sup> section throughout the entire hippocampus and cortex dorsal to the hippocampus, the Optical Fractionator as the stereological probe was used to quantify Iba-1-labelled cells with 120 $\times$ 120 $\times$ 18 $\mu$ m of a disector and 400 $\times$ 400 $\mu$ m of a sampling grid. The estimated coefficient of error (CE) was less than 0.08. Tissue thickness was measured at each

disector location, using a focus drive with  $\pm 0.1\mu\text{m}$  accuracy. In each disector, only Iba-1 positive cells with clear haematoxylin nucleus staining were counted.

The proliferating microglia, which appeared with typical brown microglial processes and dark blue nuclei, were counted in the total hippocampus area in the randomly selected sections as described above. Data were reported as the number of antibody-labeling cells divided by the full area ( $\text{mm}^2$ ) of interest. All immunohistochemical analyses were performed by an experimenter blinded to the genotype of mice.

### 5.2.8 Congo red staining

To identify compacted amyloid in a beta-sheet secondary structure in the brain tissue, we stained paraffin-embedded sections as described above with Congo red according to the standard laboratory procedures (Wilcock et al., 2006). Detailed procedures are as follows:

1. The slides were serially deparaffinized in the solutions (2 x 5 min Xylene, 2 x 5 min 100% ethanol, 5 min 96% ethanol, 5 min 70% ethanol, and 5 min 50% ethanol).
2. Rehydrate the sections by incubating for 30 s in distilled water (dish a).
3. Incubate the slides for 20 min in the alkaline saturated NaCl solution (dish b).
4. Incubate the slides for 20 min in the Congo red solution (dish C).
5. Rinse by dipping ten times in 95% ethanol (dish d).
6. Rinse by dipping ten times in 100% ethanol (dishes e and f).
7. Incubate the slides for 5 min in each of the three xylenes (dishes g-i).
8. Mount with Mowiol.

To demonstrate the A $\beta$  deposits in the blood vessel, we cooked Congo red-stained sections in citrate buffer and then treated them with pepsin (Life Technologies) for the antigen retrieval. After being blocked in goat serum, the sections were incubated with a rabbit polyclonal against collagen type IV (Cat. ab6586, Abcam) as the first antibody and Alexa488-conjugated goat anti-rabbit IgG as the second antibody.

To analyze the distribution of A $\beta$  plaque size, we acquired images of hippocampus after Congo red staining with a 10 $\times$  objective (Carl Zeiss) using the Virtual Tissue Module (MicroBrightField). The hippocampus was delineated and the area of individual plaques was

determined after performing histogram-based segmentation with Image-Pro Plus 6.0 software (Media Cybernetics, Silver Spring, MD, USA).

### **5.2.9 Immunofluorescent staining**

To demonstrate the co-localization of IKK $\beta$  or GFP and different cellular markers, e.g. Iba-1, S100 and NeuN, the paraffin-embedded sections were used. The primary antibodies, rabbit polyclonal anti-IKK $\beta$  (Cat. NB600-477, Novus Biologicals), and rabbit or chicken polyclonal anti-GFP (Cat. ab290 and Cat. ab13970, Abcam) were first incubated with deparaffinised brain section and thereafter with Alexa488-conjugated goat anti-rabbit IgG or chicken IgY. After thorough washing, further antibodies against different cellular markers [mouse monoclonal anti-Iba-1 (clone 20A12.1, Merck Millipore, Billerica, USA), mouse monoclonal anti-S100 (clone 4C4.9, Abcam) or mouse monoclonal anti-NeuN (clone A60, Merck Millipore)] were used and visualized with relevant Alexa546-conjugated second antibodies (all second antibodies were from Life Technologies).

To detect CCR2-RFP positive cells in the brain, brain sections from 6-month-old bone marrow chimera APP-transgenic mice, which were constructed as in our published study (Hao et al., 2011) with ROSAmT/mG mice as the bone marrow donor, were used as positive controls. A rabbit polyclonal anti-RFP and its variants, e.g. tdTomato, (Rockland Immunochemicals, Gilbertsville, USA) was used as the first antibody and Alexa546-conjugated anti-rabbit IgG as the second antibody (Life Technologies).

### **5.2.10 Confocal microscopy**

To investigate the relationship between microglia and A $\beta$  deposits, four equidistant (120 $\mu$ m interval) serial sections from each mouse (see the last section) were co-stained with rabbit Iba-1 (Wako Chemicals) and monoclonal anti-A $\beta$  (clone 6F/3D, Dako), and then Alexa488- or Cy3-conjugated second antibodies. Under Zeiss LSM 510 Meta Confocal Microscope (Carl Zeiss) with  $\times 40$  objective, A $\beta$  deposits labeled with Cy3 were imaged after excitation with a 543nm laser. Thereafter, Z-stack serial scanning at 1 $\mu$ m interval from -15 to +15mm was performed under the excitation of 488 and 543nm lasers. From each section, five randomly chosen areas were analyzed. In order to count the number of Iba-1-positive cells co-localizing with A $\beta$



deposits, the images of Alexa488 (Iba-1) and Cy3 (A $\beta$ ) were color-coded and a 3-dimensional structure was reconstructed with the software Imaris 7.2.3 (Bitplane AG, Zurich, Switzerland). At the same time, the area of A $\beta$  from each layer of serial scanning was determined using ImageJ. Finally, the total number of microglia in each section was normalized by the total area of A $\beta$  deposits.

#### **5.2.11 Brain homogenates**

The brain was homogenized as previously described (Liu et al., 2012). Briefly, frozen hemispheres were bounce-homogenized in the TBS containing protease inhibitor cocktail (Roche Applied Science, Mannheim, Germany) and centrifuged at 16,000 $\times$ g for 30 minutes at 4°C. The supernatant (TBS-soluble fraction) was collected and stored at -80°C. The pellets were re-suspended in the TBS plus 1% Triton-X (TBS-T), sonicated for 5 minutes in 4°C water bath and centrifuged at 16,000 $\times$ g for another 30 minutes at 4°C. The supernatant was collected and stored at -80°C as the TBS-T-soluble fraction. The pellets were extracted for a third time using an ice-cold guanidine buffer (5M guanidine-HCl/50mM Tris, pH 8.0, herein referred to as guanidine-soluble fraction). The protein concentration of all samples was measured using Bio-Rad Protein Assay (Bio-Rad Laboratories GmbH, Munich, Germany). The A $\beta$  concentrations in 3 different fractions of brain homogenates were determined by A $\beta$ 42 and A $\beta$ 40 ELISA kits (both from Life Technologies). The TNF- $\alpha$  concentration in the TBS-soluble brain fraction was measured by ELISA (eBioscience), with results normalized based on the sample's protein concentration.

#### **5.2.12 Bio-Rad Protein Assay**

Protein concentration Bio-Rad Assay was completed with Protein Assay Reagent (Bio-Rad), based on the Bradford dye-binding procedure (Bradford, 1976), a simple colorimetric assay for measuring total protein concentration. Protein concentrations between 200  $\mu$ g/ml and 1,400  $\mu$ g/ml (20-140  $\mu$ g totals) can be assayed in a microplate format. Briefly, in high-concentration assay, 10  $\mu$ l sample or serial diluted standards were loaded on a 96-well format microplate, and then 200  $\mu$ l 1 $\times$  assay reagent was added to each well. Absorption at 595 nm was read with a Micro-plate reader and protein concentration was determined according to a standard curve.

### 5.2.13 ELISA

#### 5.2.13.1 A $\beta$ ELISA

A $\beta$ 1-40 and A $\beta$ 1-42 concentrations in three different fractions of brain homogenates were determined by A $\beta$ 42/40 ELISA kits (both from Invitrogen). Procedure is as follows:

1. Prepare samples and through serial dilution prepare the following A $\beta$ 1-40/ A $\beta$ 1-42 standards: 250, 125, 62.5, 31.25, 15.63, 7.81, and 0 pg/ml Hu A $\beta$ 40/ A $\beta$ 42.
2. Add 50  $\mu$ l of A $\beta$ 1-40/ A $\beta$ 1-42 peptide standards, controls, and samples to each plate well.
3. Add 50  $\mu$ l of anti-Hu A $\beta$ 40/ A $\beta$ 42 (Detection Antibody) solution to each well. Cover plate with plate cover and incubate for 3 hrs at room temperature with shaking.
4. Thoroughly aspirate solution from wells and discard the liquid. Wash wells 4 times.
5. Add 100  $\mu$ l Anti-rabbit Ig's-HRP Working Solution to each well. Cover plate with the plate cover and incubate for 30 min at room temperature.
6. Thoroughly aspirate solution from wells and discard the liquid. Wash wells 4 times.
7. Add 100  $\mu$ l of Stabilized Chromogen to each well. The liquid in the wells will begin to turn blue. Incubate for 30 min at room temperature and in the dark.
8. Add 100  $\mu$ l of Stop Solution to each well. Tap side of plate gently to mix. The solution in the wells would change from blue to yellow.
9. Read the absorbance of each well at 450 nm having blanked the plate reader against a chromogen blank composed of 100  $\mu$ l each of Stabilized Chromogen and Stop Solution. Read the plate within 30 min after adding the Stop Solution.
10. Use curve fitting software to generate the standard curve. Read the concentrations for test samples and controls from the standard curve. Multiply value(s) obtained for sample(s) by the appropriate factor to correct for the sample dilution.

#### 5.2.13.2 TNF- $\alpha$ ELISA

TNF- $\alpha$  concentrations in TBS fractions of brain homogenates and plasma were determined by TNF- $\alpha$  ELISA kits (from eBioscience). Procedure is as follows:

1. Coat ELISA plate with 100  $\mu$ L/well of TNF- $\alpha$  capture antibody in 1X Coating Buffer. Seal the plate and incubate overnight at 4°C.

2. Aspirate wells and wash 3 times with >250  $\mu$ L/well Wash Buffer. Allowing time for soaking (~1 minute) during each wash step increases the effectiveness of the washes. Blot plate on absorbent paper to remove any residual buffer.
3. Dilute 1 part 5X ELISA/ELISPOT Diluent with 4 parts DI water. Block wells with 200  $\mu$ L/well of 1X ELISA/ELISPOT Diluent. Incubate at room temperature for 1 hour.
4. Prepare samples and through serial dilution prepare the following TNF- $\alpha$  standards: 1000, 500, 250, 125, 62.5, 31.25, and 0 pg/ml mouse TNF- $\alpha$ . Add 100  $\mu$ L/well of your samples to the appropriate wells. Seal the plate and incubate at room temperature for 2 hours.
5. Aspirate/wash as in step 2. Repeat for a total of 3-5 washes.
6. Add 100  $\mu$ L/well of TNF- $\alpha$  detection antibody diluted in 1X ELISA/ELISPOT Diluent. Seal the plate and incubate at room temperature for 1 hour.
7. Aspirate/wash as in step 2. Repeat for a total of 3-5 washes.
8. Add 100  $\mu$ L/well of Avidin-HRP diluted in 1X ELISA/ELISPOT Diluent. Seal the plate and incubate at room temperature for 30 minutes.
9. Aspirate and wash as in step 2. In this wash step, soak wells in Wash Buffer for 1 to 2 minutes prior to aspiration. Repeat for a total of 5-7 washes.
10. Add 100  $\mu$ L/well of 1X TMB Solution to each well. Incubate plate at room temperature for 15 minutes.
11. Add 50  $\mu$ L of Stop Solution to each well.
12. Read plate at 450 nm and 570nm. Subtract the values of 570 nm from those of 450 nm and analyse data.

### 5.2.14 Western blot analysis

For evaluation of IKK $\beta$  protein, microglia and BMDM cells derived from *ikkbk<sup>fl/fl</sup>Cre<sup>-/-</sup>* and *ikkbk<sup>fl/fl</sup>Cre<sup>+/-</sup>* mice were washed with PBS and lysed in the buffer [50mM Tris/HCl, pH=7.4, 145mM NaCl, 1% Triton-100 and protease inhibitor cocktail (Roche Applied Science)]. For detection of phosphorylated and total amount of p65 component of NF- $\kappa$ B complex, microglia were activated with 10 $\mu$ M oligomeric A $\beta$ 42 for 12 minutes and immediately lysed in the buffer [50mM Tris/HCl, pH=7.4, 2mM EDTA, 50nM Okadaic acid, 5mM Sodium pyrophosphate, 50mM NaF, 1mM DTT, 1% Triton-100 and protease inhibitor cocktail (Roche Applied Science)]. To detect IKK $\beta$ , phosphorylated and total p65, phosphorylated and total SMAD2 and

phosphorylated and total SMAD5 in microglia and BMDM cells and synaptic proteins in the brains, cell lysates and TBS-T-soluble brain fractions derived from APP-transgenic and non-transgenic littermate mice differing in IKK $\beta$  expression were separated by 10% Tris-glycine PAGE.

#### **5.2.14.1 Sodium dodecyl sulfate-polyacrylamide gel electrophoresis**

The sodium dodecyl sulfate-polyacrylamide gel electrophoresis (SDS-PAGE) technique separates proteins according to their mobility difference in an electric field. Protein samples treated with SDS show an identical charge per unit mass and migrate in SDS gels only according to their molecular masses. The SDS-PAGE system used in this study is the Mini-PROTEAN® 3 Cell electrophoresis system (Bio-Rad). One gel is composed of a lower separating gel and an upper stacking gel. The stacking gel is 5%, while the percentage of the separating gel varies from 8% to 15%. Low percentage gels are used for large proteins, while small proteins are separated in high percentage gels. In this study, 10% separating gel was used. The gel and the electrodes were assembled in the SDS-PAGE chamber. The samples were diluted 1:2 in 3  $\times$  SDS-PAGE Sample loading buffer and heated at 95°C for 5min. Then, 20  $\mu$ l sample per well was loaded to 10% Acrylamide gel for electrophoresis running at 120 V until the Bromophenol blue front runs out of the gel. Proteins on the gel were transferred to membranes of nitrocellulose (NC) or polyvinylidene fluoride (PVDF) and detected by immunoblotting.

#### **5.2.14.2 Protein detection using immunoblotting**

Proteins separated by SDS-PAGE were further transferred to NC or PVDF membranes. PVDF membranes must be activated prior to the transfer by short incubation in 100 % methanol.

In this work, the membrane and sponges were immersed in transfer buffer before the transfer and the transfer buffer was cooled at 4 °C. In the transfer, the gel and membrane were sandwiched between sponge and paper (sponge/paper/gel/membrane/paper/sponge) and all are clamped tightly together after ensuring no air bubbles have formed between the gel and membrane. The transfer chamber was completely filled with transfer buffer and completed the transfer at 250 mA for 65 min. Subsequently, the sandwich was unpacked and the SDS gel discarded. The membrane with the immobilized protein was 10% skim milk powder (w/v) in PBS for 1 h at RT or 4 °C overnight in order to saturate unspecific binding sites. Then, the membrane was washed

twice for 5 minutes each with PBS. The primary antibody was diluted in PBS with 1% skimmed milk powder (w/v) at the concentration indicated below, and incubated with the membrane at 4 °C overnight. The membrane was washed 3x10 min in TBS + 0.05% Tween 20 to remove residual primary antibody. The membrane was then incubated with the appropriate secondary antibody at the concentration indicated below. The secondary antibody was diluted in PBS +1% skim milk powder (w/v) and the incubation period was 1 hours. Therefore, the membrane was washed 3x10 min with TBS + 0.05% Tween 20. Lightning ECL substrate (Perkin Elmer) was developed. According to the manufacturer charges substrate solution A and B substrate solution were mixed in a 1:1 ratio and evenly distributed on the membrane. After 2 minutes, the substrate mixture was removed and the chemiluminescence detected using Amersham Hyperfilm ECL (GE Healthcare) in a darkroom. Kodak GBX developer and fixer were used to make signals visible.

The western blot films were scanned with the Epson Perfection V700 Photo Scanner. Densitometric analyzes were performed with the image processing program Image J (NIH, Version 1.43).

#### **5.2.15 Purification of membrane components and $\beta$ - and $\gamma$ -secretase activity assays**

Membrane components were purified from 6-month-old APP-transgenic and non-transgenic littermate mouse brains with established methods (Burg et al., 2013; Hao et al., 2011; Xie et al., 2013). Briefly, brain tissue was homogenized in sucrose buffer (10mM Tris/HCl, pH=7.4, 1mM EDTA, 200mM sucrose). Cell nuclei were removed by centrifugation at 1,000×g and 4°C for 10 minutes. The supernatant was transferred to a new tube and centrifuged again at 10,000×g and 4°C for 10 minutes. The resulting supernatant was centrifuged at 187,000×g and 4°C for 75 minutes in an Optima MAX Ultracentrifuge (Beckman Coulter, Krefeld, Germany). The supernatant was discarded and the pellet containing the crude membrane fraction was stored at -80°C until use.  $\beta$ - and  $\gamma$ -secretase activities were measured by incubating the crude membrane fraction at 0.1mg/ml for  $\beta$ -secretase and 1mg/ml for  $\gamma$ -secretase with 8 $\mu$ M secretase-specific FRET substrates. At 37°C, in the  $\beta$ -secretase buffer (0.1M sodium acetate, pH=4.5) and  $\gamma$ -secretase buffer (50mM Tris/HCl, pH=6.8, 2mM EDTA), both secretases cleaved the fluorogenic substrates resulting in continuous accumulation of fluorescence signals which were measured by

Synergy Mx Monochromator-Based Multi-Mode Microplate Reader (BioTek, Winooski, USA). For both secretase assays, dynamic reading of fluorescence intensity in each well was performed for 73 cycles with intervals of 5 minutes. Fluorescence intensity of the first cycle was considered to be background and subtracted for each well. Data were presented as an activity-time curve.

#### **5.2.16 Reverse transcription and quantitative PCR for analysis of gene transcripts**

Real-time PCR is a quantitative PCR method for the determination of cope number of PCR templates such as DNA or complementary DNA (cDNA) in a PCR reaction. There are two types of real-time PCR: intercalator-based and probe-based. Both methods require a special thermocycler equipped with a sensitive camera that monitors the fluorescence in each well of the 96-well plate at frequent intervals during the PCR Reaction. Intercalator-based method (also known as SYBR Green method) requires a double-stranded DNA dye in the PCR reaction which binds to newly synthesized double-stranded DNA and gives fluorescence. Probe-based real-time PCR (also known as TaqMan PCR) requires a pair of PCR primers (as regular PCR does) an additional fluorogenic probe which is an oligonucleotide of 20-26 nucleotides with both a reporter fluorescent dye and a quencher dye attached. The probe is designed to bind only the DNA sequence between the two specific PCR primers. Only a specific PCR product can generate a fluorescent signal in TaqMan PCR. Therefore, the TaqMan method is more accurate and more reliable than SYBR green method.

In our study, real-time PCR was performed using SYBR green (Roche Applied Science) or Taqman® probes (Life Technologies) with the 7500 Fast Real-Time PCR System (Life Technologies). The primer sequences for detecting transcripts of *tnf-α*, *il-1β*, *inos*, *il-10*, *ccl-2* and *glyceraldehyde 3-phosphate dehydrogenase (gapdh)* were the same as used in our earlier study (Liu et al., 2006). Taqman® gene expression assays from Life Technologies were used to measure transcripts of the following genes: mouse *tnf-α*, *il-1β*, *mrc1*, *arg1*, *ikbkb*, *chi3l3*, *cd36*, *sra*, *ide*, *nep*, *rage*, *lrp1* and 18s RNA. For the *ikbkb* transcript detection, the Taqman® gene expression assay (Mm01222249\_m1) was used with the amplified PCR product overlapping 6-7 exon boundary of *ikbkb*.

### 5.2.16.1 Brain total RNA isolation with Trizol

Homogenization: The 0.5 mm-thick piece of tissue sagittally cut from the right hemi-brain (see above tissue preparation section 3.2.6) was homogenized in 1 ml Trizol (Invitrogen).

1. Phase separation: Incubate the homogenized samples for 5 min at room temperature to permit complete dissociation of nucleoprotein complexes. Then add 0.2 ml of chloroform and shake vigorously by hand for 15 sec, and then incubate at room temperature for 3 min. Centrifuge the samples at  $12,000 \times g$  for 15 min at 4 °C. The sample mixture was separated into a lower red, phenol-chloroform phase, an interphase and a colorless upper aqueous phase. RNA remains in the aqueous phase.
2. RNA precipitation: Transfer the colourless aqueous phase to a fresh tube; precipitate the RNA from the aqueous phase by mixing with 0.5 ml isopropyl alcohol. Incubate at room temperature for 10 min and then centrifuge at  $12,000 \times g$  for 10 min at 4 °C. The precipitated RNA is the gel-like pellet on the bottom side of the tube.
3. RNA wash: remove the supernatant and wash the RNA once with 1 ml 75% ethanol. Mix by vortexing and centrifuge at  $7,600 \times g$  for 5 min at 4 °C.
4. Redissolve the RNA: briefly dry the RNA pellet, incubating for 10 min at RT and then dissolve it in appropriate volume of RNase-free water.

### 5.2.16.2 Genome DNA degradation prior to RT-PCR

To erase trace genomic DNA contamination in the RNA sample, RQ1 (RNA Qualified) RNase-Free DNase (Promega), which is a DNase I that degrades both double-stranded and single-stranded DNA endonucleolytically, was used. The reaction was set up as following:

RNA sample in water	8 $\mu$ l
RQ1 RNase-Free DNase 10 $\times$ Reaction buffer	1 $\mu$ l
RQ1 RNase-Free DNase	1 U/ $\mu$ g RNA
Nuclease-free water	To a final volume of 10 $\mu$ l

Incubate at 37 °C for 30 min, and then add 1 µl of RQ1 DNase Stop solution to terminate the reaction. The DNase was then inactivated by incubating at 65 °C for 10 min.

### 5.2.16.3 First strand cDNA synthesis

First-strand cDNA was synthesized by priming total RNA with hexamer random primers (Invitrogen) and using Superscript II reverse transcriptase (Invitrogen), which is an engineered version of Moloney Murine Leukemia Virus RT with reduced RNase H activity and increased thermal stability. This enzyme can be used to generate cDNA up to 12.3kb. The reaction is:

Total RNA	3 µg
Rndom primer (250 ng/µl)	1 µl
dNTP mix (10 mM each)	1 µl
Nuclease-free water	To a final volume of 12 µl
Heat the mixture to 70 °C for 5 min and quick chill on ice for 2min. And then add:	
5x First-strand buffer	4 µl
0.1 M DTT	2 µl
Mix contents gently. Incubate at 25 °C for 2 min.	
Add 1 µl (200 units) Superscript <sup>TM</sup> II and mix gently.	
Incubate at 25 °C for 10 min and 45 °C for 50 min.	
Inactivate the reaction by heating at 70 °C for 15min. The cDNA can be ready for use.	

### 5.2.16.4 Real-time quantitative PCR

For quantification of *tnf-α*, *il-1β*, *mrc1*, *arg1*, *ikkb*, *chi3l3*, *cd36*, *sra*, *ide*, *nep*, *rage*, *lrp1*, *gapdh* and 18S transcription level, real-time quantitative PCR with the Taqman® gene expression



assays o was performed using the 7500 Fast real-time PCR system (Applied Biosystems) with a DyNAmo™Flash Probe qPCR kit (Roche Applied Science).

Reaction setup for Taqman probe:

Components	Volume	Concentration
2x DyNAmo™ Flash Probe Master Mix	10 µl	1x
Primer Mix (10 µM)	1 µl	0.5 µM
50x ROX reference dye	0.06 µl	0.3x
cDNA	1 µl	max. 150 ng
ddH <sub>2</sub> O	Up to 20 µl	

Select FAM-labeled detectors and set up reaction system cycling to run:

step	purpose	temp	time	cycles
1	Initial denaturation	95 °C	10 min	1
2	Denaturation	95 °C	10 s	45
	Annealing+extension	60 °C	30 s	

The amount of double-stranded PCR product synthesized in each cycle was measured by detecting the free FAM dye cleaved from the Taqman® probes. Threshold cycle (Ct) values for each test gene from the replicate PCRs was normalized to the Ct values for the 18s RNA control from the same cDNA preparations. The ratio of transcription of each gene was calculated as  $2^{(\Delta Ct)}$ , where  $\Delta Ct$  is the difference Ct (18s RNA) – Ct (test gene).

### 5.2.17 Statistics

Data shown in the Figures are presented as mean  $\pm$  SD (for in vitro data) or mean  $\pm$  SEM (for in vivo data). For multiple comparisons, one-way or two-way ANOVA followed by Bonferroni's, Tukey's Honestly Significant Difference or Tamhane's T2 post hoc test (dependent on the result of Levene's test to determine the equality of variances) was applied. Two-independent-samples

t-test was used to compare means for two groups of cases. All statistical analysis was performed on Statistical Package for the Social Sciences 15.0 for Windows (SPSS, Chicago). Statistical significance was set at  $p < 0.05$ .

## 6 RESULTS

### 6.1 Establishment of APP-transgenic mice with IKK $\beta$ deficiency in myeloid cells, i.e., endogenous microglia in the brain

To ablate IKK $\beta$  specifically in the myeloid cell lineage, especially in microglia, we cross-bred TgCRND8 APP-transgenic mice (*app*<sup>tg</sup>) to *ikkbk*-floxed mice (*ikkbk*<sup>fl/fl</sup>) and LysM-Cre knock-in mice (LysM-Cre<sup>+/+</sup>). In the brains of 3-month-old *app*<sup>tg</sup>*ikkbk*<sup>fl/fl</sup>Cre<sup>+/+</sup> mice, immunofluorescence staining determined that IKK $\beta$  protein levels were greatly reduced by Cre-mediated gene recombination in Iba-1<sup>+</sup> cells in the parenchyma, which represent endogenous microglia and potentially infiltrating brain macrophages, but not in NeuN<sup>+</sup> cells (neurons) (Figure. 4.1 A, B). IKK $\beta$  was undetectable in S100-stained cells (astrocytes) (Figure. 4.1, C). Accordingly, Western blotting results showed that the amount of IKK $\beta$  in CD11b<sup>+</sup> cells isolated from *app*<sup>tg</sup>*ikkbk*<sup>fl/fl</sup>Cre<sup>+/+</sup> mice was significantly less than that in control cells isolated from *app*<sup>tg</sup>*ikkbk*<sup>fl/fl</sup>Cre<sup>-/-</sup> littermates (IKK $\beta$ /actin: 0.037 $\pm$ 0.004 vs. 0.051 $\pm$ 0.003; *t* test, *p*=0.022; Figure. 4.1.1, D E). Similarly, quantitative PCR analysis showed that the levels of *ikkbk* transcripts in CD11b<sup>+</sup> brain cells from *app*<sup>tg</sup>*ikkbk*<sup>fl/fl</sup>Cre<sup>+/+</sup> mice were 34.53% $\pm$ 1.61% of the levels of *ikkbk* transcripts from *app*<sup>tg</sup>*ikkbk*<sup>fl/fl</sup>Cre<sup>-/-</sup> littermate mice (Figure. 4.1, F). In contrast, in CD11b<sup>-</sup> brain cells, including neurons, astrocytes, and oligodendrocytes, the levels of general *ikkbk* transcripts were unaffected by Cre expression (Figure. 4.1, F).

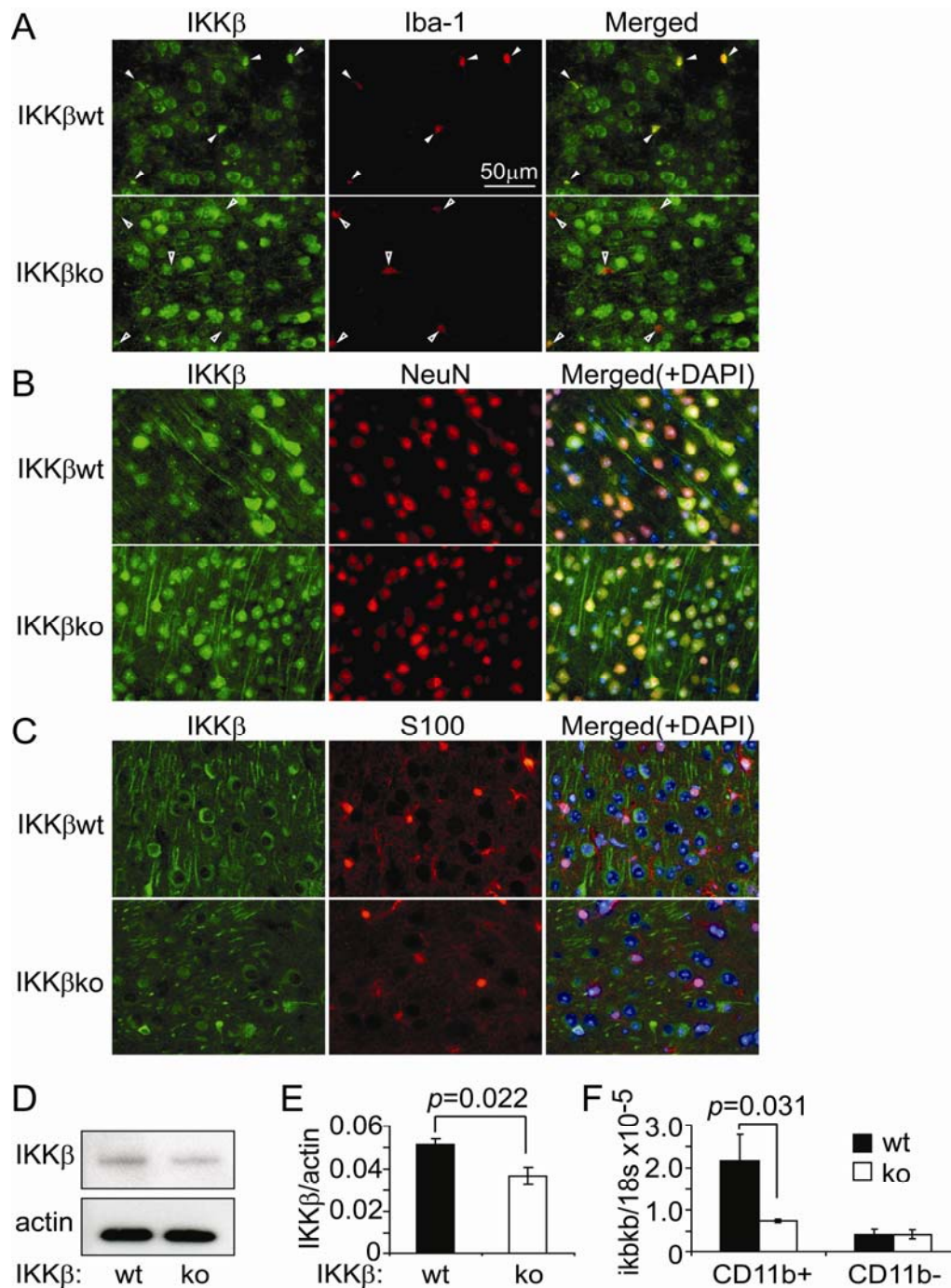


**Figure 4.1. LysM-Cre efficiently excises the floxed *ikkbb* gene in microglia and brain macrophages.** A-C. Brain sections derived from 3-month-old *ikkbb<sup>fl/fl</sup>Cre<sup>+/+</sup>* (IKK $\beta$ ko) and *ikkbb<sup>fl/fl</sup>Cre<sup>-/-</sup>* (IKK $\beta$ wt) mice were stained for IKK $\beta$  (in green) and various cellular markers: Iba-1, NeuN, and S100 (in red). To determine the ablation efficiency of the *ikkbb* gene by Cre recombinase, CD11b<sup>+</sup> and CD11b<sup>-</sup> cells were isolated from the brains of these two groups of mice. IKK $\beta$  protein was detected and quantified by Western blot (D-E. *t* test; n=4 per group) and the *ikkbb* gene transcripts were measured by quantitative PCR (F. *t* test; n=4 per group).

In additional experiments, we also measured IKK $\beta$  protein levels in CD11b<sup>+</sup> circulating monocytes and cultured bone marrow–derived macrophages, which had been prepared according to our established protocol (Hao et al., 2011). LysM-Cre could more efficiently recombine the floxed genes in these peripheral myeloid cells than in microglia (Figure, 4.2; IKK $\beta$ /actin:  $0.095 \pm 0.014$  vs.  $0.332 \pm 0.034$ , *t* test,  $p < 0.001$ , in monocytes;  $0.013 \pm 0.002$  vs.  $0.266 \pm 0.063$ , *t* test,  $p = 0.013$ , in cultured macrophages derived from *app<sup>tg</sup>ikkb<sup>fl/fl</sup>Cre<sup>+/-</sup>* and *app<sup>tg</sup>ikkb<sup>fl/fl</sup>Cre<sup>-/-</sup>* littermates, respectively). Our results were in accordance with those of a previous published report stating that the rate of LysM-Cre–mediated gene recombination is approximately 40% in microglia and 60% in monocytes (Goldmann et al., 2013).

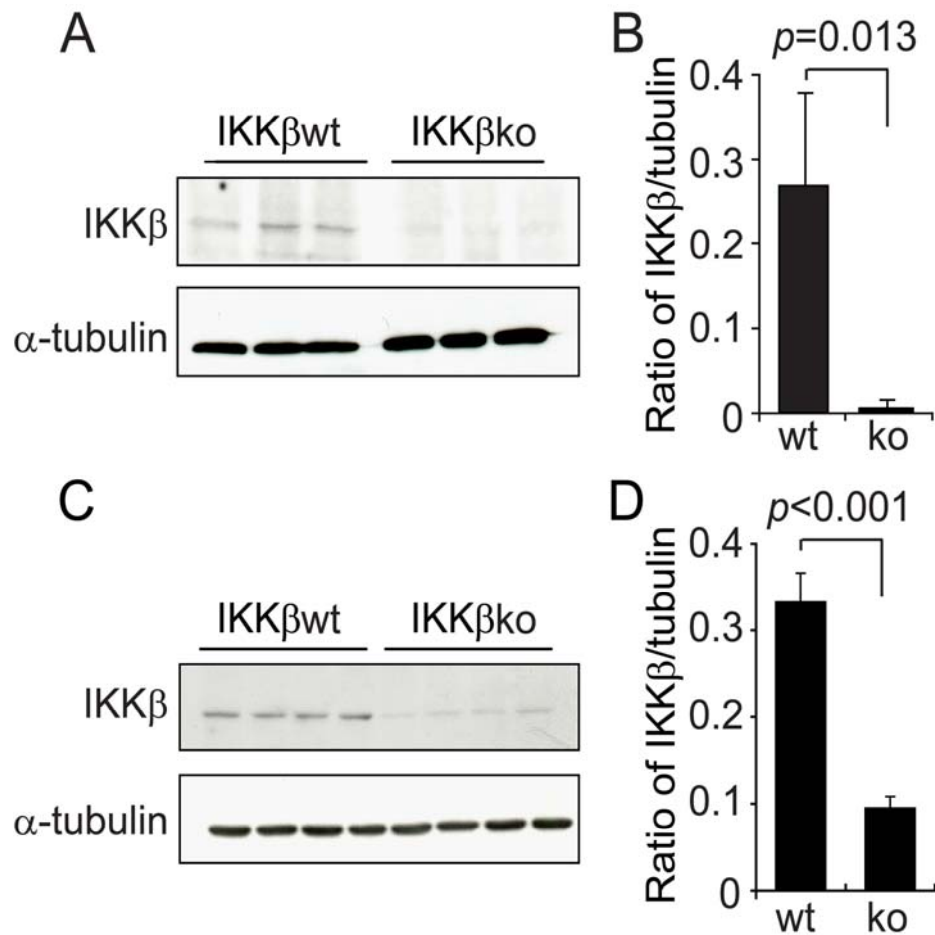


**Figure 4.2. LysM-Cre efficiently excises the floxed *ikkb* gene in bone marrow derived macrophages and peripheral monocytes.** Cultured bone marrow–derived macrophages and CD11b<sup>+</sup> circulating monocytes were isolated from *ikkb<sup>fl/fl</sup>Cre<sup>+/-</sup>* (IKK $\beta$ ko) and *ikkb<sup>fl/fl</sup>Cre<sup>-/-</sup>* (IKK $\beta$ wt) mice. IKK $\beta$  protein in BMDM (A, B) and peripheral monocytes (C, D) was detected and quantified by Western blot (*t* test,  $n \geq 3$  per group).

To further confirm the cell selectivity of Cre, LysM-Cre mice were cross-bred to ROSA<sup>mT/mG</sup> Cre report mice (Muzumdar et al., 2007). This report system confirmed that Cre recombinase was active only in Iba-1<sup>+</sup> cells, not in S100<sup>+</sup> cells (Figure. 4.3).

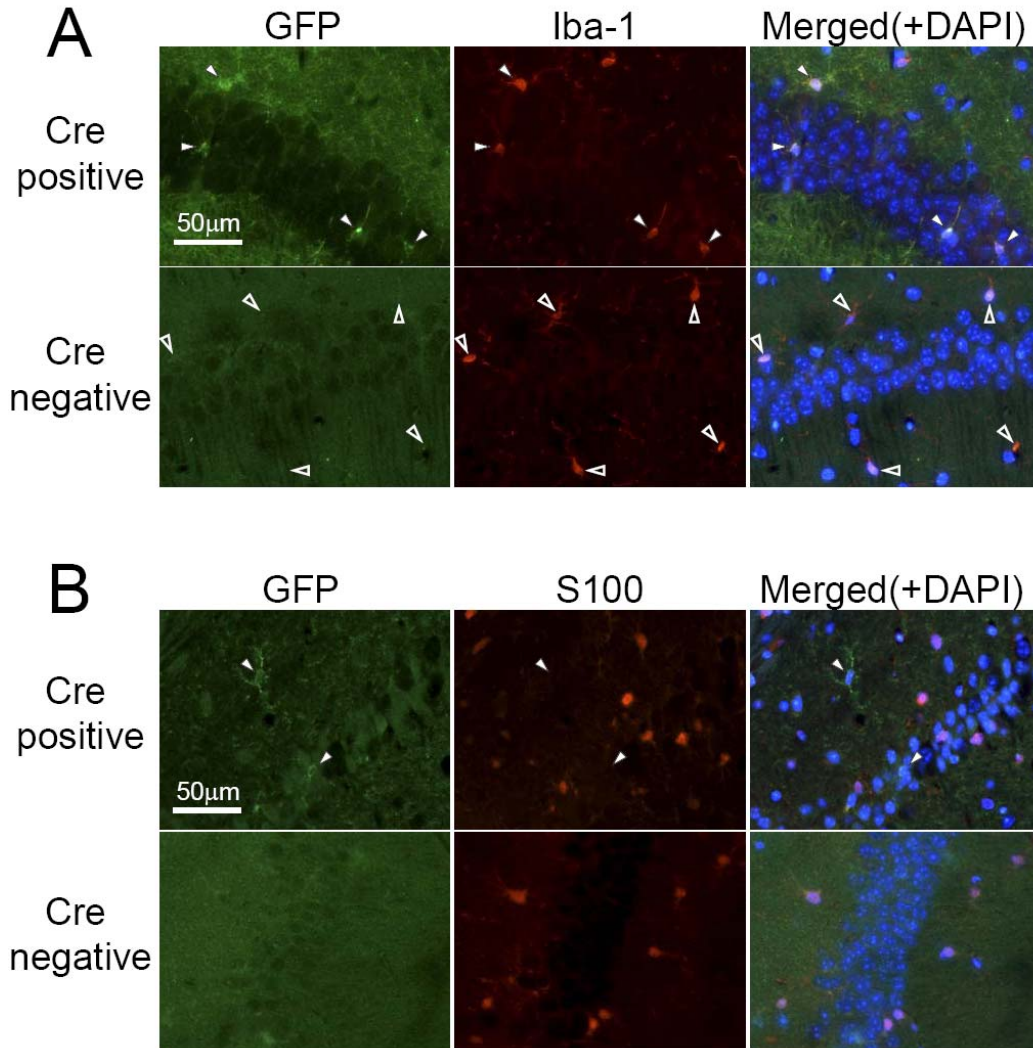


**Figure 4.3. LysM-Cre does not affect IKK $\beta$  expression in neurons and astrocytes.** Brain sections derived from 3-month-old *app<sup>tg</sup>ikkb<sup>fl/fl</sup>Cre<sup>+/-</sup>* (IKK $\beta$ ko) and *app<sup>tg</sup>ikkb<sup>fl/fl</sup>Cre<sup>-/-</sup>* (IKK $\beta$ wt) mice were stained with rabbit anti-IKK $\beta$  (visualized in green fluorescence) and mouse monoclonal antibodies against NeuN and S100 (visualized in red fluorescence). Co-localization of IKK $\beta$  and NeuN or S100 was shown by yellow color and the co-localization of IKK $\beta$ , NeuN and DAPI (in blue fluorescence) was shown in white. In both IKK $\beta$ wt and IKK $\beta$ ko mice, IKK $\beta$  was detected in NeuN-positive cells (A), but not in S100-positive cells (B).

It is known that LysM-Cre recombines floxed genes in myeloid cells outside the brain, including monocytes, macrophages, and neutrophils (Clausen et al., 1999; Goldmann et al., 2013). We

wondered whether peripheral myeloid cells had migrated into the brain and affected brain pathology in our APP mice, although one published study found a negative answer to this question (Mildner et al., 2011). We found no positive immunohistochemical staining with neutrophil-specific or CD3-specific antibodies in the brains of 6-month-old APP-transgenic mice (data not shown). Therefore, we excluded the possibility of brain infiltration of neutrophils and T-lymphocytes, both of which are CD45<sup>+</sup>. However, we did observe a few CD45<sup>+</sup> cells in the same brain; these cells were diffused or clustered within a region of the brain parenchyma but were not distributed throughout the entire brain area where A $\beta$  was deposited. The density of CD45<sup>+</sup> cells was  $2.01 \pm 0.42/\text{mm}^2$  in the hippocampus and cortex of *app<sup>tg</sup>ikbb<sup>fl/fl</sup>Cre<sup>+/-</sup>* mice and  $1.88 \pm 0.38/\text{mm}^2$  in the hippocampus and cortex of *app<sup>tg</sup>ikbb<sup>fl/fl</sup>Cre<sup>-/-</sup>* mice (Figure. 4.4, A, B; *t* test between two groups,  $p > 0.05$ ). In addition, we used flow cytometry to count fluorescence-labeled cells and found that in the CD11b<sup>+</sup> brain cell populations derived from *app<sup>tg</sup>ikbb<sup>fl/fl</sup>Cre<sup>+/-</sup>*, *app<sup>tg</sup>ikbb<sup>fl/fl</sup>Cre<sup>-/-</sup>*, and even *app<sup>wt</sup>ikbb<sup>fl/fl</sup>Cre<sup>-/-</sup>* mice approximately 2% of cells were CD45<sup>+</sup>. This ratio did not differ between the three groups of mice (Figure. 4.4, C, D; One-way ANOVA,  $p > 0.05$ ) but was significantly higher in the experimental autoimmune encephalitis (EAE) mice than in *app<sup>wt</sup>ikbb<sup>fl/fl</sup>Cre<sup>-/-</sup>* mice ( $10.30\% \pm 0.54\%$ , Bonferroni's post-hoc test,  $p < 0.001$ ). EAE is a mouse model of multiple sclerosis with infiltration of peripheral leukocytes in the central nerve system. We considered these CD45/CD11b<sup>+</sup> cells with limited numbers to be potentially infiltrating brain macrophages.

As an additional confirmation of the existence of brain macrophages in AD mice, we performed immunohistochemical staining with a popularly used macrophage-recognizing antibody, anti-CD68. We did not observe CD68<sup>+</sup> cells in the brain parenchyma of either *app<sup>tg</sup>ikbb<sup>fl/fl</sup>Cre<sup>+/-</sup>* or *app<sup>tg</sup>ikbb<sup>fl/fl</sup>Cre<sup>-/-</sup>* mice. We cross-bred TgCRND8 APP-transgenic mice to CCR2-RFP mice (Saederup et al., 2010). In 6-month-old APP-transgenic mice heterozygous for the *ccr2-rfp* gene, we found no RFP<sup>+</sup> cells in the brain parenchyma and only a few cells in close proximity to cerebral blood vessels (Figure. 4.4, E;  $n=3$ ). As a positive control we used brains from 6-month-old bone marrow chimera APP-transgenic mice, which were constructed as previously described (Hao et al., 2011) with ROSA<sup>mT/mG</sup> mice as the bone marrow donor. The bone marrow-derived cells were distributed in the brain parenchyma and expressed TFP, which reacts with the same antibody against RFP in CCR2-RFP mice. The results of this experiment provide evidence for



the limited infiltration of brain macrophages in AD mice, given that brain macrophages are derived from  $\text{Ly6C}^{\text{high}}\text{CCR2}^+$  monocytes (Mildner et al., 2007; Mizutani et al., 2012; Varvel et al., 2012).

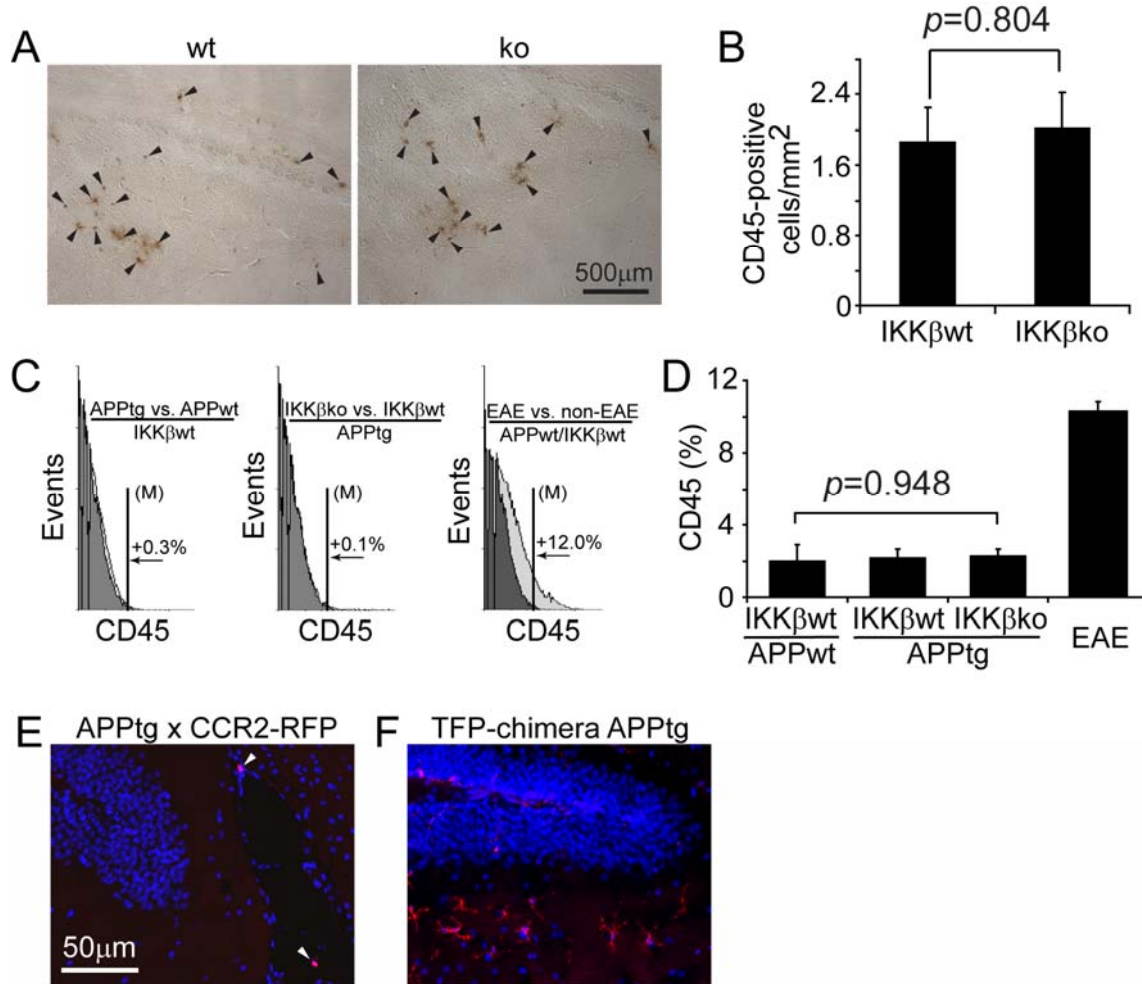


**Figure 4.4. Infiltration of  $\text{CD45}^+$  or  $\text{CCR2}^+$  cells in APP-transgenic mouse brain.** **A.** Brain sections derived from 6-month-old APP-transgenic mice with (ko) and without (wt) ablation of IKK $\beta$  in myeloid cells were stained for CD45 (in brown, arrowhead). IKK $\beta$  ablation did not affect the density of  $\text{CD45}^+$  cells in the hippocampus and cortex (**B.** *t* test;  $n=6$  per group). **C.**  $\text{CD11b}^+$  cells were isolated from 6-month-old IKK $\beta$ ko and wt APP-transgenic mice and fluorescently labeled with CD45 antibody for flow cytometry. Histograms show  $\text{CD45}^+$  cells and comparisons between two groups with control in gray color. **D.** Columns summarize percentages of  $\text{CD45}^+$  cells in the  $\text{CD11b}^+$  brain cell populations (One-way ANOVA;  $n>7$  per group). **E.** Brain sections derived from 6-month-old APP-transgenic mice that were mated to CCR2-RFP knock-in mice were stained for RFP. A brain section from a 6-month-old tdTomato-transgenic bone marrow chimera APP-transgenic mouse was used as a positive control, because the chosen antibody recognized both RFP and tdTomato (**F**). TdTomato $^+$  cells are distributed in the brain parenchyma with typical microglial morphology.



We also investigated the effects of IKK $\beta$  deficiency in myeloid cells on peripheral inflammatory status by measuring plasma TNF- $\alpha$  levels. We observed no difference in plasma TNF- $\alpha$  levels between the four mouse groups (*app<sup>wt</sup>ikkb<sup>fl/fl</sup>Cre<sup>+/-</sup>*, 35.38 $\pm$ 10.56 pg/mL; *app<sup>wt</sup>ikkb<sup>fl/fl</sup>Cre<sup>-/-</sup>*, 34.84 $\pm$ 11.39 pg/mL; *app<sup>tg</sup>ikkb<sup>fl/fl</sup>Cre<sup>+/-</sup>*, 32.68 $\pm$ 13.88 pg/mL; and *app<sup>tg</sup>ikkb<sup>fl/fl</sup>Cre<sup>-/-</sup>*, 35.88 $\pm$ 9.09 pg/mL; One-way ANOVA,  $p>0.05$ ;  $n=9$  per group).

Finally, we investigated the effects of IKK $\beta$  deficiency on microglial NF- $\kappa$ B activation. Western blot analysis showed that the amount of IKK $\beta$  protein detected in cultured primary microglia derived from *ikkb<sup>fl/fl</sup>Cre<sup>+/-</sup>* mice was 49.18% $\pm$ 6.90% of the amount detected in cultured microglia derived from *ikkb<sup>fl/fl</sup>Cre<sup>-/-</sup>* mice (Figure. 4.5, A, B). The approximately 50% reduction in IKK $\beta$  protein suppressed the phosphorylation of p65 in the NF- $\kappa$ B complex in the microglia both at the basal level and after activation with 10  $\mu$ M oligomeric A $\beta$ 42 (the ratio of phosphorylated p65 to total p65 was 0.40 $\pm$ 0.09 in *ikkb<sup>fl/fl</sup>Cre<sup>-/-</sup>* cells and 0.11 $\pm$ 0.01 in *ikkb<sup>fl/fl</sup>Cre<sup>+/-</sup>* cells at the basal level, and 1.29 $\pm$ 0.20 in *ikkb<sup>fl/fl</sup>Cre<sup>-/-</sup>* cells and 0.26 $\pm$ 0.05 in *ikkb<sup>fl/fl</sup>Cre<sup>+/-</sup>* cells after A $\beta$  activation; One-way ANOVA,  $p<0.05$ ; Figure. 4.5, C, D). However, IKK $\beta$  deficiency did not completely block NF- $\kappa$ B activation by A $\beta$ 42 oligomers, because A $\beta$  significantly increased the level of phosphorylated p65 in microglia derived from *ikkb<sup>fl/fl</sup>Cre<sup>+/-</sup>* mice ( $t$  test,  $p<0.05$ ; Figure. 4.5, C, D).

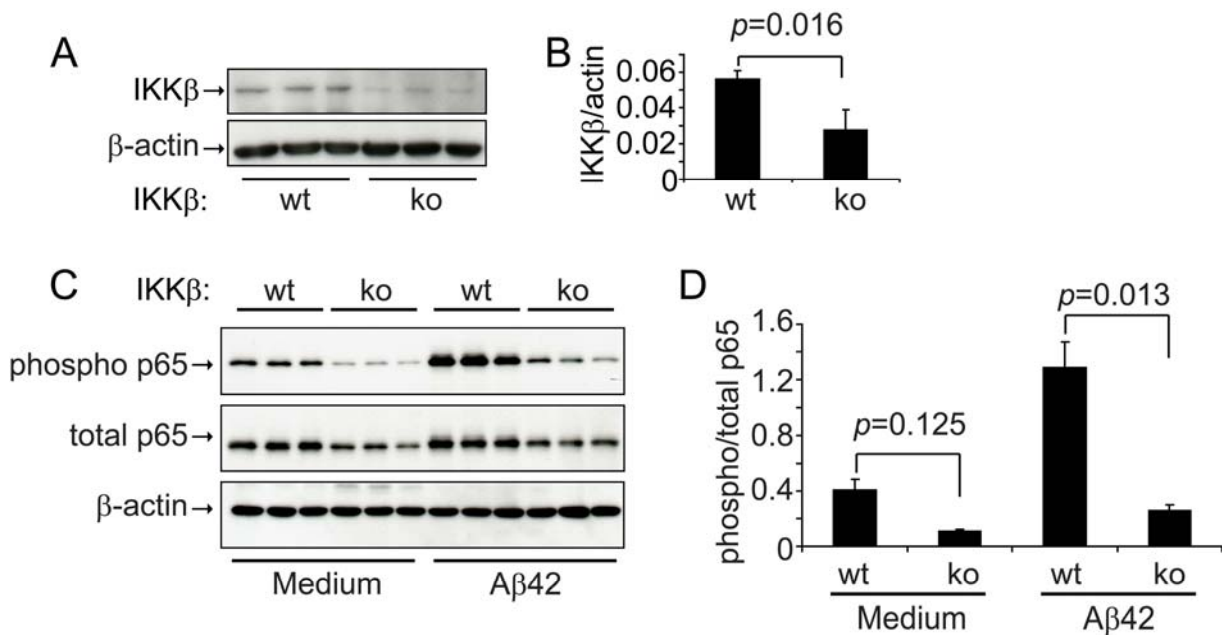


**Figure 4.5. IKK $\beta$  ablation inhibits NF- $\kappa$ B activation in primary cultured microglia.** IKK $\beta$  protein (A, B. *t* test; *n*=3 per group) and phosphorylated and total NF- $\kappa$ B p65 (C, D. *t* test; *n*=3 per group) in the primary cultured microglial cell lysate derived from *ikkbk<sup>fl/fl</sup>Cre<sup>+/-</sup>* (IKK $\beta$ ko) and *ikkbk<sup>fl/fl</sup>Cre<sup>-/-</sup>* (IKK $\beta$ wt) mice were detected and quantified with Western blotting. For NF- $\kappa$ B activation assays, IKK $\beta$  wt and ko microglia were activated with 10  $\mu$ M oligomeric A $\beta$ 42 for 12 minutes.

## 6.2 Deficiency of IKK $\beta$ in myeloid cells (microglia) rescues cognitive deficits in APP-transgenic mice

Because deficiencies in TLR2, MyD88, and IRAK4 in myeloid cells, especially in microglia, have been shown to ameliorate AD-like pathology and improve neuronal functions in AD mice (Hao et al., 2011; Cameron et al., 2012; Liu et al., 2012), we investigated whether deficiency of IKK $\beta$  in myeloid cells (microglia) improves the cognitive function of APP-transgenic mice. In the Barnes maze (Hao et al., 2011; Liu et al., 2012), the traveling time and distance traveled was significantly shorter for all tested mice when training time increased (Figure. 4, A, B, C; One-way ANOVA, *p*<0.05). During the test there were no significant differences in running speed between various groups of mice or for the same mice on different training dates (Two-way ANOVA, *p*>0.05). Thus, both APP-transgenic (*app<sup>tg</sup>*) and non-APP-transgenic (*app<sup>wt</sup>*) littermate mice with different myeloid expressions of IKK $\beta$  retained the ability to use spatial reference points to learn the location of an escape hole (Figure. 4.6, A, B, C).

There were no differences in traveling time and distance traveled between non-APP-transgenic littermate mice with deficiencies in IKK $\beta$  or with wild-type IKK $\beta$  in myeloid cells (*app<sup>wt</sup>ikkbk<sup>fl/fl</sup>Cre<sup>-/-</sup>* and *app<sup>wt</sup>ikkbk<sup>fl/fl</sup>Cre<sup>+/-</sup>*) (Figure. 4.6, B, C; Two-way ANOVA, *p*>0.05). However, compared to their *app<sup>wt</sup>ikkbk<sup>fl/fl</sup>Cre<sup>-/-</sup>* and *app<sup>wt</sup>ikkbk<sup>fl/fl</sup>Cre<sup>+/-</sup>* littermates, 6-month-old APP-transgenic mice with wild-type IKK $\beta$  expression in myeloid cells (*app<sup>tg</sup>ikkbk<sup>fl/fl</sup>Cre<sup>-/-</sup>*) spent significantly more time (Figure. 4, B; Two-way ANOVA, *p*<0.05) and traveled longer distances (Figure. 4.6, C; Two-way ANOVA, *p*<0.05) before reaching the escape hole. Interestingly, ablation of IKK $\beta$  specifically in myeloid cells, especially microglia (*app<sup>tg</sup>ikkbk<sup>fl/fl</sup>Cre<sup>+/-</sup>* mice), completely rescued these cognitive deficits in 6-month-old APP-transgenic mice as assessed by the Barnes maze test (Figure. 4.6, B, C). Moreover, in the probe trials, *app<sup>wt</sup>ikkbk<sup>fl/fl</sup>Cre<sup>-/-</sup>* and *app<sup>wt</sup>ikkbk<sup>fl/fl</sup>Cre<sup>+/-</sup>* mice visited the escape hole similarly, and *app<sup>tg</sup>ikkbk<sup>fl/fl</sup>Cre<sup>-/-</sup>* mice spent less time around the escape hole and visited the hole less frequently than did non-APP-transgenic

mice, although the difference did not reach statistical significance (Figure. 4.6, D, E). Interestingly, in comparison to *app<sup>tg</sup>ikbb<sup>fl/fl</sup>Cre<sup>-/-</sup>* mice, *app<sup>tg</sup>ikbb<sup>fl/fl</sup>Cre<sup>+/-</sup>* mice with IKK $\beta$  deficiency in myeloid cells visited the escaping area significantly more frequently and spent significantly more time there (Figure. 4.6, D, E).

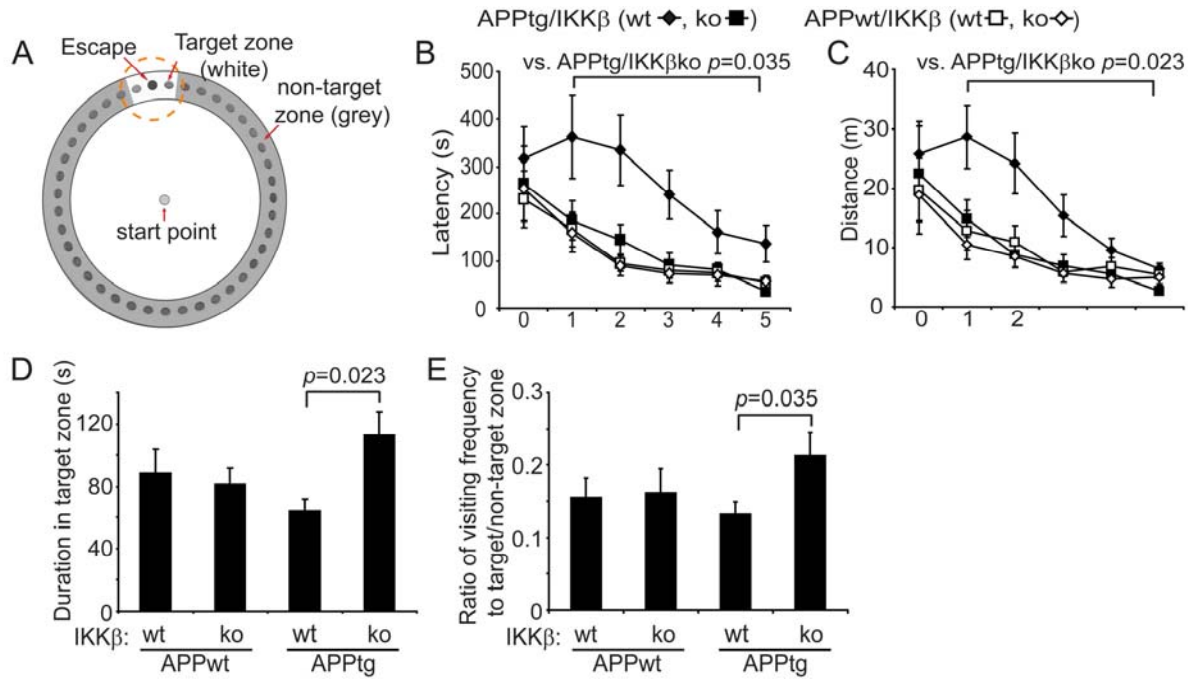


**Figure 4.6. Deficiency in IKK $\beta$  in myeloid cells improves cognitive function in APP-transgenic mice.** Schematic of the Barnes maze used (A). During the training phase, 6-month-old APP-transgenic mice (APPtg) spent more time in the maze and traveled longer distances to reach the escape hole than did their non-APP-transgenic littermates (APPwt). Ablation of IKK $\beta$  in myeloid cells (IKK $\beta$ ko) significantly reduced the traveling time and distance of APPtg mice but not of APPwt mice (B, C. Two-way ANOVA;  $n \geq 9$  per group). In the probe trial, APPtg/IKK $\beta$ ko mice remained in the target zone significantly longer and visited the escape hole more frequently than the APPtg/IKK $\beta$ wt mice (D, E. One-way ANOVA;  $n \geq 9$  per group).

Western blot analysis was also used to quantify the protein levels of PSD-95 (also known as disks large homolog 4) and pre-synaptic Munc18-1 in brain homogenates from 6-month-old APP-transgenic and wild-type littermate control mice. Both PSD-95 and Munc18-1 levels were markedly lower in *app<sup>tg</sup>ikbb<sup>fl/fl</sup>Cre<sup>-/-</sup>* mice than in their *app<sup>wt</sup>ikbb<sup>fl/fl</sup>Cre<sup>-/-</sup>* and *app<sup>wt</sup>ikbb<sup>fl/fl</sup>Cre<sup>+/-</sup>* littermates (Figure. 4.7; One-way ANOVA,  $p < 0.05$ ). Similarly, the amounts of PSD-95 and Munc18-1 proteins did not differ significantly between *app<sup>wt</sup>ikbb<sup>fl/fl</sup>Cre<sup>-/-</sup>* and *app<sup>wt</sup>ikbb<sup>fl/fl</sup>Cre<sup>+/-</sup>* mice (Figure. 4.7; One-way ANOVA,  $p > 0.05$ ). Interestingly, the reduction in PSD-95 and Munc18-1 proteins due to APP-transgenic expression was attenuated by the

deficiency of IKK $\beta$  in myeloid cells. The levels of PSD-95 and Munc18-1 proteins were significantly higher in brains from *app<sup>tg</sup>ikkbk<sup>fl/fl</sup>Cre<sup>+/-</sup>* mice than in brains from *app<sup>tg</sup>ikkbk<sup>fl/fl</sup>Cre<sup>-/-</sup>* control mice (Figure. 4.7; One-way ANOVA,  $p < 0.05$ ).

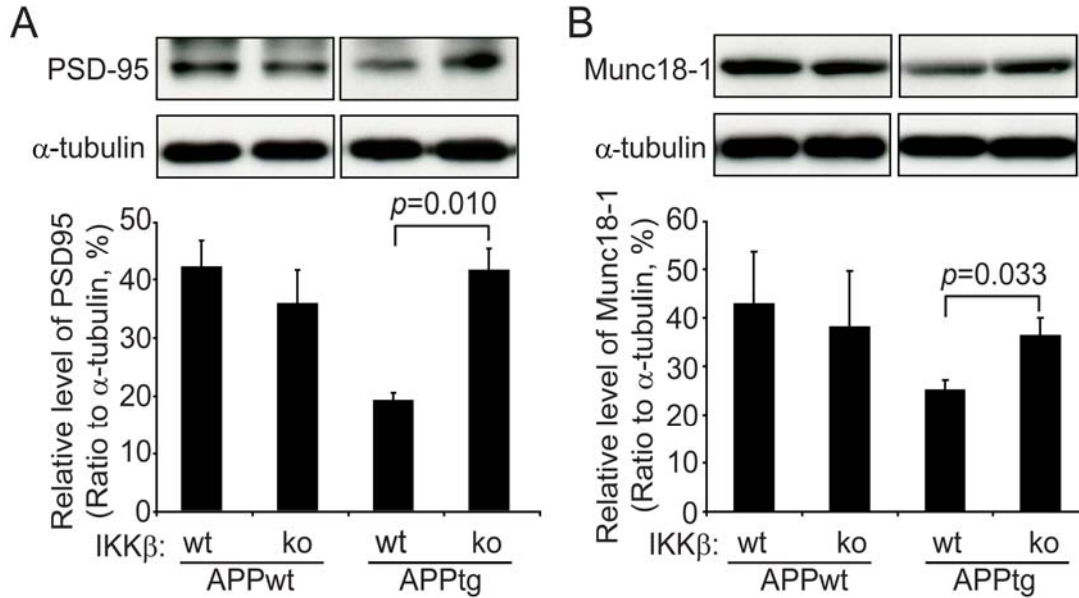


**Figure 4.7. Deficiency in IKK $\beta$  in myeloid cells attenuated synaptic protein loss in APP-transgenic mice.** The amount of PSD-95 and Munc18-1 in the brain homogenate was quantified with Western blotting (F, G). Deficiency in myeloid IKK $\beta$  was associated with a higher level of PSD-95 and Munc18-1 in the APPtg mouse but not in the APPwt mouse (One-way ANOVA;  $n \geq 6$  per group).

### 6.3 Deficiency of IKK $\beta$ in myeloid cells (microglia) reduces inflammatory activation in aged APP-transgenic mouse brains

Because proinflammatory activation contributes to AD pathogenesis, we investigated whether a deficiency of IKK $\beta$  in myeloid cells (microglia) might reduce inflammatory activity in the brain. We used the stereological technique to estimate the total number of Iba-1<sup>+</sup> cells, including microglia and potentially infiltrating brain macrophages, in the hippocampus and cortex of 6-month-old APP-transgenic and non-APP-transgenic mice with or without IKK $\beta$  expression in myeloid cells (*app<sup>tg</sup>ikkbk<sup>fl/fl</sup>Cre<sup>+/-</sup>*, *app<sup>tg</sup>ikkbk<sup>fl/fl</sup>Cre<sup>-/-</sup>*, *app<sup>wt</sup>ikkbk<sup>fl/fl</sup>Cre<sup>+/-</sup>* and *app<sup>wt</sup>ikkbk<sup>fl/fl</sup>Cre<sup>-/-</sup>* mice). The total number of Iba-1<sup>+</sup> cells was significantly higher in APP-transgenic mice than in non-APP-transgenic mice (Figure. 4.8, A, B, C; One-way ANOVA,  $p < 0.05$ ). The two groups of transgenic mice differed significantly in the total number of Iba-1<sup>+</sup> cells: *app<sup>tg</sup>ikkbk<sup>fl/fl</sup>Cre<sup>+/-</sup>* mice,  $20.46 \pm 0.70 \times 10^3$  cells in the hippocampus and  $23.74 \pm 0.86 \times 10^3$  cells in the cortex dorsal to the

hippocampus; *app<sup>tg</sup>ikbb<sup>fl/fl</sup>Cre<sup>-/-</sup>* mice,  $25.49 \pm 1.17 \times 10^3$  cells in the hippocampus and  $29.54 \pm 0.89 \times 10^3$  cells in the cortex dorsal to the hippocampus (Figure. 4.8, B, C; One-way ANOVA,  $p < 0.05$ ). However, there was no significant difference in the number of Iba-1<sup>+</sup> cells between the two groups of non-APP-transgenic mice (*app<sup>wt</sup>ikbb<sup>fl/fl</sup>Cre<sup>+/-</sup>* mice and *app<sup>wt</sup>ikbb<sup>fl/fl</sup>Cre<sup>-/-</sup>* mice; Figure. 4.8, B, C; One-way ANOVA,  $p > 0.05$ ).

We next investigated the mechanisms by which IKK $\beta$  deficiency decreases the number of Iba-1<sup>+</sup> cells. Because we had observed no significant difference between groups in the recruitment of monocyte-derived brain macrophages (Figure. 4.4), we evaluated endogenous microglial proliferation by costaining Iba-1 and Ki67, a cell-proliferation marker (Liu et al., 2013). Because there were too few cells, we could not use the stereological technique. As shown in Figure. 4.8, D, E, there were indeed significantly fewer double-positive cells in the hippocampus of *app<sup>tg</sup>ikbb<sup>fl/fl</sup>Cre<sup>+/-</sup>* mice ( $3.67 \pm 0.50$  cells per mm<sup>2</sup>) than in that of *app<sup>tg</sup>ikbb<sup>fl/fl</sup>Cre<sup>-/-</sup>* mice ( $5.53 \pm 0.77$  cells per mm<sup>2</sup>; *t* test,  $p < 0.05$ ).

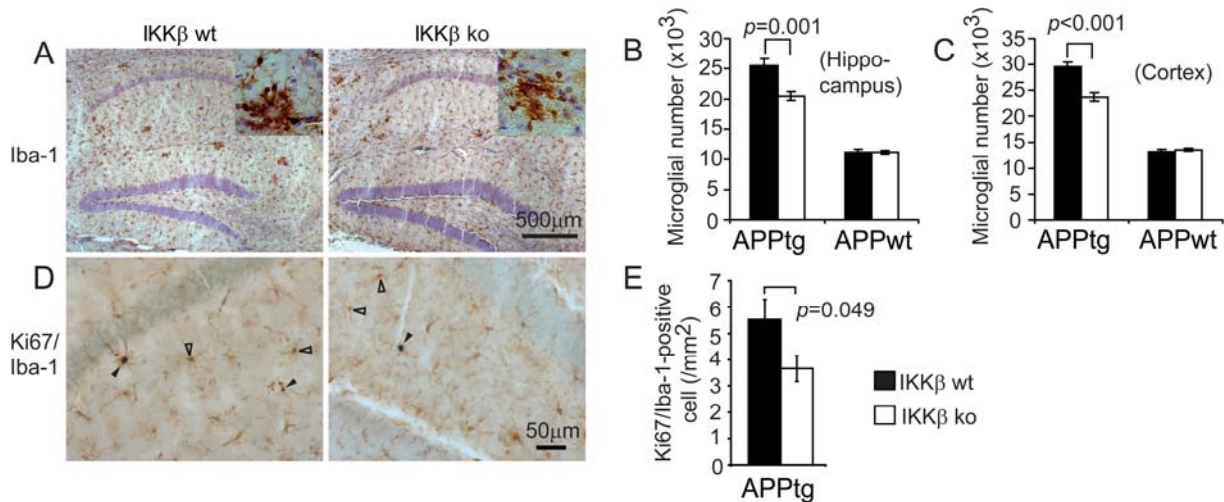


**Figure 4.8. Deficiency of IKK $\beta$  in myeloid cells reduces the number of microglia in APP-transgenic mice.** Six-month-old APP-transgenic mice (APPtg) and their non-APP-transgenic littermates (APPwt) were tested for inflammatory activation. Microglial cell numbers were estimated with stereological methods after immunohistochemical staining of Iba-1 (A, in brown). Proliferating microglia were identified by double staining of Iba-1 and Ki67, which appear in blue nucleus and brown cytoplasm (D, E, marked with closed arrowheads; pure Iba-1<sup>+</sup> cells are marked with open arrowheads).

We then used ELISA to quantify TNF- $\alpha$  protein levels in the TBS-soluble brain homogenate derived from 6-month-old APP-transgenic and non-transgenic mice and found that TNF- $\alpha$  production was significantly higher in APP mice than in their non-APP-transgenic littermates

(Figure. 4.9; One-way ANOVA,  $p < 0.001$ ). A deficiency in IKK $\beta$  in myeloid cells did not affect the levels of cerebral TNF- $\alpha$  protein in non-APP-transgenic mice (Figure. 4.9), but did significantly decrease levels of TNF- $\alpha$  protein in the brain of APP-transgenic mice, compared to littermate APP mice with wild-type IKK $\beta$  expression in myeloid cells (Figure. 4.9; One-way ANOVA,  $p = 0.002$ ).

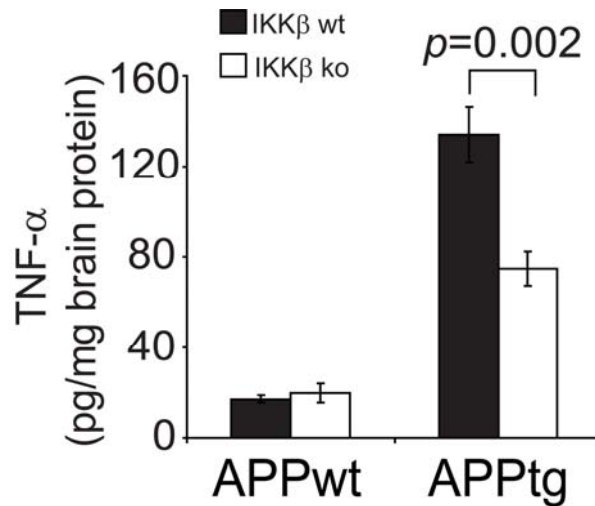


**Figure 4.9. Deficiency of IKK $\beta$  in myeloid cells decreased TNF- $\alpha$  protein level in the brains.** TNF- $\alpha$  protein concentration in brain homogenates derived from APPtg and APPwt mice was determined by ELISA (One-way ANOVA;  $n \geq 6$  per group).

We also quantified transcripts of M1-inflammatory gene markers (*tnf- $\alpha$* , *il-1 $\beta$* , *inos*, and *ccl2*) and M2-inflammatory gene markers (*il-10*, *mrc1*, *arg1*, and *chi3l3*) (Colton et al., 2006) in the brains of four separate groups of 6-month-old littermate mice (myeloid IKK $\beta$ : deficient [*ikkbk<sup>fl/fl</sup>Cre<sup>+/-</sup>*] and wild-type [*ikkbk<sup>fl/fl</sup>Cre<sup>-/-</sup>*] mice; APP-transgenic expression: positive [*app<sup>tg</sup>* mice] and negative [*app<sup>wt</sup>* mice]). As shown in Figure. 4.10, A, B, levels of *tnf- $\alpha$*  and *il-1 $\beta$*  transcripts were significantly higher in APP mice than in non-APP mice (One-way ANOVA,  $p < 0.05$ ). A deficiency in IKK $\beta$  in myeloid cells (microglia) completely abolished the transcriptional upregulation of *tnf- $\alpha$*  and *il-1 $\beta$*  by APP-transgenic expression (One-way ANOVA,  $p < 0.05$ ). In non-APP-transgenic mice, an IKK $\beta$  deficiency in myeloid cells did not change the transcription of *tnf- $\alpha$*  and *il-1 $\beta$*  genes (Figure. 4.10, A, B; One-way ANOVA,  $p > 0.05$ ). Neither the transcription of the other M1 genes (*inos* and *ccl2*) that we tested, nor the transcription of the M2 activation markers differed between myeloid IKK $\beta$ -deficient and wild-type APP-transgenic



or non-transgenic mice (Figure. 4.10, C-H). In an additional experiment, we isolated microglia and potential brain macrophages from 6-month-old APP-transgenic mice. We observed that transcription of the inflammatory gene *tnf- $\alpha$*  but not that of other proinflammatory and antiinflammatory genes was significantly lower in CD11b<sup>+</sup> cells isolated from *app<sup>tg</sup>ikbb<sup>fl/fl</sup>Cre<sup>+/-</sup>* mice than in cells from *app<sup>tg</sup>ikbb<sup>fl/fl</sup>Cre<sup>-/-</sup>* mice (Figure. 4.10, I; *t* test,  $p < 0.05$ ).

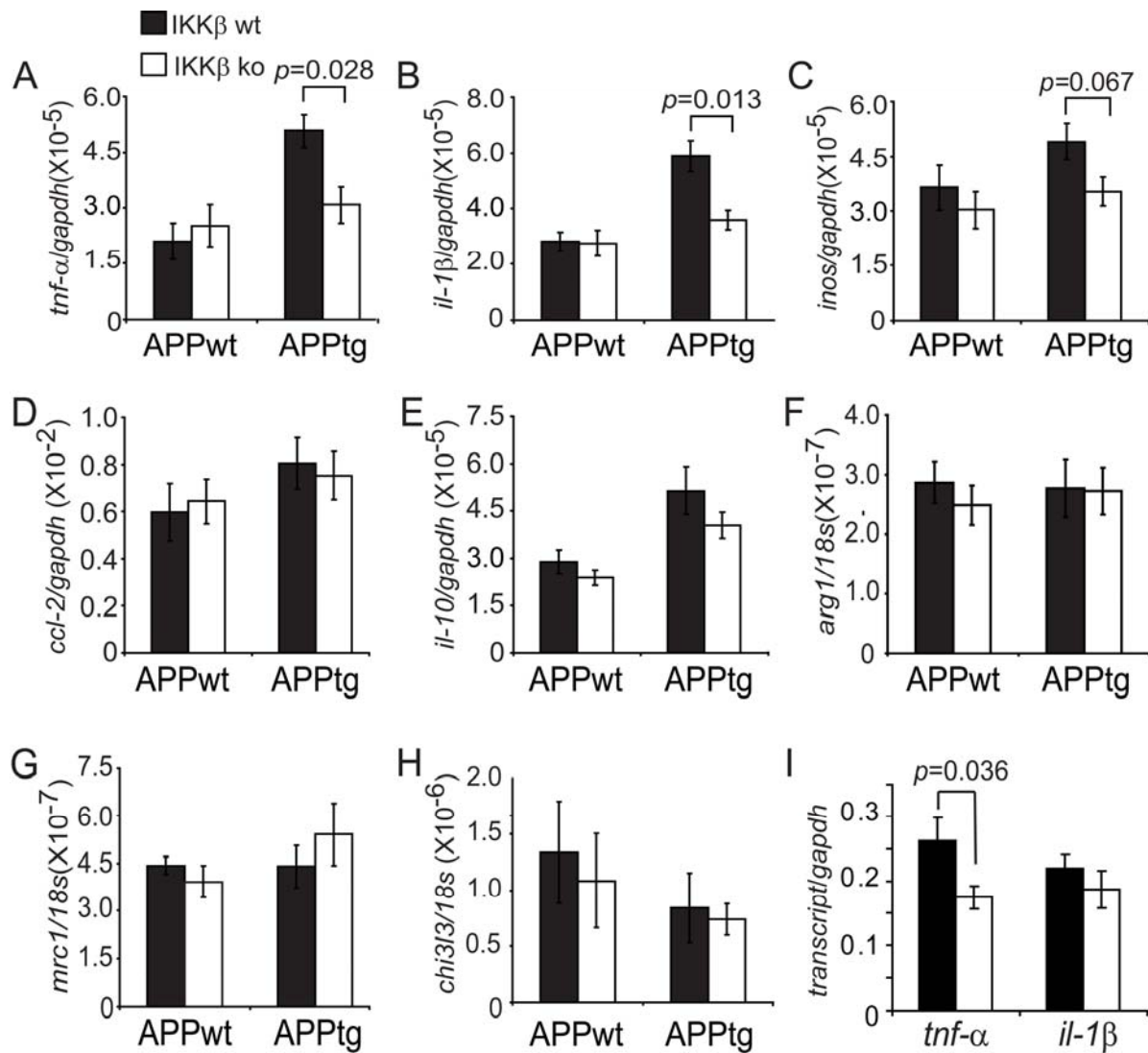


**Figure 4.10. Myeloid IKK $\beta$  deficiency reduces proinflammatory gene transcription in AD mouse brain.** Inflammatory gene transcripts in the brain (A-H) and in isolated microglia from 6-month-old APPtg mice (I) were measured by quantitative RT-PCR.

## 6.4 Deficiency of IKK $\beta$ in myeloid cells (microglia) reduces A $\beta$ load in aged APP-transgenic mouse brains

Because A $\beta$  pathology is considered to be the key mechanism mediating neuronal death in AD (Mucke and Selkoe, 2012), we continued to investigate the effects on the cerebral A $\beta$  load of IKK $\beta$  deficiency in myeloid cells. We separated brain homogenate from 6-month-old *app<sup>tg</sup>ikkb<sup>fl/fl</sup>Cre<sup>+/-</sup>* and *app<sup>tg</sup>ikkb<sup>fl/fl</sup>Cre<sup>-/-</sup>* mice into 3 $\times$  TBS-soluble, TBS-T-soluble, and guanidine chloride-soluble fractions according to our established protocols (Hao et al., 2011; Liu et al., 2012). Compared to *app<sup>tg</sup>ikkb<sup>fl/fl</sup>Cre<sup>-/-</sup>* mice, *app<sup>tg</sup>ikkb<sup>fl/fl</sup>Cre<sup>+/-</sup>* mice exhibited significantly lower concentrations of A $\beta$ 42 and A $\beta$ 40 in both TBS-T-soluble fractions and guanidine chloride-soluble fractions, which were enriched in oligomeric and high-molecular-weight aggregated A $\beta$  species (Hao et al., 2011) (Figure. 4.11; *t* test,  $p < 0.05$ ). Using the commercially available oligomeric A $\beta$  ELISA kit, we confirmed that the aggregated level of A $\beta$  ( $106.58 \pm 6.20$  pg per mg of wet brain tissue) in TBS-T-soluble brain homogenate from *app<sup>tg</sup>ikkb<sup>fl/fl</sup>Cre<sup>+/-</sup>* mice was significantly lower than that ( $130.52 \pm 6.20$  pg per mg of wet brain tissue) in homogenate from *app<sup>tg</sup>ikkb<sup>fl/fl</sup>Cre<sup>-/-</sup>* mice (*t* test,  $p = 0.036$ ). In the TBS-soluble brain homogenate fraction, which contained most of the monomeric A $\beta$  species (Hao et al., 2011), a deficiency in IKK $\beta$  in myeloid cells did not significantly affect A $\beta$  concentrations (Figure. 4.11; *t* test,  $p > 0.05$ ).

We used Congo red staining and immunohistochemical analysis to determine the A $\beta$  load in the brain. As shown in Figure. 4.12, A and C, the extent and morphology of the congophilic amyloid load or of antibody-labelled diffused A $\beta$  or A $\beta$  plaques with dense cores were not changed by a deficiency in IKK $\beta$  in the myeloid cell lineage. When we measured A $\beta$  volume (adjusted by the volume of analyzed tissues) with the stereological *Cavalieri* method (Gundersen and Jensen, 1987), we observed that, after ablation of IKK $\beta$  in myeloid cells, the volume of congophilic A $\beta$  load ( $0.074\% \pm 0.009\%$  in the hippocampus and  $0.143\% \pm 0.015\%$  in the cortex) was significantly reduced (to  $0.048\% \pm 0.006\%$  in the hippocampus [ $p = 0.038$ ] and  $0.095\% \pm 0.012\%$  in the cortex [ $p = 0.019$ ]) (Figure. 4.12, A, B; *t* test for relevant comparisons).



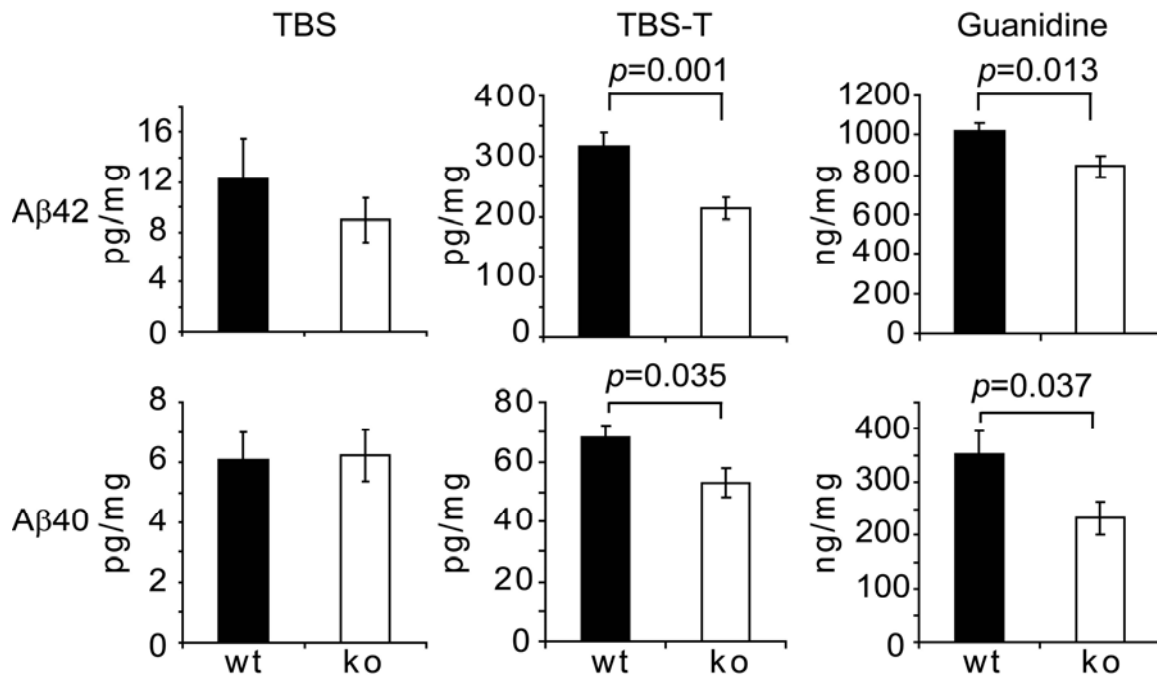


**Figure. 4.11. Deficiency of IKK $\beta$  in myeloid cells relieved A $\beta$  load in APP-transgenic mouse brain.** The brains of 6-month-old APP-transgenic (APPtg) mice were analyzed for A $\beta$  load. The brain was homogenized and separated into TBS, TBS-T and guanidine-soluble fractions. Amounts of A $\beta$ 40 and A $\beta$ 42 were measured by ELISA and normalized to the homogenate protein concentration. (*t* test; *n*=11 per group).

Similarly, the volume of immunoreactive A $\beta$  load was markedly higher in *app<sup>tg</sup>ikkb<sup>fl/fl</sup>Cre<sup>-/-</sup>* mice ( $2.687\% \pm 0.020\%$  in the hippocampus and  $2.801\% \pm 0.234\%$  in the cortex) than in *app<sup>tg</sup>ikkb<sup>fl/fl</sup>Cre<sup>+/-</sup>* mice ( $2.062\% \pm 0.152\%$  in the hippocampus [ $p=0.027$ ] and  $2.139\% \pm 0.178\%$  in the cortex [ $p=0.041$ ]) (Figure. 4.12, C, D; *t* test for relevant comparisons). Because Congo red typically binds to the  $\beta$  sheet structure of A $\beta$  plaques (Lorenzo and Yankner, 1994), we calculated the ratio of volumes of Congo red staining to volumes of immunohistochemical staining, which were not altered by the deficiency in myeloid IKK $\beta$  (Figure. 4.12, E; *t* test,  $p>0.05$ ), a fact suggesting that the ablation of myeloid IKK $\beta$  does not affect A $\beta$  aggregation. Furthermore, we quantified A $\beta$  deposits in the hippocampus and analyzed the distribution of their size. As shown in Figure. 4.12, F, IKK $\beta$  ablation in the myeloid cell lineage tended to shift A $\beta$  plaques from large to small, although the difference in the distribution of plaque size between IKK $\beta$ -deficient and wild-type mice was not statistically significant (Two-way ANOVA,  $p>0.05$ ).

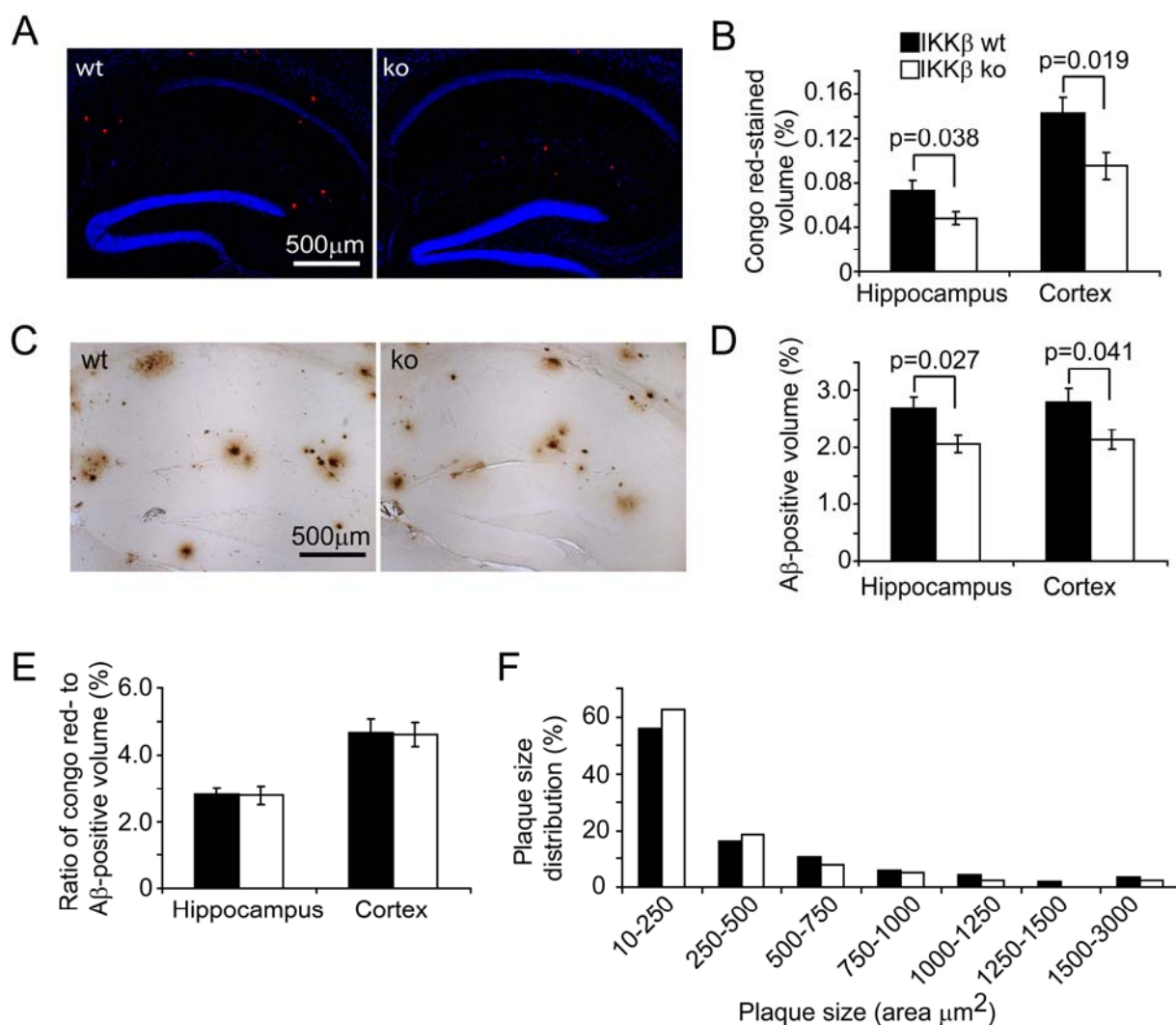


**Figure 4.12. Myeloid IKK $\beta$  deficiency reduces A $\beta$  plaque in APP-transgenic mouse brain.** The A $\beta$  volume in the whole hippocampus and cortex was estimated after both Congo red staining (A, B) and immunohistochemistry with human A $\beta$ -specific antibody (C, D) and adjusted by volumes of the relevant brain tissues. Myeloid IKK $\beta$  deficiency significantly reduces cerebral A $\beta$  load (*t* test; *n*=8 per group for Congo red staining and *n*=13 per group for immunohistochemistry). E. The ratio of Congo red-stained volume to A $\beta$ -immunohistochemically stained volume is calculated (*t* test; *n*=8 per group). F. The size of A $\beta$  plaque was measured and the frequency of A $\beta$  plaques with a certain size was showed as percentage of the total number of plaques (Two-way ANOVA, *p*>0.05; *n*=8 per wt or ko group).

## 6.5 Deficiency in IKK $\beta$ enhances microglial and macrophage recruitment toward A $\beta$ deposits and A $\beta$ internalization

Given that a deficiency in IKK $\beta$  in microglia reduced both inflammatory activation and A $\beta$  load in the APP-transgenic mouse brain, we hypothesized that IKK $\beta$  deficiency might enhance A $\beta$

clearance by internalization into microglia or macrophages. Because it is difficult to measure intracellular A $\beta$  directly in the brain, we first counted microglia and macrophages interacting with A $\beta$  deposits; we found that significantly more Iba-1<sup>+</sup> cells were recruited to the A $\beta$  deposits in *app<sup>tg</sup>ikkb<sup>fl/fl</sup>Cre<sup>+/-</sup>* mice than to the A $\beta$  deposits in their *app<sup>tg</sup>ikkb<sup>fl/fl</sup>Cre<sup>-/-</sup>* littermates (Figure. 4.13, A, B; *t* test, *p*=0.008), a finding in accordance with our previous findings in AD mice with a deficiency in MyD88 in myeloid cells (Hao et al., 2011). However, the amoeboid morphology of microglia surrounding A $\beta$  appeared not to be changed by myeloid IKK $\beta$  deficiency, when the IKK $\beta$ -deficient cells were tracked by Cre-mediated GFP expression (Figure. 4.13, C).

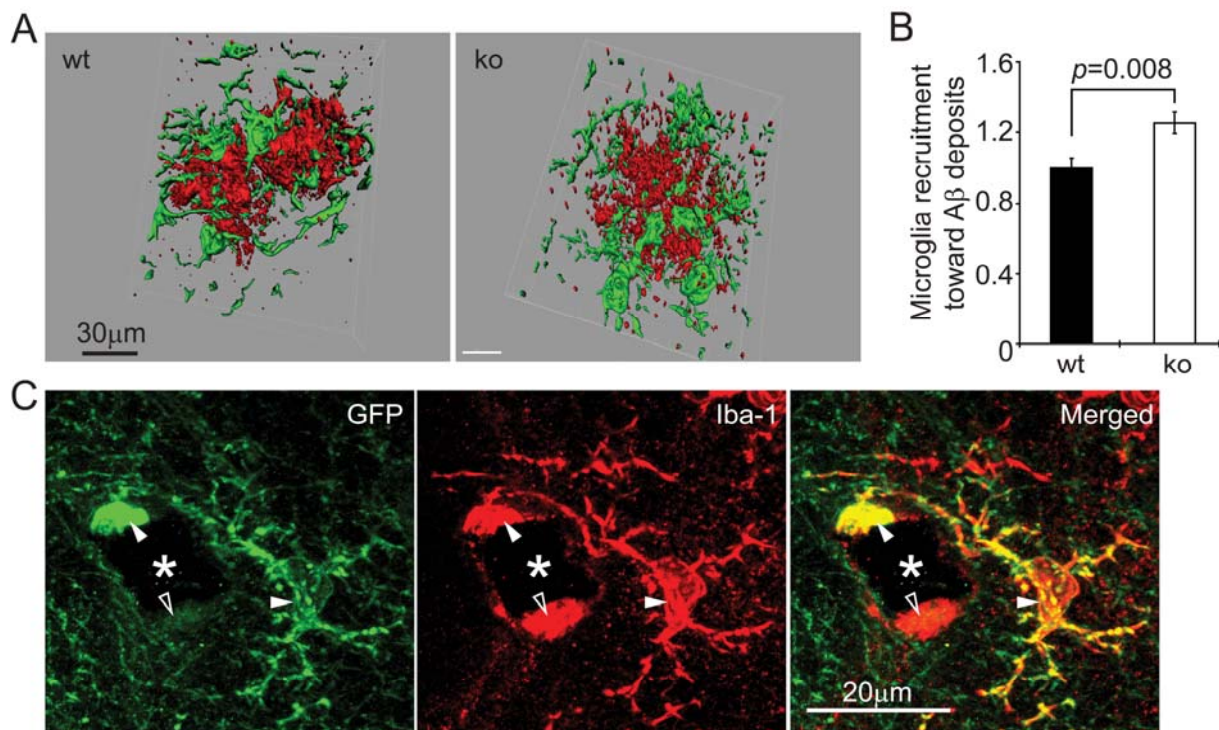


**Figure. 4.13. IKK $\beta$  deficiency increases microglial/brain macrophage recruitment toward A $\beta$  deposits in the APP-transgenic mouse brain.** The 6-month-old APP-transgenic (APPtg) mouse brain was analyzed for the interaction between A $\beta$  and microglia and brain macrophages under confocal microscopy after immunofluorescent staining with antibodies against A $\beta$  and Iba-1 (A. A $\beta$  in red and Iba-1 in green). The numbers of microglia and macrophages that colocalized with A $\beta$  were counted and adjusted by A $\beta$  volume. (*t* test; *n*=6 per group). C. IKK $\beta$ -ablated microglia and macrophages were tracked by GFP expression. After co-staining GFP in green and Iba-1 in red fluorescence, microglia and macrophages expressing both proteins appeared in yellow (closed arrowheads) and cells expressing Iba-1 alone were shown in red (open arrowhead). A $\beta$  plaques were stained in blue color in the bright field and appeared as black holes under confocal microscopy (marked with “\*”).

IKK $\beta$  deficiency also significantly upregulated the transcription of A $\beta$ -cleaning SRA (Frenkel et al., 2013) in the brains of APP-transgenic mice but not in the brains of their non-APP-transgenic

littermates (Figure. 4.14 A; One-way ANOVA,  $p < 0.05$ ). CD36 transcription was lower in *app<sup>tg</sup>ikkb<sup>fl/fl</sup>Cre<sup>-/-</sup>* mice than in *app<sup>wt</sup>ikkb<sup>fl/fl</sup>Cre<sup>-/-</sup>* littermate controls (Figure. 4.14 B; One-way ANOVA,  $p < 0.05$ ), a finding consistent with the observations of El Khoury's group (Hickman et al., 2008). Interestingly, a deficiency in IKK $\beta$  in microglia was associated with the complete recovery of CD36 expression in the brains of APP-transgenic mice (Figure. 4.14, B; One-way ANOVA,  $p < 0.05$ ) but had no effects on CD36 transcription in non-APP-transgenic mice (Figure. 4.14, B; One-way ANOVA,  $p > 0.05$ ).

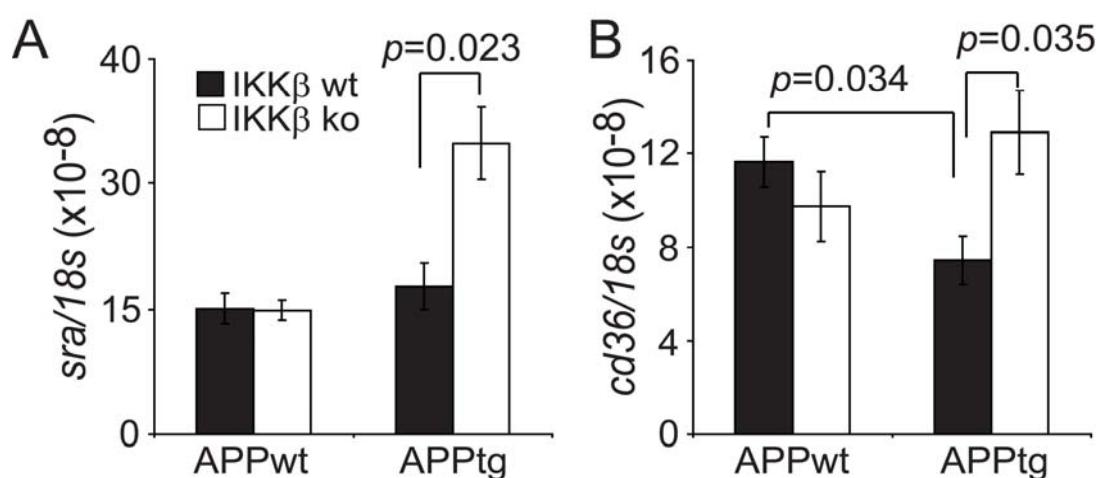


**Figure. 4.14. IKK $\beta$  deficiency enhances cerebral expression of A $\beta$ -interacting receptors.** The transcription of scavenger receptor *A* (*sra*) and *cd36* was measured with quantitative RT-PCR and was upregulated by myeloid IKK $\beta$  deficiency in APPtg mouse brains but not in APP-wildtype (APPwt) mouse brains (A, B. One-way ANOVA;  $n \geq 9$  per group).

In further experiments, we challenged primary cultured microglia with HiLyte Fluor 488-labelled A $\beta$ 42 enriched in oligomeric and fibrillar species (Figure. 4.15, A) to model the A $\beta$  species in TBS-T-soluble and guanidine-soluble brain homogenates. When microglia were treated with aggregated A $\beta$  at a concentration of 1  $\mu$ M, internalization was detectable within 1 hour, and levels of internalized A $\beta$  increased as the incubation time increased (Figure. 4.15, B, C). Significantly more oligomeric A $\beta$ 42 than fibrillar A $\beta$ 42 was internalized by microglia (with or without IKK $\beta$  expression), as measured by mFI (Figure. 4.15, B; Two-way ANOVA,  $p < 0.001$ ). After cells were incubated with A $\beta$ 42 for 3 hours, the mFI of cells treated with A $\beta$  oligomers decreased more quickly than did that of microglia treated with A $\beta$  fibrils. This difference could be due to the difference in the efficiency of degradation and extracellular release

between A $\beta$  oligomers and fibrils in microglia (Chung et al., 1999; Yamamoto et al., 2008). Comparison of the internalizing capability of IKK $\beta$ -deficient and wild-type microglia showed that IKK $\beta$  deficiency significantly increased the uptake of A $\beta$ 42 oligomers at a concentration of 1  $\mu$ M but not of A $\beta$  fibrils. This difference remained when A $\beta$ 42 treatment was extended to 24 hours (Figure. 4.15, B, C; Two-way ANOVA,  $p < 0.001$ ). Interestingly, when microglia were treated with oligomeric A $\beta$ 42 at a concentration of 0.2  $\mu$ M, IKK $\beta$  deficiency did not enhance A $\beta$  internalization (Figure. 4.15, B, C; Two-way ANOVA,  $p > 0.05$ ). Similar results were seen in internalization assays with bone marrow-derived macrophages, in which IKK $\beta$ -deficient macrophages showed a significantly higher uptake of A $\beta$  than IKK $\beta$ -wild-type macrophages when cells were treated with oligomeric A $\beta$ 42 at concentrations of 1 or 10  $\mu$ M. This A $\beta$  internalization enhanced by IKK $\beta$  deficiency disappeared when oligomeric A $\beta$ 42 was administered at a concentration of 0.5  $\mu$ M or when fibrillar A $\beta$ 42 was administered at a concentration of 1  $\mu$ M.

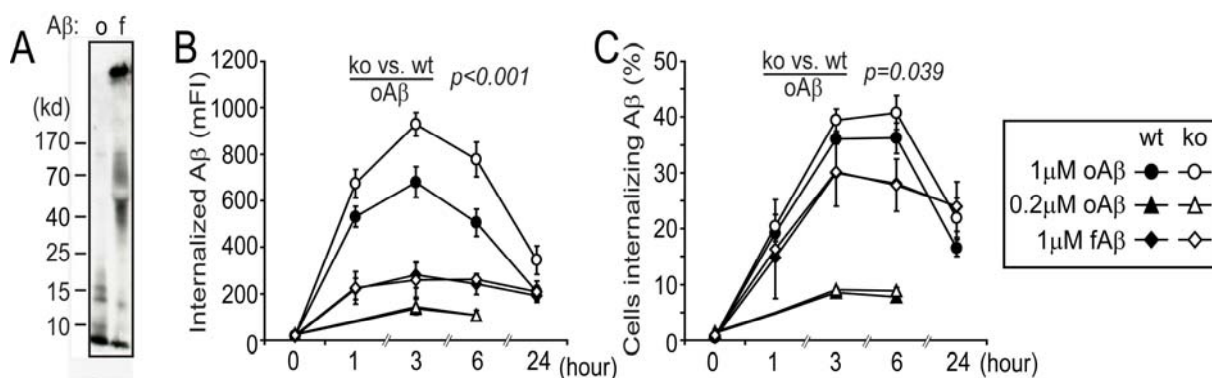


**Fig. 4.15. IKK $\beta$  deficiency enhances internalization of oligomeric A $\beta$ 42 in microglia.** **A.** Aggregating patterns (o, oligomeric; f, fibrillar) of HiLyte Fluor 488-labelled A $\beta$ 42. **B, C.** Line curves showing the internalization of 1 or 0.2  $\mu$ M oligomeric A $\beta$ 42 (oA $\beta$ ) and 1  $\mu$ M fibrillar A $\beta$ 42 (fA $\beta$ ) by primary cultured microglia derived from IKK $\beta$ -ablated (IKK $\beta$ ko) and wild-type (IKK $\beta$ wt) mice for various time periods (Two-way ANOVA;  $n = 3$  per group). **D, E.** Histograms show the inflammatory gene transcripts in primary microglia 6 hours after the A $\beta$  internalization ( $t$ -test;  $n \geq 6$  per group).

To determine whether elevated inflammatory activation might be inversely related to the internalization of A $\beta$  into microglia (Hao et al., 2011; Liu et al., 2012), we performed two additional experiments. First, we analyzed the pathological changes in 3-month-old APP-transgenic mice with or without IKK $\beta$  ablation in myeloid cells as controls for the 6-month-old AD mice that we described above. A deficiency in myeloid IKK $\beta$  neither changed cerebral

transcripts of *tnf- $\alpha$* , *il-1 $\beta$* , and *inos* genes nor altered A $\beta$  concentrations in all TBS-soluble, TBS-T-soluble, and guanidine chloride-soluble brain homogenate fractions (Figure. 4.16, A, B). Second, we measured the inflammatory activation of cultured microglia during internalization of A $\beta$  over a 6-hour interval. As shown in Figure. 4.17, A, B, IKK $\beta$ -deficiency significantly suppressed inflammatory gene (e.g., *tnf- $\alpha$*  and *il-1 $\beta$* ) transcription triggered by oligomeric A $\beta$  at a concentration of 1  $\mu$ M (Two-way ANOVA,  $p < 0.05$ ). Microglial inflammatory gene transcription was not significantly induced by fibrillar A $\beta$ 42 at a concentration of 1  $\mu$ M (Figure. 4.17, A, B; Two-way ANOVA,  $p > 0.05$ ).

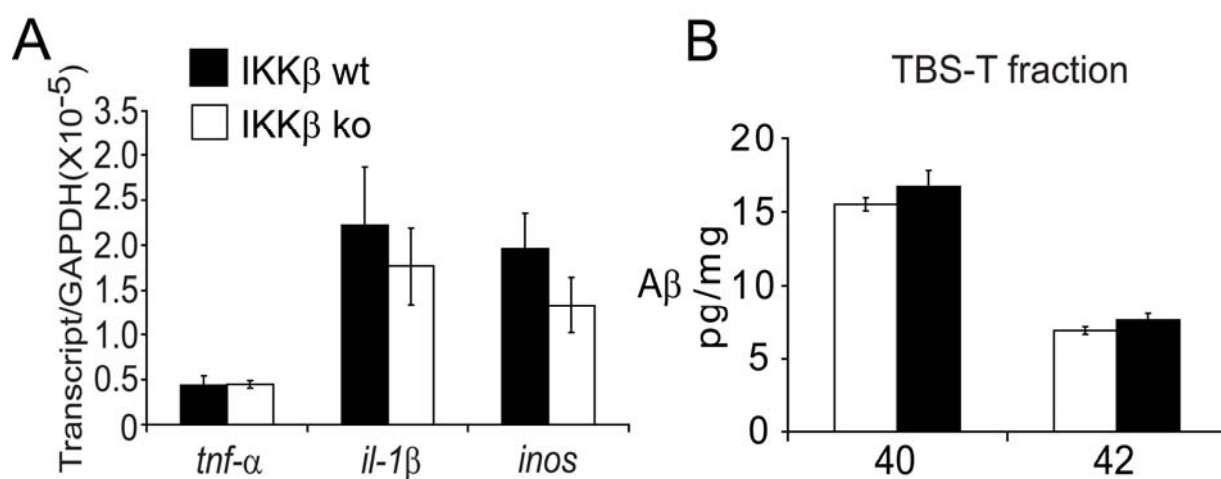


**Figure. 4.16. IKK $\beta$  deficiency neither changes proinflammatory gene transcription nor alters A $\beta$  load in 3-month-old mice.** The brains of 3-month-old APP-transgenic (APPTg) mice were analyzed for proinflammatory gene transcription (A) and A $\beta$  load (B).

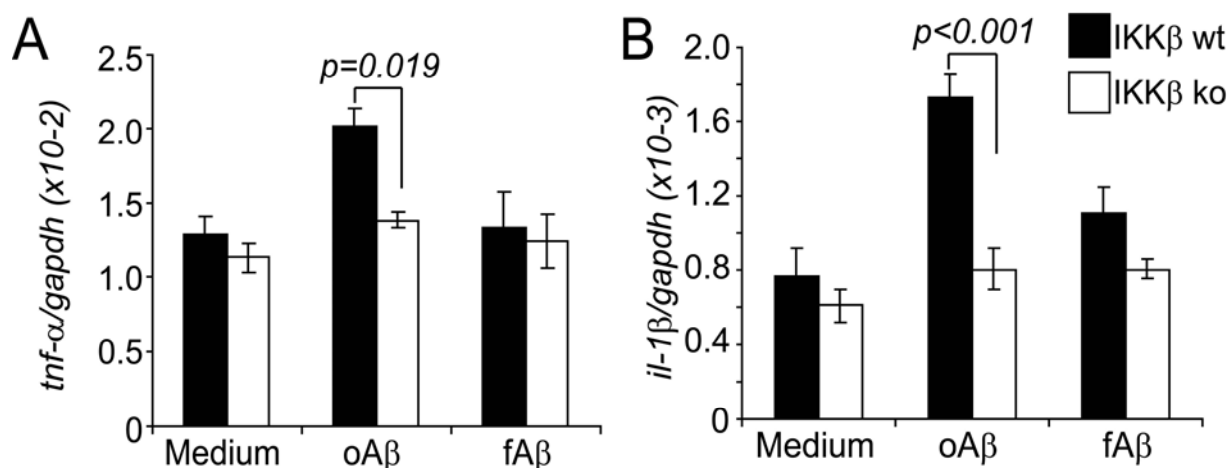


**Figure. 4.17. IKK $\beta$  deficiency reduces oligomeric A $\beta$ -induced inflammatory genes expression in microglia.** Primary culture microglia derived from wild-type (wt) and IKK $\beta$  deficiency (ko) mice were challenged with 1  $\mu$ M oligomeric and fibrillar A $\beta$ 42 for 6 hours. The gene transcriptions of *tnf- $\alpha$*  (A) and *il-1 $\beta$*  (B) were detected by RT-PCR.



---

## 6.6 Inhibition of TGF- $\beta$ –SMAD2/3 signaling could be involved in microglial A $\beta$ internalization enhanced by IKK $\beta$ deficiency

Because it has been reported that blocking either CD40 or the TGF- $\beta$  signaling cascade in AD mice leads to a reduction in both inflammatory activation and A $\beta$  load in the brain (Tan et al., 1999 and 2002; Town et al., 2008), the same phenomenon we observed in myeloid IKK $\beta$ –deficient AD mice, we decided to investigate whether IKK $\beta$  modulates CD40 and TGF- $\beta$  signaling. Indeed, a deficiency in myeloid IKK $\beta$  significantly decreased transcription levels of TGF- $\beta$  receptor types 1 and 2 (*tgfb-r1* and *-r2*) in microglia isolated from APP-transgenic mice (Figure. 4.18, B; *t* test,  $p < 0.05$ ), although IKK $\beta$  deficiency did not change the transcription level of these two receptors or of TGF- $\beta$ 1 in the entire brain (Figure. 4.18, A; *t* test,  $p > 0.05$ ). In cultured microglia, IKK $\beta$  deficiency reduced *tgf- $\beta$ 1* transcription at the basal level and reduced both *tgf- $\beta$ 1* and *tgfb-r1* transcription after challenge with oligomeric A $\beta$ 42 at a concentration of 1  $\mu$ M (Figure. 4.18, C; *t* test,  $p < 0.05$ ). Notably, we observed that IKK $\beta$  deficiency inhibited SMAD2 phosphorylation but did not change SMAD5 phosphorylation in microglia in response to stimulation with TGF- $\beta$ 1 at a concentration of 1 or 10 ng/mL (Figure. 4.18, D, E, F; Two-way ANOVA). However, CD40 gene transcription was not changed by IKK $\beta$  deficiency in either adult or cultured microglia.

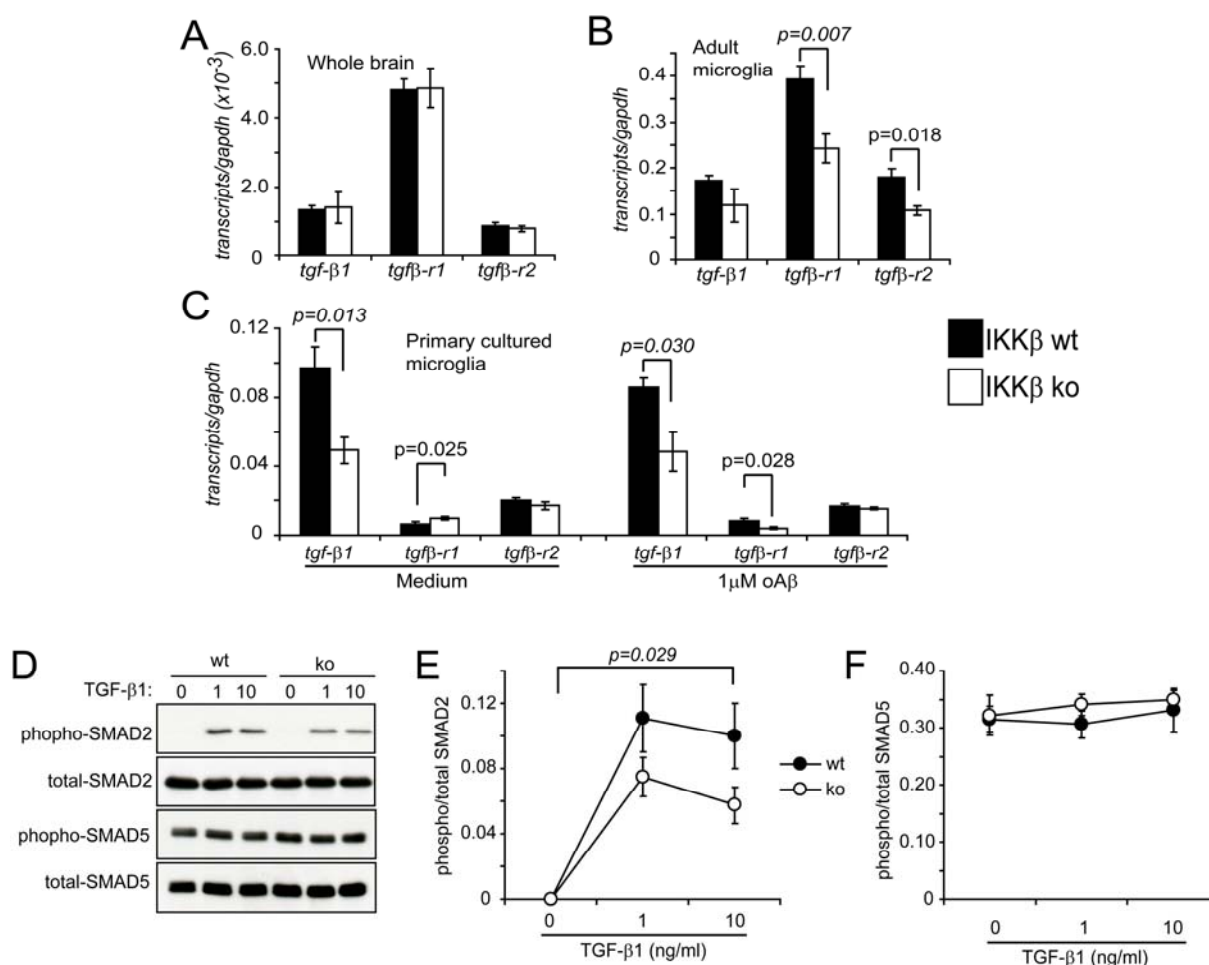


**Figure. 4.18. IKKβ deficiency blocks TGF-β-SMAD2/3 signal pathway.** A-C, Transcripts of *tgf-β1*, *tgfβ-r1* and *r2* genes in the entire hippocampus and cortex, in adult microglia isolated from APP-transgenic mice and in cultured primary microglia with and without treatment of 1μM oAβ were measured using real-time PCR (*t* test;  $n \geq 5$  per group). Primary cultured IKKβwt and IKKβko microglia were activated with TGF-β1 at 0, 1 and 10ng/ml for 30 minutes. After stimulation, the phosphorylated and total SMAD2 and SMAD5 proteins were detected by Western blotting (D-F). The ratios of phospho-/total SMAD2 and SMAD5 reflect SMAD2/3 and SMAD1/5/8 signaling.

Thereafter, whether Aβ internalization in microglia was increased by blockade of TGF-β-SMAD2/3 signaling was tested, as Town's group reported (Town et al., 2008). Two ALK-5 inhibitors, SB-505124 and SB-431542, at concentrations of 1 and 10 μM, had been shown to inhibit both SMAD2/3 and SMAD1/5/8 signaling in response to exogenous TGF-β1 activation (Town et al., 2008). We observed that both SB-505124 and SB-431542 at concentrations of 0.1 and 0.02 μM reduced SMAD2 phosphorylation but did not markedly affect SMAD5 phosphorylation in microglia after the same challenge with TGF-β1 (Figure. 4.19, A). This partial inhibition was comparable to the inhibition caused by IKKβ deficiency, as described



above. Interestingly, the inhibitor-treated cultured microglia internalized significantly more oligomeric A $\beta$ 42 aggregates, in a dose-dependent manner, than did the microglia without special treatment (Figure. 4.19, B, C; Two-way ANOVA,  $p < 0.05$ ). The concentrations that promoted A $\beta$  internalization were between 0.5  $\mu$ M and 20 nM; the maximal effect was induced by a concentration of 20 nM (Figure. 4.19, B, C; Two-way ANOVA followed by *post-hoc* tests,  $p < 0.05$ ). At higher and lower concentrations (1  $\mu$ M and 4 nM, respectively), the inhibitors failed to promote A $\beta$  internalization.

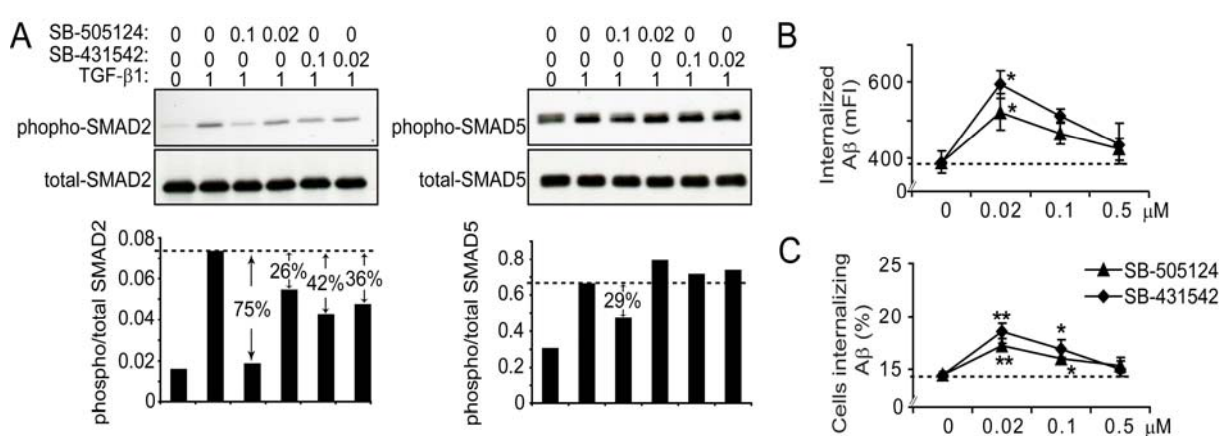


**Figure. 4.19. Blockade of TGF- $\beta$ -SMAD2/3 signal increases A $\beta$  internalization in microglia.** Primary cultured IKK $\beta$ wt microglia were treated with SB-505124 and SB-431542 at 0, 0.02 and 0.1  $\mu$ M and then with 1 ng/ml TGF- $\beta$ 1 for 30 minutes (A). B, C. IKK $\beta$ wt microglia were pre-treated with SB-505124 and SB-431542 at 0, 0.02 and 0.1  $\mu$ M for 1 hour and then incubated with 1  $\mu$ M fluorescent oA $\beta$  for 6 hours in the presence of inhibitors. The internalization of oA $\beta$  was assayed with flow cytometry (Two-way ANOVA followed by *post-hoc* tests, \*:  $p < 0.05$  and \*\*:  $p < 0.01$  vs. the A $\beta$  internalization without inhibitor treatment;  $n = 4$  per group).

## 6.7 Deficiency in IKK $\beta$ in myeloid cells does not increase A $\beta$ clearance through brain-to-blood transportation

Deane and colleagues (2004) reported that altered communication of A $\beta$  between the brain interstitial fluid and the peripheral bloodstream affects cerebral A $\beta$  load (Deane et al., 2004). Peripheral myeloid cells could clear A $\beta$  in the perivascular area so as to reduce A $\beta$  deposition in the parenchyma (Hawkes and McLaurin, 2009; Mildner et al., 2011). Neither the volume of A $\beta$  that was deposited in the blood vessels nor the number of vessels that tested positive for A $\beta$  deposits differed between myeloid IKK $\beta$ -deficient and wild-type APP-transgenic mice was observed (Figure. 4.20, A, B, C;  $t$  test,  $p > 0.05$ ). We also measured A $\beta$  levels in the plasma and

the expression of RAGE and LRP1 in the brain, two receptors that act as shuttles to transport A $\beta$  across the blood-brain barrier (Deane et al., 2003 and 2004). As shown in Figure. 9, neither plasma A $\beta$ 40 and A $\beta$ 42 concentrations in APP-transgenic mice (Figure. 4.20, F) nor receptor expression in APP-transgenic and non-transgenic mouse brains (Figure. 4.20, D, E) was affected by IKK $\beta$  deficiency in myeloid cells (*t* test,  $p > 0.05$ ).

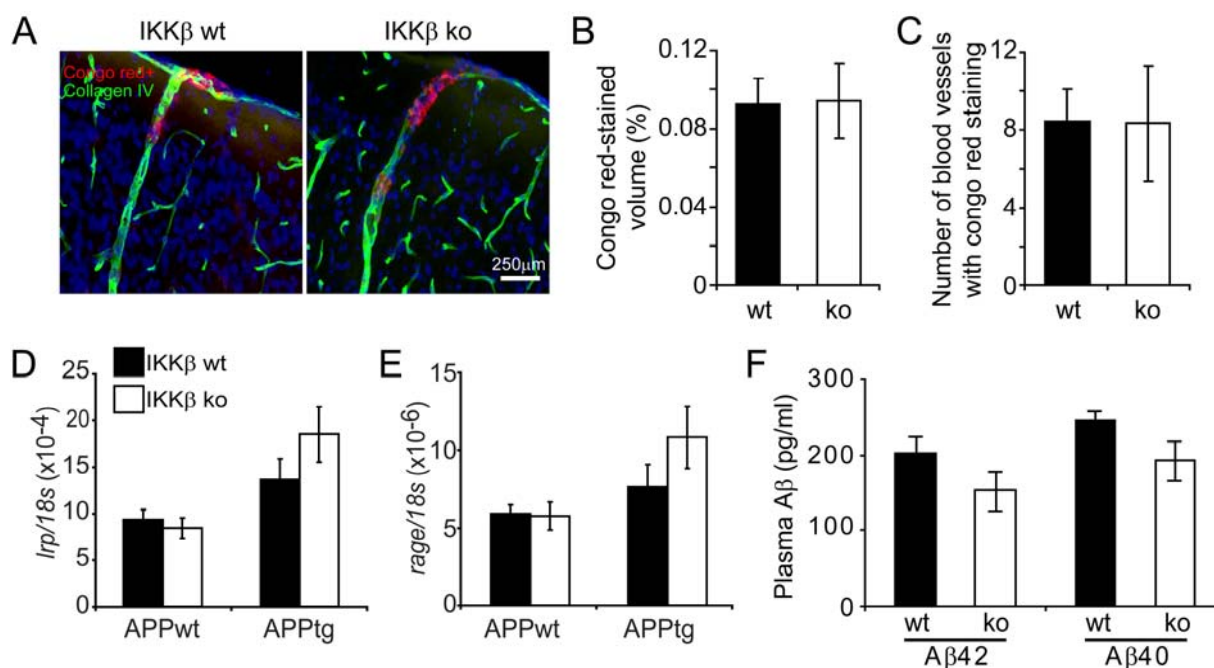


**Figure. 4.20. Deficiency of IKK $\beta$  in myeloid cells does not increase A $\beta$  clearance through brain-to-blood transportation.** The 6-month-old APP-transgenic (APPtg) and non-APP-transgenic (APPwt) littermate mice with (IKK $\beta$ ko) and without IKK $\beta$  ablation (IKK $\beta$ wt) in myeloid cells were analyzed for cerebral vascular A $\beta$  deposits after tissues were costained with Congo red and collagen type IV antibodies (A-C), and for transcription of *lrp1* and *rage* in the brain with quantitative RT-PCR (D, E). Concentrations of A $\beta$ 40 and A $\beta$ 42 in the plasma from IKK $\beta$ ko and IKK $\beta$ wt APPtg mice were quantified by ELISA (F).

## 6.8 Deficiency in IKK $\beta$ in myeloid cells does not reduce amyloidogenic APP metabolism

To explore whether IKK $\beta$  deficiency in myeloid cells affects A $\beta$  production in APP-transgenic mice, we measured the activities of  $\beta$ -secretase and  $\gamma$ -secretase, the two main enzymes that cleave APP to produce A $\beta$  (Mucke and Selkoe, 2012). Surprisingly, neither  $\beta$ -secretase activity nor  $\gamma$ -secretase activity was changed by IKK $\beta$  deficiency (Figure. 4.21, A, B).

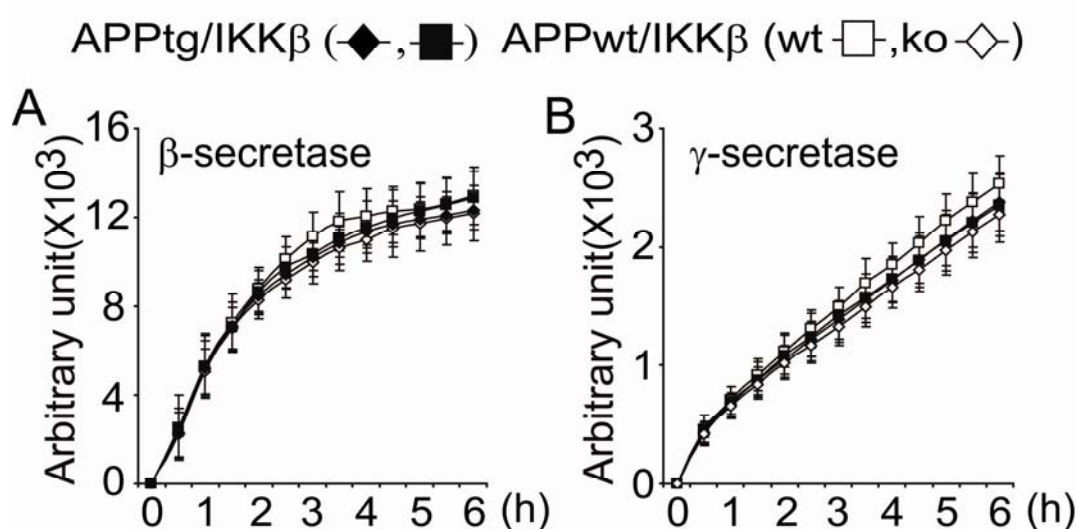


**Figure. 4.21, Deficiency of microglial IKK $\beta$  does not affect  $\beta$ - and  $\gamma$ -secretase activity in APP-transgenic mouse brain.** Membrane components were prepared from 6-month-old microglial IKK $\beta$ -deficient (ko) and wildtype (wt) APP-transgenic (APPtg) and non-APP transgenic (APPwt) littermate mice.  $\beta$ - and  $\gamma$ -secretase activity was determined by incubating membrane components with fluorogenic  $\beta$ - and  $\gamma$ -secretase substrates (two-way ANOVA shows no difference between different mouse groups,  $p > 0.05$ ,  $n \geq 6$  per group).

## 6.9 Deficiency in IKK $\beta$ in myeloid cells does not increase A $\beta$ clearance through endogenous degradation

Quantitative RT-PCR investigation of the A $\beta$ -degrading enzyme neprilysin and the insulin-degrading enzyme (Leissring et al., 2003; Miners et al., 2008) showed no significant increase in the transcription of *nep* and *ide* genes in *app<sup>tg</sup>ikkb<sup>fl/fl</sup>Cre<sup>+/-</sup>* mice compared to *app<sup>tg</sup>ikkb<sup>fl/fl</sup>Cre<sup>-/-</sup>* littermate controls (Figure. 4.22, A, B), a finding suggesting that microglial IKK $\beta$  deficiency has no effect on A $\beta$  catabolism.

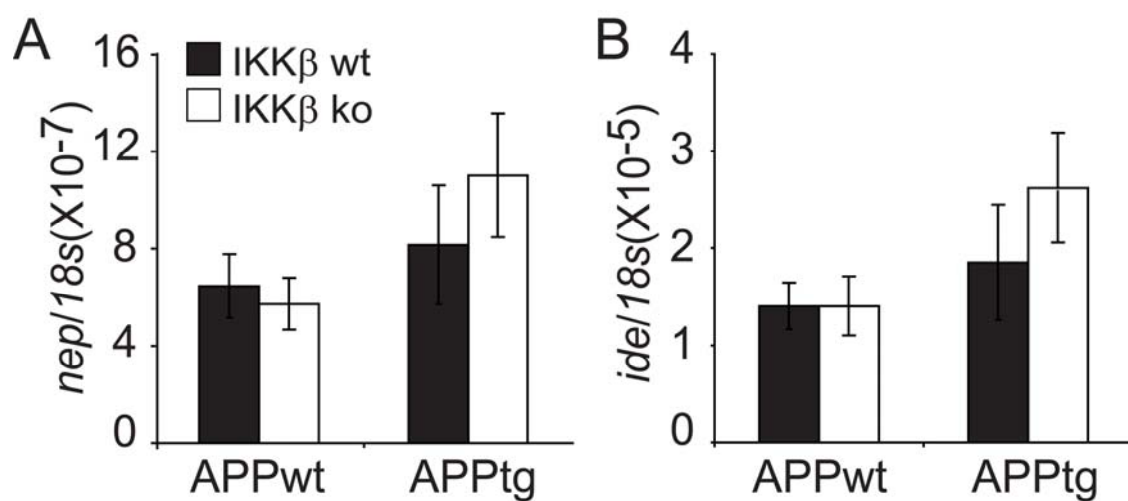


**Figure. 4.22, Deficiency of microglial IKK $\beta$  does not change gene transcriptions of A $\beta$ -degrading enzymes in APP-transgenic mouse brain.** The transcripts of *neprilysin* (*nep*) and *insulin degrading enzyme* (*ide*) genes were quantified by real-time PCR (t-test,  $p > 0.05$ , between IKK $\beta$ ko and IKK $\beta$ wt mice,  $n \geq 9$  per group).

## 7 DISCUSSION

AD is a progressive neurodegenerative disorder and the most common form of dementia, which is characterized by A $\beta$  deposits, hyperphosphorylated tau-composed neurofibrillary tangle and microglia activation. Emerging evidences have suggested that microglia act as a double-edged sword in AD pathogenesis: on one side, they contribute to neuronal death by secreting inflammatory mediators; and on the other side, they clear neurotoxic A $\beta$  to prevent AD progression. Innate immune signaling cascade, *e.g.* TLRs-MyD88-NF- $\kappa$ B, regulate the inflammatory mediators, and modify AD pathogenesis (Tahara et al., 2006; Reed-Geaghan et al., 2010; Hao et al., 2011; Lim et al., 2011; Michaud et al., 2011 and 2012; Song et al., 2011; Cameron et al., 2012; Liu et al., 2012). However, the net effect of microglial activation in AD is still unclear. The mechanism switching between detrimental and beneficial effects need to be understood. In this study, we demonstrated that a deficiency in IKK $\beta$  in myeloid cells, especially in endogenous microglia, simultaneously reduces inflammatory activation and A $\beta$  load in the brain and improves cognitive function in AD mice. These findings corroborate the results of our earlier studies of the deficiency of myeloid TLR2 or MyD88 in APP-transgenic mice (Hao et al., 2011; Liu et al., 2012).

### 7.1 IKK $\beta$ was specifically deleted in myeloid cells of APP-transgenic mice

To the best of our knowledge, we were the first to use the Cre-Lox technique in cross-breeding experiments to conditionally delete the protein of interest in APP-transgenic mice. This deletion allows us to investigate in detail the functions of this protein in AD pathogenesis in a specific tissue and within a certain time frame. We investigated IKK $\beta$  in microglia by specifically ablating IKK $\beta$  in myeloid cells of APP-transgenic mice, thereby excluding any confounding effects from neuronal IKK $\beta$ . Neuronal IKK $\beta$  has been reported to activate neuronal NF- $\kappa$ B, thus modifying A $\beta$  generation and the degeneration and plasticity of neurons (He et al., 2007; Kaltschmidt and Kaltschmidt, 2009; Gutierrez and Davies, 2011; Zhang et al., 2013; Jun et al., 2013).

However, in my AD mouse model, the *ikkb* gene was deleted not only in endogenous microglia but also in peripheral myeloid cells (Clausen et al., 1999; Goldmann et al., 2013). One subset of

myeloid cells potentially circulates to the brain parenchyma and serves as brain macrophages (Hao et al., 2011). In our APP-transgenic mouse brains we observed a small population of CD45<sup>+</sup> cells whose distribution was localized within one brain region instead of around most A $\beta$  deposits, a finding indicating that these cells are not activated endogenous microglia. These CD45<sup>+</sup> cells are also neither neutrophils nor T lymphocytes, because they do not express neutrophil or CD3 markers. Thus, this cell population may be brain macrophages. Surprisingly, the number of CD45<sup>+</sup> cells in this population is very limited (<2% of Iba-1<sup>+</sup> cells, as estimated on the basis of our observations (Hao et al., 2011; Liu et al., 2012; Xie et al., 2013). Moreover, flow cytometry showed that approximately 2% of CD11b<sup>+</sup> brain cells are CD45<sup>+</sup> not only in IKK $\beta$ -deficient and wild-type APP-transgenic mice but also in non-APP-transgenic mice. Thus, the recruitment of potential brain macrophages appears to be independent of neuroinflammatory status and of IKK $\beta$  expression in AD mice.

Brain macrophages have been shown to originate from CCR2<sup>+</sup> monocytes (Mildner et al., 2007; Varvel et al., 2012). In another APP-transgenic mouse model, one allele of the *ccr2* gene was replaced by the RFP-encoding sequence, whereas the other allele expressed CCR2 to exert full cellular physiological function. In this model, recruitment of brain macrophages in AD mice is limited. APP-transgenic mouse brains that have not been preconditioned by irradiation are devoid of parenchymal peripherally infiltrated macrophages (Mildner et al., 2011; Kierdorf et al., 2013), a condition that makes it unlikely that IKK $\beta$ -ablated brain macrophages can affect A $\beta$  pathology in the brain parenchyma.

In the perivascular area, peripheral myeloid cells can interact with A $\beta$  and modify the cerebral A $\beta$  load (Hawkes and McLaurin, 2009; Mildner et al., 2011). In my AD mouse models, neither the concentration of plasma A $\beta$  (especially A $\beta$ 42) and TNF- $\alpha$  nor the volume of A $\beta$  deposited in the blood vessels was changed by the ablation of IKK $\beta$  in the myeloid cells. Thus, although the effects of peripheral myeloid cells on A $\beta$  pathology cannot be completely excluded, the anti-AD phenotype observed in our study appears to result primarily from a deficiency in IKK $\beta$  in the endogenous microglia.

## 7.2 Myeloid deficiency of IKK $\beta$ reduces neuroinflammation in the brain

A $\beta$  is currently believed to be the key molecule in the pathogenesis of AD, due to its role as a trigger of chronic neuroinflammation (Akiyama et al., 2000; Latta et al., 2014). In AD animal models, which over-express human APP, microglia are observed to be activated and recruited to A $\beta$  plaque. In AD patients, positron emission tomography (PET) analysis also suggests that AD progression relates to microglial activation. In recent years, a number of receptors of the innate immunity (CD14, TLR2 and TLR4) and their downstream adapter proteins (MyD88 and IRAK4) were identified to mediate A $\beta$ -induced microglial activation, which included M1 and M2 inflammatory activation. M1 inflammatory activation contributes to local liberation of various proinflammatory cytokines (e.g. TNF- $\alpha$  and IL-1 $\beta$ ), chemokines (e.g. CCL-2) and reactive oxygen species. (Fassbender et al., 2004; Walter et al., 2007; Jana et al., 2008; Hao et al., 2011; Liu et al., 2012). Although cytokines such as TNF- $\alpha$  and IL-1 $\beta$  at low levels activate NF- $\kappa$ B-dependent signaling pathways and might promote cellular growth and survival (Piani et al., 1992; Tracey and Cerami 1994; Chao et al., 1995; Nguyen et al., 2002), these cytokines at high concentrations are neurotoxic over a longer term (Simard and Rivest, 2006; Moore et al., 2009; Michaud et al., 2013). It has been recently established that uncontrolled TNF- $\alpha$  induces neuronal damage and chronic TNF- $\alpha$  infusion in the brain causes neuronal death by apoptosis (Stepanichev et al., 2003; Simard and Rivest 2006; Cheng et al., 2014). In the case of AD mouse model, the pathology was attenuated when neuroinflammation reduced, whether caused by a deficiency in CD40 ligand (Tan et al., 1999 and 2002), IRAK4 (Cameron et al., 2012), NLRP3 (Heneka et al., 2013), or Mrp14 (a neuroinflammation-amplifying protein; Kummer et al., 2012), by blocking TGF- $\beta$ –SMAD2/3 signaling (Town et al., 2008), by stimulating PPAR $\gamma$  and retinoid X receptors (Yamanaka et al., 2012), or by anti-inflammatory agents (Jantzen et al., 2002). In another study, adoptive transfer of interferon- $\gamma$ -producing A $\beta$ -specific T lymphocytes into AD mice severely exacerbated AD pathogenesis (Browne et al., 2013). In contrast, M2 inflammatory activation appears to produce beneficial effects in AD by facilitating neurotoxic inflammatory resolution and promoting neuronal protection and regeneration (Colton et al., 2006; Qian et al., 2006; Martinez et al., 2009; Ma et al., 2010; Sharma et al., 2011; Liu et al., 2012).

Indeed, in my AD mouse model, I found that the number of microglia in the cortex and hippocampus of myeloid *ikbk2*-deficient APP mice significantly decreased than that in myeloid *ikbk2*-WT APP mice. Meanwhile, the transcriptional levels of M1 inflammatory cytokines such as TNF- $\alpha$ , IL-1 $\beta$  and CCL-2 were significantly decreased in the brains of APP mice. And less TNF- $\alpha$  protein was detected in the brain of APP mice. Although astrocytes could also mediate inflammatory response (Avila-Munoz and Arias, 2014), as IKK $\beta$  protein level was not change in non-myeloid original cells in our model. Thus, in this study, the reduced inflammation effect should come from a myeloid source, specifically microglia.

In our studies, ablation of microglial MyD88 and IKK $\beta$  reduced only M1 inflammatory activation without affecting M2 activation in the APP-transgenic mouse brain (Hao et al., 2011). In AD mice with a deficiency in CD14 (Reed-Geaghan et al., 2010), TLR2 (Liu et al., 2012), or IRAK4 (Cameron et al., 2012), microglia were skewed from M1 to M2 inflammatory activation, although the underlying mechanisms were not explained.

### 7.3 Myeloid deficiency of IKK $\beta$ reduces A $\beta$ load in the brain

A $\beta$  is considered to be the major risk factor in the AD pathogenesis because of its neurotoxicity. The A $\beta$  peptide derives from APP via proteolytic cleavage by  $\beta$ - and  $\gamma$ - secretases (Strooper et al., 2010). The 4 kDa monomer transitions from a random coil or  $\alpha$  helix conformation to a  $\beta$ -hairpin. This facilitates a dynamic nucleation-dependent polymerisation reaction which forms short, soluble, metastable intermediates called oligomers. These assemble to form an oligomeric nucleus which can be rapidly extended by monomer addition to form curvilinear protofibrils. Finally, protofibrils are bundled together to form the large, insoluble, cross  $\beta$ -sheet fibrils which accumulate in plaques (Gilbert, 2013). In vitro model, A $\beta$  oligomers increase oxidative stress through calcium homeostasis (Decker et al., 2010). Aggregated A $\beta$  also directly injures synaptic junctions in the neocortex and limbic system, thereafter causing neuronal loss in AD mouse model (Mucke and Selkoe, 2012). The soluble A $\beta$  oligomers, especially dimers, were observed to inhibit long-term potentiation (LTP) by increasing activation of extrasynaptic NR2B-containing receptors and cause neuritic degeneration in which Tau hyperphosphorylation is involved (Shankar et al., 2008; Li et al., 2011). Furthermore, aggregated A $\beta$  could decrease adult neurogenesis, thereby interfering with the recovery from neuronal



damage in AD pathogenesis (Crews et al., 2010a; Crews et al., 2010b). In AD patients, A $\beta$  deposition which can be assessed by Pittsburgh Compound B- PET co-localizes anatomically with other imaging abnormalities associated with AD in many regions of the brain. Abnormalities include brain atrophy as shown on brain magnetic resonance imaging, hypometabolism measured by fluorodeoxyglucose- PET, and dysfunction of the default mode network (DMN) as measured by functional magnetic resonance imaging (Lucey and Bateman, 2014).

Microglia have a beneficial effect on AD pathogenesis by clearing A $\beta$  deposits in the brain (Simard et al., 2006; Grathwohl et al., 2009). But does the inhibition of innate immune signal pathways of microglia simultaneously attenuate A $\beta$  pathology and pro-inflammatory activation? Our previous studies focusing on TLR2 (Liu et al., 2012) and MyD88 (Hao et al., 2011) and the current study addressing IKK $\beta$  have consistently given a positive answer to this question. Indeed, other published observations show that inflammatory activation inhibits phagocytosis in mononuclear phagocytes (Koenigsknecht-Talboo and Landreth, 2005; Townsend et al., 2005; Zelcer et al., 2007; Hickman et al., 2008). In both patients with Alzheimer's disease and AD mice, decreased A $\beta$  clearance correlates with higher cytokine production (Fiala et al., 2005 and 2007; Hickman et al., 2008). The enhancement of A $\beta$  clearance results from reduced inflammatory activation rather than from direct effects of the innate immune molecules *per se*. In the brains of 3-month-old APP-transgenic mice and in the microglial/macrophage internalization assays with A $\beta$  at low concentrations (e.g., 0.2  $\mu$ M), the inflammatory activation level is low. Thus, the presence or absence of MyD88 or IKK $\beta$  does not affect A $\beta$  internalization (Hao et al., 2011).

However, it has been shown that inflammatory activation by the systemic administration of TLR4 ligands can facilitate microglial internalization of A $\beta$ , which decreases the A $\beta$  burden in APP-transgenic mice (Michaud et al., 2013). These results raise an apparent discrepancy with our findings. In our study, we observed that IKK $\beta$  deficiency specifically blocks TGF- $\beta$ –SMAD2/3 signaling but does not affect the SMAD1/5/8 pathway in microglia. Microglial SMAD1/5/8 signaling is constitutively active. Town reported (2008) that SMAD2/3 signaling inhibits macrophage uptake of A $\beta$ , whereas SMAD1/5/8 signaling promotes it; however, an

IKK $\beta$  deficiency in the microglia of our AD mice may have attenuated the inhibitory effects of SMAD2/3 signaling, thereby enhancing microglial clearance of A $\beta$  in the brain. Using cultured microglia, we have confirmed that the pharmacological inhibition of SMAD2/3 signaling increases A $\beta$  internalization. In Michaud's AD mice, microglial SMAD1/5/8 signaling could be further induced by TLR4-mediated inflammatory activation, so that the A $\beta$  internalization–promoting effect is relatively stronger than the inhibitory effect contributed by SMAD2/3. Thus, activation of the SMAD1/5/8 signaling cascade by exogenous stimulators may resolve this apparent discrepancy. The hypothesis that the signaling balance between SMAD2/3 and SMAD1/5/8 modulates microglial A $\beta$  internalization could function also in other AD mice deficient in NLRP3 (Heneka et al., 2013) or with PPAR $\gamma$  activation (Yamanaka et al., 2012), because a deficiency in NLRP3 attenuates (Wang et al., 2013) SMAD2/3 phosphorylation in the kidney epithelium, whereas a deficiency in PPAR $\gamma$  increases SMAD2/3 phosphorylation in embryo fibroblasts (Ghosh et al., 2008). Additional studies are needed to further investigate whether this TGF- $\beta$  hypothesis is a general rule in enhanced microglial A $\beta$  clearance after the inhibition of innate immune signaling and exactly how TGF- $\beta$  regulates microglial endocytosis.

In our study, a deficiency in IKK $\beta$  in myeloid cells did not appear to affect A $\beta$  generation, degradation and A $\beta$  efflux from the brain parenchyma. This observation was surprising in light of the fact that neuroinflammation has been reported to change  $\beta$ -secretase and  $\gamma$ -secretase expression and activity (Sheng et al., 2003; He et al., 2007; Xie et al., 2013) and to alter the A $\beta$  transporter function in the blood-brain barrier (Erickson et al., 2012).

In summary, our study shows that the signaling cascade of TLRs-MyD88-IRAK4-IKK $\beta$  mediates A $\beta$ -triggered microglial inflammatory activation. Ablation of IKK $\beta$  inhibits detrimental neuroinflammation and facilitates beneficial A $\beta$  clearance, thereby improving neuronal function in AD mice. These results contribute to a better understanding of AD pathogenic mechanisms that may eventually translate to therapeutic options for the prevention or treatment of AD progression.

## 8 APPENDIX

## Liu et al., Brain, Behavior, and Immunity, 2015

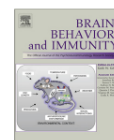
## ARTICLE IN PRESS

Brain, Behavior, and Immunity xxx (2015) xxx–xxx



Contents lists available at ScienceDirect

## Brain, Behavior, and Immunity

journal homepage: [www.elsevier.com/locate/ybrbi](http://www.elsevier.com/locate/ybrbi)Long-term treatment with *Ginkgo biloba* extract EGb 761 improves symptoms and pathology in a transgenic mouse model of Alzheimer's diseaseXu Liu<sup>a,b</sup>, Wenlin Hao<sup>a,b</sup>, Yiren Qin<sup>a,b,c</sup>, Yann Decker<sup>a,b</sup>, Xuan Wang<sup>d</sup>, Martin Burkart<sup>e</sup>, Karl Schötz<sup>f</sup>, Michael D. Menger<sup>g</sup>, Klaus Fassbender<sup>a,b</sup>, Yang Liu<sup>a,b,\*</sup><sup>a</sup>Department of Neurology, University of the Saarland, 66421 Homburg/Saar, Germany<sup>b</sup>German Institute for Dementia Prevention (DIDP), University of the Saarland, 66421 Homburg/Saar, Germany<sup>c</sup>The Institute of Neuroscience, Soochow University, 215123 Suzhou, China<sup>d</sup>Department of Pharmacy, Putuo People's Hospital, 200060 Shanghai, China<sup>e</sup>Dr. Willmar Schwabe GmbH & Co. KG, 76227 Karlsruhe, Germany<sup>f</sup>Preclinical Research, Dr. Willmar Schwabe GmbH & Co. KG, 76227 Karlsruhe, Germany<sup>g</sup>Institute for Clinical and Experimental Surgery, University of the Saarland, 66421 Homburg/Saar, Germany

## ARTICLE INFO

## Article history:

Received 31 October 2014

Received in revised form 4 January 2015

Accepted 12 January 2015

Available online xxxxx

## Keywords:

Alzheimer's disease

Aβ

Autophagy

Inflammation

Microglia

Neurodegeneration

## ABSTRACT

Alzheimer's disease (AD) is a neurodegenerative disease characterized by extracellular deposits of amyloid  $\beta$  peptide (A $\beta$ ) and microglia-dominated neuroinflammation. The therapeutic options for AD are currently limited. In this study, we investigated the antiinflammatory effects and the underlying molecular mechanisms of *Ginkgo biloba* extract EGb 761 when administered to TgCRND8 AD mice, which overexpress human Alzheimer's amyloid precursor protein (APP) specifically in neurons. We gave APP-transgenic mice EGb 761 as a dietary supplement for 2 or 5 months. Plasma concentrations of EGb 761 components in mice were in the same range as such concentrations in humans taking EGb 761 at the recommended dose (240 mg daily). Treatment with EGb 761 for 5 months significantly improved the cognitive function of the mice as measured by the Barnes Maze test. It also attenuated the loss of synaptic structure proteins, such as PSD-95, Munc18-1, and SNAP25. Treatment with EGb 761 for 5 months inhibited microglial inflammatory activation in the brain. The effects of treatment with EGb 761 for 2 months were weak and not statistically significant. Moreover, EGb 761 activated autophagy in microglia. Treatment with EGb 761 decreased A $\beta$ -induced microglial secretion of TNF- $\alpha$  and IL-1 $\beta$  and activation of caspase-1, both of which were abolished by the inhibition of autophagy. Treatment with EGb 761 also reduced the concentrations of NLRP3 protein that colocalized with LC3-positive autophagosomes or autolysosomes in microglia. Additionally, long-term treatment with EGb 761 may reduce cerebral A $\beta$  pathology by inhibiting  $\beta$ -secretase activity and A $\beta$  aggregation. Therefore, long-term treatment with *G. biloba* extract EGb 761, a clinically available and well-tolerated herbal medication, ameliorates AD pathology by antiinflammatory and A $\beta$ -directed mechanisms.

© 2015 Elsevier Inc. All rights reserved.

## 1. Introduction

Alzheimer's disease (AD) is a neurodegenerative disease characterized by extracellular amyloid  $\beta$  (A $\beta$ ) deposits surrounded by activated microglia. Aggregated A $\beta$  directly injures synaptic junctions in the neocortex and limbic system and causes loss of neurons (Selkoe, 2002; Shankar et al., 2008). Aggregated A $\beta$  also

damages neurons by activating microglia to release neurotoxic inflammatory mediators, such as tumor necrosis factor (TNF)- $\alpha$ , interleukin (IL)-1 $\beta$ , and reactive oxygen species (Akiyama et al., 2000; Wyss-Coray and Rogers, 2012). However, activated microglia are beneficial in clearing A $\beta$  from the brain by endocytosis (Liu et al., 2005, 2014). Thus, therapeutic strategies that can protect neurons, attenuate A $\beta$  generation, inhibit microglial inflammatory neurotoxicity, and preserve or even enhance microglial clearance of A $\beta$  in the brain are desirable.

EGb 761 is a dry extract from *Ginkgo biloba* leaves that is adjusted to contain 22–27% ginkgo flavonoids and 5–7% terpene lactones (Ude et al., 2013). The current worldwide guidelines for

\* Corresponding author at: Department of Neurology, University of the Saarland, Kirrberger Straße, 66421 Homburg/Saar, Germany. Tel.: +49 6841 1624260; fax: +49 6841 1624175.

E-mail address: [a.liu@mx.uni-saarland.de](mailto:a.liu@mx.uni-saarland.de) (Y. Liu).

<http://dx.doi.org/10.1016/j.bbi.2015.01.011>  
0889-1591/© 2015 Elsevier Inc. All rights reserved.

dementia therapy recommend EGb 761 as an antidementia drug at the same level as cholinesterase inhibitors and memantine (Ihl and Bachinskaya, 2011). EGb 761 has exhibited multiple anti-AD effects in preclinical (DeFeudis and Drieu, 2000) and clinical studies (Weinmann et al., 2010; Tan et al., 2015). EGb 761 interferes with free cholesterol levels and decreases neuronal production of A $\beta$  (Yao et al., 2004), enhances  $\alpha$ -secretase activity (Colciaghi et al., 2004), and reduces the levels of Alzheimer's amyloid precursor protein (APP) in the brain (Augustin et al., 2009). EGb 761 inhibits A $\beta$  aggregation (Luo et al., 2002). In the AD mouse brain, EGb 761 stabilizes mitochondrial function (Eckert, 2012) and attenuates oxidative stress-triggered neuronal cytotoxicity (Bastianetto et al., 2000; Smith and Luo, 2003). Moreover, feeding EGb 761 to APP-transgenic mice enhances hippocampal neurogenesis and synaptogenesis (Tchanchou et al., 2007, 2009). Recently, treatment with EGb 761 was found to inhibit inflammatory reactions in inflammatory disorders of the colon and the lung (Kotakadi et al., 2008; Haines et al., 2011) and to reduce the expression of Toll-like receptor 4 (TLR4) by decreasing the stability of TLR4 mRNA in human monocytes (Lee et al., 2011). However, the antiinflammatory effects of EGb 761 in AD brains are still unclear.

In this study, we evaluated the anti-AD effects of EGb 761, with a focus on its antiinflammatory effects and potential molecular mechanisms in AD mouse models that overexpress human mutated APP in neurons.

## 2. Materials and methods

### 2.1. Mice

TgCRND8 APP-transgenic mice in a C57BL/6J129 (1:1) background (continuously interbred for more than 5 generations) were kindly provided by D. Westaway (University of Toronto; Chishti et al., 2001). C57BL/6 mice were purchased from Charles River Laboratories (Sulzfeld, Germany). All animal experiments were approved by the regional ethics committee of the Saarland, Germany.

### 2.2. EGb 761-supplemented diets

Female APP-transgenic mice were randomly assigned to one of four groups ( $n \geq 15$  per group): Group 1 consisted of 2-month-old mice treated with a low-flavonoid control diet (C1000, Altromin Spezialfutter GmbH & Co. KG, Lage, Germany) for 5 months. Group 2 consisted of 2-month-old mice treated with C1000 supplemented with a diet containing 600 mg EGb 761 per kg (0.6%) for 5 months. EGb 761, provided by Dr. Willmar Schwabe pharmaceuticals, Karlsruhe, Germany, is a dry extract from *G. biloba* leaves (35–67:1) with an extraction solvent, acetone 60% (w/w), and adjusted to 22.0–27.0% ginkgo flavonoids calculated as ginkgo flavone glycosides; 5.0–7.0% terpene lactones consisting of 2.8–3.4% ginkgolides A, B, and C; 2.6–3.2% bilobalide; and less than 5 ppm ginkgolic acids. On the basis of *ad libitum* diet intake measures, the average dose of EGb 761 provided corresponds to 69 mg per kg body weight per day. Group 3 consisted of 5-month-old mice treated with C1000 for 2 months. Group 4 consisted of 5-month-old mice treated with C1000 supplemented with EGb 761 for 2 months. Before the intervention period, all mice were adapted to the C1000 diet for 1 week.

### 2.3. Barnes Maze test

The cognitive function of APP-transgenic mice was tested with the Barnes Maze test according to an established protocol (Hao et al., 2011). The test started at 2:00 pm and involved 5 days of

acquisition training with two trials per day. For each trial, the mouse was placed at the center of the maze. After 5–10 s, the mouse was allowed to run freely on the platform until reaching the escape hole. For each trial, latency to enter the escape hole and distance traveled were recorded by EthoVision XT (V 7.0) tracking software (Noldus Information Technology, Wageningen, The Netherlands). After each animal had run the maze twice, the averages of latency and total distance from the two trials per day were used for statistical analysis.

### 2.4. Tissue collection

After completing the diet trials, animals were put to death by inhalation of isoflurane (Abbott, Wiesbaden, Germany). Whole blood was collected by intracardial puncture and stored in heparin-containing Eppendorf tubes. After rapid transcardial perfusion with ice-cold phosphate buffered saline (PBS), the brain was removed and divided. The left hemi-brain was immediately fixed in 4% paraformaldehyde (PFA; Sigma, Schnelldorf, Germany) for immunohistochemistry. A section of tissue 0.5 mm thick was cut sagittally from the right hemisphere, and the cortex and hippocampus were carefully dissected and homogenized in Trizol (Life Technologies, Karlsruhe, Germany) for RNA isolation. The remainder of the right hemisphere was frozen in liquid nitrogen for biochemical analysis.

### 2.5. Determination of terpene lactone content in plasma

Plasma was obtained from whole blood after centrifugation (2000 $\times$ g for 10 min at 4 °C). After the addition of 1/10 volume 1 N hydrochloric acid, the plasma was stored at –80 °C until analysis. Concentrations of bilobalide, ginkgolide A, and ginkgolide B were measured in plasma aliquots with gas chromatography tandem mass spectrometry (GC–MS/MS) in the laboratory of Dr. Willmar Schwabe, according to a published protocol (Biber and Koch, 1999).

### 2.6. Brain homogenates and A $\beta$ ELISA

Brains were homogenized according to a published protocol (Liu et al., 2014). Briefly, frozen hemispheres were bounce-homogenized in a Tris-buffered saline (TBS) buffer containing protease inhibitor cocktail (Roche Applied Science, Mannheim, Germany) and centrifuged at 16,000 $\times$ g for 30 min at 4 °C. The supernatant (TBS-soluble fraction) was collected and stored at –80 °C. The pellets were resuspended in TBS plus 1% Triton-X (TBS-T), sonicated for 5 min in a 4 °C water bath, and centrifuged at 16,000 $\times$ g for another 30 min at 4 °C. The supernatant was collected and stored at –80 °C as the TBS-T-soluble fraction. The pellets were extracted for a third time with an ice-cold guanidine buffer (5 M guanidine-HCl/50 mM Tris, pH 8.0, hereinafter referred to as guanidine-soluble fraction). The protein concentration of all samples was measured with the Bio-Rad Protein Assay (Bio-Rad Laboratories GmbH, Munich, Germany). The A $\beta$  concentrations in 3 separate fractions of brain homogenates were determined by A $\beta$ 42 and A $\beta$ 40 enzyme-linked immunosorbent assay (ELISA) kits (both from Life Technologies). The A $\beta$  results were normalized by the protein concentration of the same sample.

### 2.7. Histologic image acquisition and analysis

The PFA-fixed brain was embedded in paraffin, and serial sagittal sections 40  $\mu$ m thick were cut and mounted on glass slides. Immunofluorescent staining was performed on these sections with the primary antibodies: rabbit anti-ionized calcium-binding adaptor molecule 1 (Iba-1) (1:500, Wako Chemicals GmbH, Neuss,



Germany) or mouse monoclonal anti-human A $\beta$  antibody (clone 6F/3D, Dako, Hamburg, Germany). The staining was visualized by Alexa488- or Alexa546-conjugated goat anti-rabbit or anti-mouse immunoglobulin G (IgG; Life Technologies).

All images were acquired with a Zeiss AxioImager.Z2 microscope (Carl Zeiss, Göttingen, Germany) equipped with a Stereo Investigator system (MicroBrightField, Williston, VT, USA). We used the stereologic technique for all histologic analyses and were blinded to the diets given to the mice during the entire experiment. Briefly, after systematic random sampling of every tenth section throughout the entire hippocampus and the cortex, we used the Optical Fractionator (MicroBrightField) as a stereologic probe to quantify Iba-1-labeled cells with a  $120 \times 120 \times 18 \mu\text{m}$  disector and a  $400 \times 400 \mu\text{m}$  sampling grid. The estimated coefficient of error (CE) was less than 0.05. Volumes of A $\beta$  and brain tissues (hippocampus and cortex) were estimated with the Cavalieri probe (Gundersen and Jensen, 1987) with a  $20\text{-}\mu\text{m}$  grid, which provided CE estimates less than 0.04. The A $\beta$  load was calculated as the ratio of A $\beta$  volume to relevant brain tissue volume.

## 2.8. Reverse transcription and quantitative PCR for analysis of gene transcripts

Total RNA was isolated from the brain homogenate in Trizol. First-strand cDNA was synthesized by priming total RNA with hexamer random primers and using Superscript III reverse transcriptase (Life Technologies). For quantification, we used the 7500 Fast real-time PCR system (Life Technologies) to perform real-time quantitative polymerase chain reaction (PCR) with the Taqman gene expression assays of mouse *tnf- $\alpha$* , *il-1 $\beta$* , *inducible nitric oxide synthase (inos)*, *chemokine (C-C motif) ligand 2 (ccl2)*, *il-10*, *brain-derived neurotrophic factor (bdnf)*, *insulin-like growth factor (igf)-1*, *glyceraldehyde 3-phosphate dehydrogenase (gapdh)* and 18s RNA (all from Life Technologies).

## 2.9. Cell culture

Primary microglia were prepared from brains of 3- to 5-day-old C57BL/6 mice, as previously described (Liu et al., 2005). SH-SY5Y neuroblastoma cells were obtained from LGC Standards GmbH (Wesel, Germany). A human APP695-transgenic cell line was established by transfecting cells with human APP695-encoded protein expressing vectors with a CMV promoter. The transfected cells were selected with G418 until the transgene was stably expressed.

## 2.10. Treatments of microglia and inflammatory analysis

Chemically synthesized human A $\beta$ 42 was kindly provided by Livia Fülöp (Albert Szent Gyorgyi Medical University, Szeged, Hungary). The oligomeric A $\beta$  aggregates were prepared according to a published protocol (Dahlgren et al., 2002). Endotoxin concentrations of peptide samples were less than 0.01 EU/ml, as determined by the Limulus amoebocyte lysate assay (Lonza, Basel, Switzerland). The oligomeric conformation of A $\beta$ 42 peptides was confirmed by Western blot analysis and electron microscopy (data not shown).

Microglia plated in 48-well plates (BD, Heidelberg, Germany) at  $2 \times 10^5$  cells per well were pretreated with EGb 761 at 0, 5, 10, 50, or 100  $\mu\text{g/ml}$  for 24 h. Aggregated A $\beta$ 42 at 10  $\mu\text{M}$  was added to the culture medium in the presence of EGb 761 for another 24 h. Supernatants were collected for detecting TNF- $\alpha$ , IL-1 $\beta$ , and CCL-2 by ELISA kits (eBioscience, San Diego, CA, USA). Autophagy and caspase 1 activity were analyzed with a commercial kit (Abcam, Cambridge, UK); microglia plated in 6-well plates (BD) at  $1 \times 10^6$  cells per well were treated as in the inflammatory cytokine assays. To analyze the involvement of autophagy in inflammatory

inhibition induced by EGb 761, we treated cells with 1 mM 3-methyladenine (3-MA) together with EGb 761.

## 2.11. Flow cytometric analysis of HiLyte Fluor 488-conjugated A $\beta$ 42 internalization in primary microglia

To investigate the effects of EGb 761 on microglial internalization of A $\beta$ , we pretreated primary microglia cultured in a 24-well plate (BD) at a density of  $3 \times 10^5$  cells per well with 10  $\mu\text{g/ml}$  EGb 761 for 24 h and then with 5  $\mu\text{M}$  HiLyte Fluor 488-conjugated A $\beta$ 42 aggregates for 0, 3, or 6 h. Fluorescent A $\beta$  was prepared by mixing HiLyte Fluor 488-labeled human A $\beta$ 42 (AnaSpec, Fremont, CA, USA) and unlabeled A $\beta$  at a ratio of 1:10. Thereafter, microglia were washed with a  $1\times$  solution of PBS and detached from the plate with trypsin ethylenediaminetetraacetic acid (trypsin-EDTA; Life Technologies). The mean fluorescence intensity (mFI) of internalized fluorophore-conjugated A $\beta$ 42 and the percentages of positive cells with intracellular proteins were immediately determined with a BD FACSCanto II flow cytometer (Franklin Lakes, NJ, USA). To examine the surface binding of A $\beta$ , we incubated cells with 5  $\mu\text{M}$  HiLyte Fluor 488-conjugated A $\beta$ 42 aggregates for 3 h on ice and then analyzed them for mFI.

## 2.12. Immunofluorescent analysis of microglial autophagy and localization of NLRP3 inflammasomes

To analyze the effects of EGb 761 on microglial autophagy, we pretreated primary microglia cultured in an 8-well chamber slide (BD) at a density of  $2 \times 10^4$  cells per well with 10  $\mu\text{g/ml}$  EGb 761 for 24 h and fixed them with 4% PFA for 20 min. After increasing the permeability of the cell membrane with 0.2% Triton-100 and blocking cells with 1% bovine serum albumin, we incubated cells with rabbit polyclonal antibody against microtubule-associated protein light chain (LC3) A/B (Cat. No. ab128025, Abcam). The colocalization of LC3 with nucleotide-binding oligomerization domain (NOD)-, leucine-rich repeat (LRR)-, and pyrin domain-containing 3 (NLRP3) was demonstrated by further staining of the microglia with a rat monoclonal antibody against mouse NLRP3 (Clone 768319; R&D Systems, Wiesbaden-Nordenstadt, Germany). The immunofluorescent staining was visualized with Alexa488- or Alexa546-conjugated goat anti-rabbit or anti-rat IgG (Life Technologies).

To count LC3 puncta in microglia, we randomly selected more than 40 areas under a  $40\times$  objective and counted more than 200 microglia. The density of LC3 puncta in each cell was calculated as the total number of LC3 puncta divided by the total number of cells. The experiments were repeated independently 5 times.

## 2.13. Western blot analysis

For analysis of synaptic proteins and autophagy markers in the brain, TBS-T-soluble brain homogenates (see Section 2.6) were separated by 10% Tris-glycine polyacrylamide gel electrophoresis (PAGE). Postsynaptic density protein 95 (PSD-95), the mammalian homologue of unc-18 (Munc18)-1, the 25-kDa synaptosome-associated protein (SNAP25), synaptophysin, LC3B, and beclin1 were detected by Western blot analysis with rabbit or mouse monoclonal antibodies (clone D27E11 for PSD-95, clone D406V for Munc18-1, clone D110 for SNAP25, clone SY38 for synaptophysin, clone D11 for LC3B, and clone D40C5 for beclin 1; Cell Signaling Technology, Danvers, MA, USA, or Abcam) according to an established protocol (Liu et al., 2014).

For detecting the autophagy markers and NLRP3 in microglia, cells were treated with 10  $\mu\text{g/ml}$  EGb 761 for 24 h and were lysed in radioimmunoprecipitation assay (RIPA) buffer (50 mM Tris-HCl [pH 8.0], 150 mM NaCl, 5 mM EDTA, 1% NP-40, 0.5% sodium

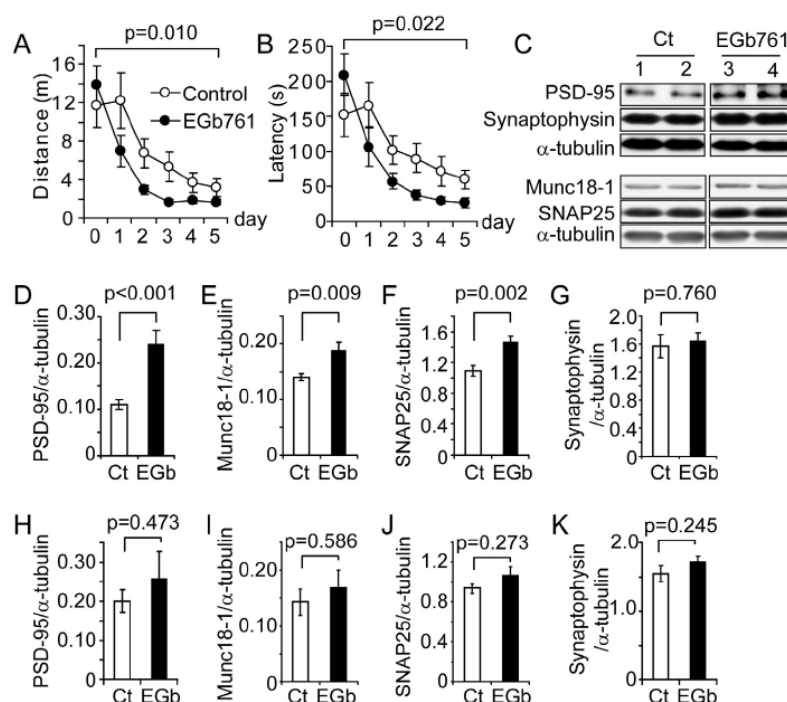


**Fig. 1.** EGb 761 improves cognitive function of APP-transgenic mice. Two-month-old TgCRND8 APP-transgenic mice were fed EGb 761-supplemented or control diets for 5 months. Alternatively, 5-month-old APP mice were fed with these two diets for 2 months. In the Barnes Maze test, the group of 2-month-old mice taking EGb 761 for 5 months spent significantly less time and traveled a markedly shorter distance to reach the escape chamber than did the control mice receiving the control diet (A–B; two-way ANOVA;  $n = 14$  per group). Synaptic structure proteins in brain homogenates were detected by Western blot analysis. The amounts of PSD-95, Munc18-1, and SNAP25 in the brains of mice receiving EGb 761 for 5 months (D–F) but not for 2 months (H–J) were significantly higher than those in the APP mice receiving the control diet ( $t$ -test;  $n = 10$  per group). The synaptophysin levels were not changed by EGb 761 treatments for 2 or 5 months (C, G, and K;  $t$ -test;  $n = 10$  per group).

deoxycholate, and 0.1% sodium dodecyl sulfate [SDS]) containing a protease inhibitor cocktail (Roche Applied Science). For Western blot analysis, we used the beclin1, LC3B, and NLRP3 antibodies described above and a rabbit polyclonal antibody against sequestosome 1 (SQSTM1)/p62 (Cat. No. 5114, Cell Signaling Technology).

For all Western blot analyses described above, mouse  $\alpha$ -tubulin or  $\beta$ -actin was detected as a loading control with the DM1A antibody (Abcam) and the 13E5 antibody (Cell Signaling Technology). Western blots were visualized with the enhanced chemiluminescence (ECL) method (Perkin Elmer, Rodgau, Germany). Densitometric analysis of bands was performed with ImageJ (version 1.4.3; National Institutes of Health, Bethesda, MD, USA). The amount of proteins of interest was calculated as a ratio between the density of proteins of interest and the density of  $\alpha$ -tubulin or  $\beta$ -actin from the same sample.

#### 2.14. Cell treatment with EGb 761 and A $\beta$ secretion

Human APP695 transgenic SH-SY5Y cells were treated with EGb 761 at 0, 5, 10, 50, or 100  $\mu$ g/ml for 1 or 3 days in Dulbecco's modified Eagle's medium (DMEM) culture medium containing 10% fetal calf serum (FCS). Thereafter, the culture medium was replaced with DMEM medium without serum. After 24 h, the conditioned medium was collected for A $\beta$  detection with A $\beta$ 40 and A $\beta$ 42 ELISA kits (Life Technologies).

#### 2.15. Thioflavin T assay to detect A $\beta$ aggregation

The monomeric A $\beta$ 42 was prepared according to a published protocol (Dahlgren et al., 2002). The peptide was diluted with

PBS to 25  $\mu$ M and incubated with EGb 761 at various concentrations (0, 1, 10, 50, and 100  $\mu$ g/ml) at 37° for 96 h. Aliquots were transferred into the measuring solution containing 5 mM thioflavin T (ThT) in 50 mM glycine–NaOH buffer (pH 8.5). Fluorescence was measured with a Synergy Mx Monochromator-Based Multi-Mode Microplate Reader (BioTek, Winooski, VT, USA) at an excitation wavelength of 440 nm and an emission wavelength of 482 nm. A control solution of A $\beta$ 42 in glycine–NaOH buffer without ThT was used as a control. The fluorescence intensity above the control level indicated the content of A $\beta$ 42 aggregates.

#### 2.16. Statistical analysis

Data shown in the figures are presented as mean  $\pm$  SEM. For multiple comparisons, we used one-way or two-way ANOVA followed by Bonferroni, Tukey's Honestly Significant Difference, or Tamhane's T2 *post hoc* test (depending on the result of Levene's test to determine the equality of variances). A two-independent-samples  $t$ -test was used to compare means for two groups of cases. All statistical analyses were performed with IBM SPSS Statistics Standard v. 19.0.0 (IBM, New York, NY, USA). Statistical significance was set at the level of  $p < 0.05$ .

### 3. Results

#### 3.1. Long-term treatment with EGb 761 improves cognitive function and preserves synaptic structure proteins in APP-transgenic mice

To evaluate the anti-AD effects of EGb 761, we first evaluated the efficacy of EGb 761 against cognitive deficits in APP-transgenic



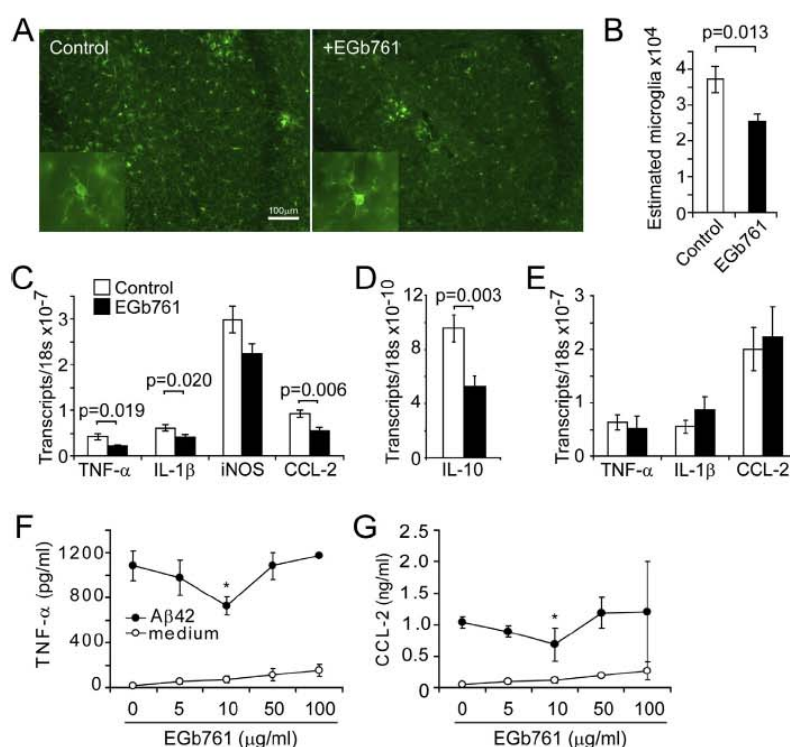


**Fig. 2.** EGb 761 inhibits neuroinflammatory activation in APP-transgenic mice. Two-month-old TgCRND8 APP-transgenic mice received EGb 761-supplemented diets or control diets for 5 months, and 5-month-old APP mice received either diet for 2 months. Microglia were immunofluorescently stained with Iba-1 antibodies (green fluorescence). The number of microglia in the entire hippocampus was reduced after 5 months of treatment with EGb 761 (B; *t*-test; *n* = 10 per group). Transcription of inflammatory gene markers *tnf-α*, *il-1β*, *ccl-2*, *inos*, and *il-10* in the brains of APP-transgenic mice was reduced by 5 months of treatment with EGb 761 (C–D) but not by 2 months of treatment (E), as determined by real-time polymerase chain reaction (*t*-test; *n* = 10 per group). Moreover, primary cultured microglia were pretreated with EGb 761 at 0, 5, 10, 50, and 100 μg/ml for 24 h and then stimulated with 10 μM oligomeric Aβ42 for another 24 h. The culture medium was collected for analysis with ELISA. EGb 761 administered at 10 μg/ml significantly reduced the secretion of Aβ-induced TNF-α and CCL-2 (one-way ANOVA; *n* = 4 per group). (For interpretation of the references to colour in this figure legend, the reader is referred to the web version of this article.)

mice. Two-month-old APP-transgenic mice were fed diets supplemented with EGb 761 for 5 months. At the end of the feeding experiments, the plasma concentration of bilobalide was 9.0–14.6 ng/ml, that of ginkgolide A was 4.1–6.5 ng/ml, and that of ginkgolide B was 1.0–1.8 ng/ml, all of which were within or very close to the range of concentrations found in humans taking EGb 761 at the recommended dosage (240 mg daily) (Zadayan et al., 2012; Ude et al., 2013). In plasma from control mice receiving standard diets these EGb 761 components were undetectable.

In the Barnes Maze test, the traveling time and the distance traveled were significantly shorter for all tested mice when the training time was increased (Fig. 1A and B; one-way ANOVA, *p* < 0.05). There was no significant difference in running speed between the two groups of mice or between different training dates for the same mice (two-way ANOVA, *p* > 0.05). Thus, APP-transgenic mice retained the ability to use spatial reference points to learn the location of an escape hole. When compared with APP-transgenic mice receiving standard diets, the APP mice receiving diets supplemented with EGb 761 required significantly less time (Fig. 1A; two-way ANOVA, *p* = 0.022) and traveled significantly shorter distances (Fig. 1B; two-way ANOVA, *p* = 0.010) before reaching the escape hole.

Our previous studies have shown that the number of synaptic structure proteins is lower in AD mice than in their littermate controls (Hao et al., 2011; Liu et al., 2012, 2014). Interestingly, the levels of the proteins PSD-95, Munc18-1, and SNAP25 but not

that of synaptophysin were significantly higher in APP-transgenic mice receiving a diet supplemented with EGb 761 for 5 months than in APP-transgenic mice receiving a standard diet (Fig. 1C–G; *t*-test, *p* < 0.05). In APP-transgenic mice that received diets supplemented with EGb 761 for 2 months, EGb 761 exerted only a weak and not statistically significant effect on the concentrations of all tested synaptic structure proteins: PSD-95, Munc18-1, SNAP25, and synaptophysin (Fig. 1H–K; *t*-test, *p* > 0.05).

In additional experiments, we also quantified transcripts of genes encoding two important neurotrophic factors (BDNF and IGF-1) in the brains of 7-month-old APP-transgenic mice. We found that BDNF but not IGF-1 gene transcription was significantly increased by 5 months of treatment with EGb 761: from  $1.50 \pm 0.28 \times 10^{-4}$  to  $2.46 \pm 0.23 \times 10^{-4}$  (*bdnf/gapdh*; *t*-test, *p* = 0.026; *n* ≥ 5 per group).

### 3.2. Long-term treatment with EGb 761 reduces inflammatory activation in the AD mouse brain

Because neurotoxic inflammatory activation contributes to AD pathogenesis (Akiyama et al., 2000; Wyss-Coray and Rogers, 2012), we determined whether long-term treatment with EGb 761 inhibited neuroinflammatory activation in AD mice. The histological analysis demonstrated that the number of Iba-1-positive cells in the hippocampus was significantly lower ( $2.54 \pm 0.22 \times 10^5$  cells; *t*-test, *p* = 0.013) in APP-transgenic mice treated with

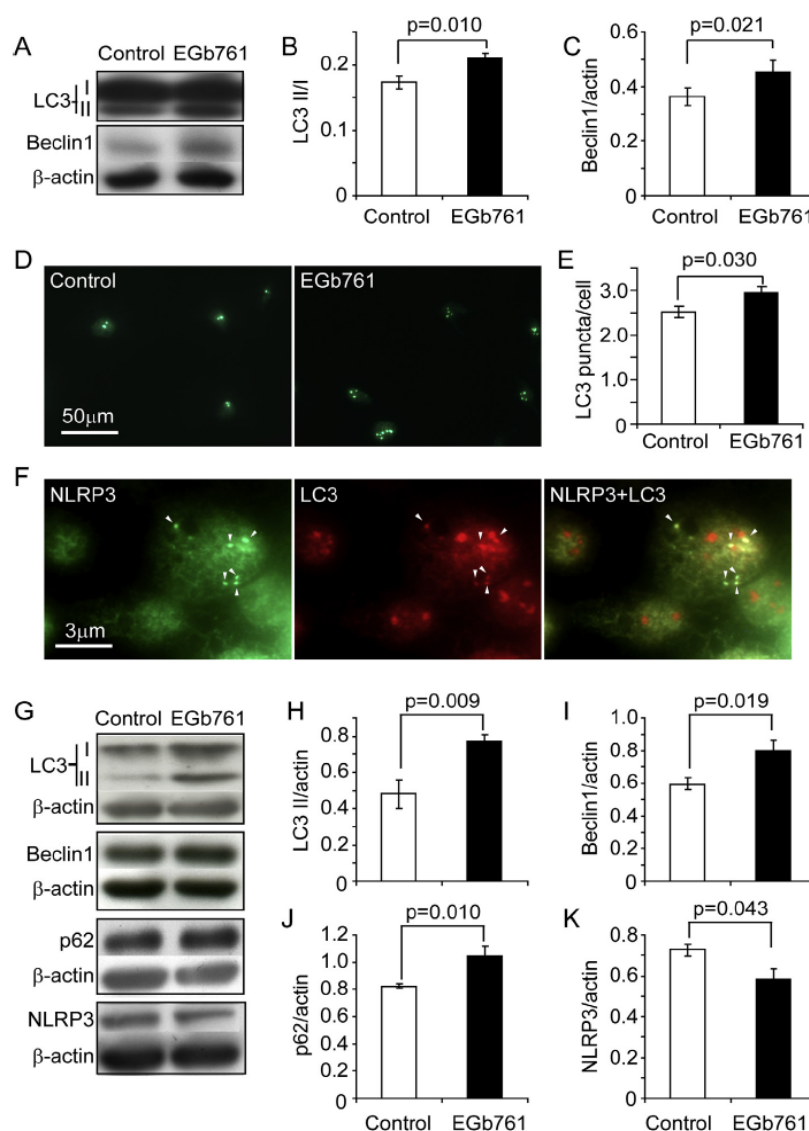


**Fig. 3.** Treatment with EGb 761 enhances autophagy both *in vivo* and *in vitro*. Two-month-old TgCRND8 APP-transgenic mice received an EGb 761-supplemented diet or a control diet for 5 months. The autophagy markers LC3, and beclin1 in the brain homogenate were detected by Western blot analysis (A–C;  $n \geq 21$  per group). Primary cultured microglia were treated with 10  $\mu$ g/ml EGb 761 for 24 h. LC3 and NLRP3 in microglia were immunofluorescently stained (D and F). The numbers of LC3 puncta were compared between EGb 761-treated and control microglia (E;  $n = 5$  per group). Colocalization between NLRP3 and LC3 is indicated by arrowheads (F). The autophagy markers LC3, beclin1, and p62, as well as NLRP3, in the cell lysate were further detected by Western blot analysis (G–K;  $n \geq 4$  per group). Student's *t*-tests were used to compare two independent groups.

EGb 761 in their diet for 5 months than in control mice ( $3.72 \pm 0.37 \times 10^5$  cells) that were given diets without EGb 761 (Fig. 2A and B). The reduction in Iba-1-positive cell number, which reflects both the decreased microglial number and inflammatory activation, indicated the neuroinflammatory inhibition in EGb 761-treated mice. The morphology of microglia (insert of figure) did not appear to be substantially changed by the administration of EGb 761 (Fig. 2A).

We further quantified transcripts of inflammatory genes in the brain. As shown in Fig. 2C and D, the transcription of both proinflammatory and antiinflammatory genes (*tnf- $\alpha$* , *il-1 $\beta$* , *ccl-2*, and *il-10*) was markedly decreased by a diet supplemented with EGb

761 for 5 months (*t*-test,  $p < 0.05$ ). However, in APP-transgenic mice that received EGb 761 for only 2 months, the transcription of inflammatory genes was not affected by EGb 761 (Fig. 2E).

To confirm the antiinflammatory effects of EGb 761, we tested the effects of EGb 761 on microglial secretion of cytokines. We observed that pretreatment with EGb 761 at concentrations not higher than 10  $\mu$ g/ml could inhibit A $\beta$ -triggered microglial secretion of TNF- $\alpha$  and CCL-2 in a dose-dependent manner (Fig. 2F and G; two-way ANOVA,  $p < 0.05$ ). Surprisingly, EGb 761 at concentrations higher than 10  $\mu$ g/ml lost their inhibitory effects on A $\beta$ -induced inflammatory activation (Fig. 2F and G). Interestingly, treatment with EGb 761 alone activated microglia, in a



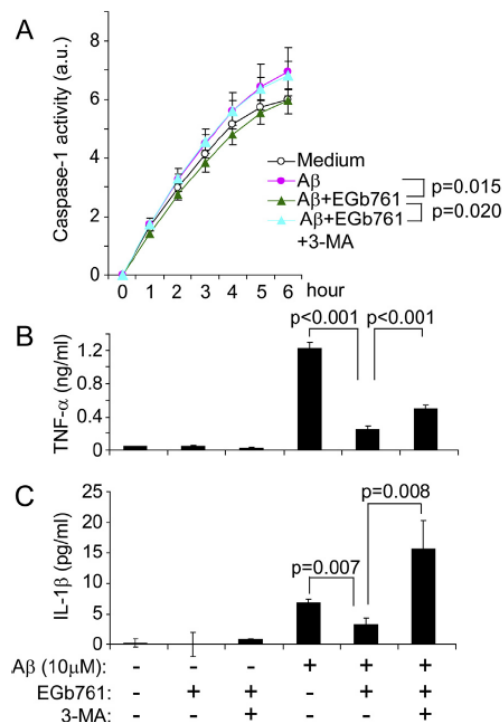


**Fig. 4.** Treatment with EGb 761 ameliorates Aβ-induced caspase 1 activation and cytokine secretion in primary microglia, both of which are abolished by inhibition of autophagy. Primary cultured microglia were pretreated with 10 μg/ml EGb 761 or vehicle for 24 h, followed by treatment with 10 μM oligomeric Aβ42 for another 24 h. To test the effects of autophagy on EGb 761-induced inflammatory inhibition, 1 mM 3-methyladenine (3-MA) was used together with EGb 761. Caspase 1 activity was detected by incubating cell lysate with a specific fluorogenic substrate (A; two-way ANOVA followed by Tukey HSD *post hoc* test;  $n = 5$  per group). TNF-α and IL-1β in the culture medium were measured by ELISA (B and C; one-way ANOVA followed by Tukey HSD *post hoc* test;  $n = 10$  per group).

concentration-dependent manner, to secrete TNF-α and CCL-2 at a level that was low but significantly higher than secretion levels in control cells (Fig. 2F and G; two-way ANOVA,  $p < 0.05$ ).

### 3.3. Autophagy enhanced by EGb 761 treatment mediates the microglial inflammatory inhibition induced by EGb 761

As described in the last section, treatment with EGb 761 reduced inflammatory signaling both in the mouse brain and in cultured microglia; the mechanism of this reduction was unclear. We found that supplementing the diet with EGb 761 significantly induced autophagy, as shown by increased protein levels of lipidated LC-3 (LC-3 type II) and beclin1 in APP-transgenic mouse brains (Fig. 3A–C;  $t$ -test,  $p < 0.05$ ). Treatment with EGb 761 increased the clustering of LC3; this clustering indicates the formation of autophagosomes or autolysosomes (Klionsky et al., 2008) in cultured microglia, as demonstrated by the fact that EGb 761-treated microglia contain more immunofluorescent LC3 puncta than do untreated control cells (Fig. 3D and E;  $t$ -test,  $p < 0.05$ ). Similarly, the concentrations of the proteins type II LC-3, beclin-1, and p62 in cultured microglia were increased by treatment with EGb 761, as shown by Western blot analysis (Fig. 3G–J;  $t$ -test,  $p < 0.05$ ). Interestingly, the key component of inflammasomes, NLRP3, was observed to colocalize with LC3-positive cytoplasmic vesicles

(Fig. 3F), and the concentration of this protein was reduced by treatment with EGb 761 (Fig. 3G and K;  $t$ -test,  $p < 0.05$ ). The NLRP3 inflammasome, which is the key enzyme complex required for the activation of proinflammatory IL-1β signaling (Schroder and Tschopp, 2010), has been reported to be degraded by autophagy (Shi et al., 2012). Thus, we questioned whether the observed increase in autophagy mediates the antiinflammatory effects of EGb 761 in microglia. We found that administering oligomeric Aβ42 at a concentration of 10 μM increased caspase-1 activity in microglia, whereas administering EGb 761 at 10 μg/ml significantly reduced Aβ-induced activation of caspase-1. The reduction of caspase-1 activity induced by EGb 761 was completely reversed when cells were co-treated with the autophagy inhibitor 3-MA (Fig. 4A; two-way ANOVA followed by Tukey HSD *post hoc* test,  $p < 0.05$ ). We continued to measure the secretion of TNF-α and IL-1β from microglia after a challenge with oligomeric Aβ. Similarly, co-treatment with EGb 761 reduced the secretion of both cytokines, whereas this reduction was abolished by 3-MA (Fig. 4B and C; one-way ANOVA followed by Tukey HSD *post hoc* test,  $p < 0.05$ ).

### 3.4. Long-term treatment with EGb 761 attenuates Aβ pathology in the AD mouse brain

Aβ is a key pathogenic molecule in AD; it interacts with microglia to trigger neuroinflammation and modulate its own metabolism (Huang and Mucke, 2012). We determined the cerebral Aβ load by using immunohistological methods. Neither the extent nor the morphology of the diffuse Aβ or Aβ plaques was changed by supplementing the diet with EGb 761 (Fig. 5A). However, we found that, after treatment with EGb 761, the volume of Aβ load ( $1.55 \pm 0.18\%$  in the hippocampus and  $2.91 \pm 0.32\%$  in the cortex) was significantly reduced (to  $1.04 \pm 0.16\%$  in the hippocampus [ $p = 0.049$ ] and to  $1.64 \pm 0.36\%$  in the cortex [ $p = 0.029$ ]) (Fig. 5A and B;  $t$ -test for relevant comparisons). However, we were unable to detect a difference in Aβ concentrations in brain homogenates derived from APP-transgenic mice receiving either a standard diet or a diet supplemented with EGb 761 for 5 months (Fig. 5C).

To further elucidate the effects of EGb 761 on Aβ pathology, we continued to investigate whether EGb 761 treatment modified the generation, aggregation, and clearance of Aβ. First, we measured the activity of β-secretase and γ-secretase, the key enzymes that generate Aβ (Vassar and Citron, 2000). We found that treatment with EGb 761 for 5 months slightly but significantly reduced β-secretase activity (Fig. 6A; two-way ANOVA,  $p < 0.05$ ) but did not change γ-secretase activity (Fig. 6B). However, in SH-SY5Y cells engineered to overexpress human APP, administering EGb 761 at concentrations of 0, 5, 10, 50, and 100 μg/ml did not affect Aβ secretion (Fig. 6C). Second, we found that EGb 761 inhibited Aβ42 aggregation *in vitro* in a dose-dependent manner in the thioflavin binding assay at an effective dose much lower than the published dose (Luo et al., 2002) (Fig. 6D; one-way ANOVA,  $p < 0.05$ ). Third, we measured microglial internalization of fluorescence-labeled oligomeric Aβ42 as in previous studies (Hao et al., 2011; Liu et al., 2014) after pretreating microglia with 10 μg/ml EGb 761. We found that EGb 761 did not reduce microglial uptake of Aβ, although Aβ-induced microglial inflammatory activation was inhibited (data not shown).

## 4. Discussion

Increasing evidence has shown that Aβ-triggered microglial inflammatory activation damages neurons in AD pathogenesis (Akiyama et al., 2000; Wyss-Coray and Rogers, 2012). In this study, we found that long-term dietary supplementation with EGb 761

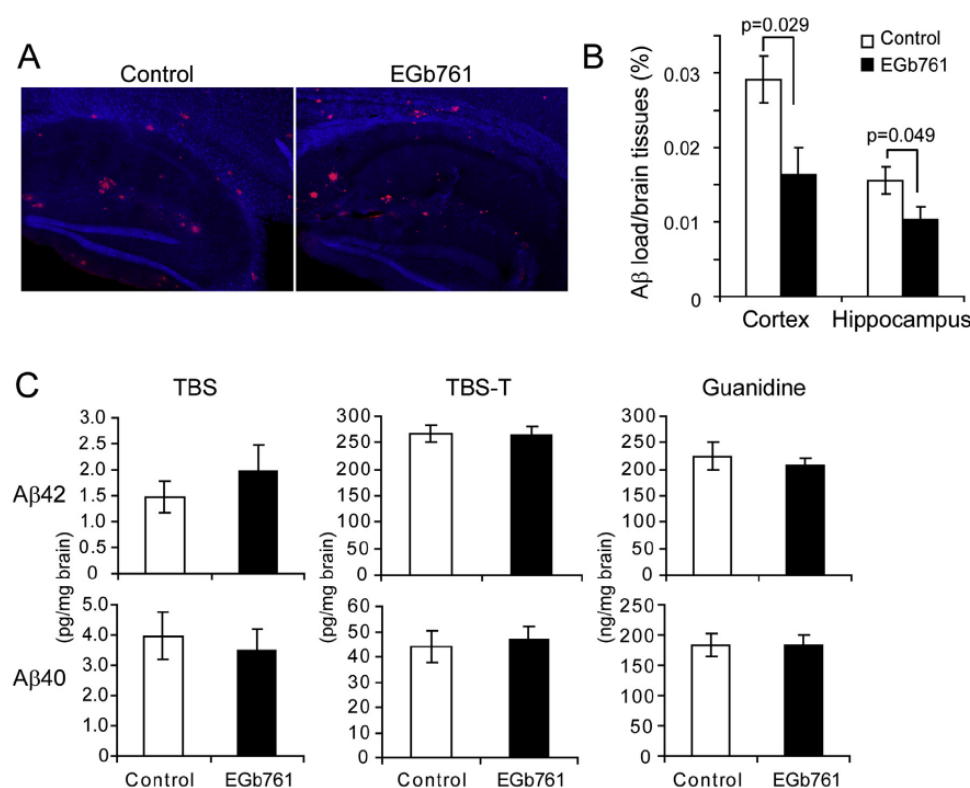


**Fig. 5.** Treatment with EGb 761 potentially attenuates cerebral Aβ load in APP-transgenic mice. Two-month-old TgCRND8 APP-transgenic mice were fed EGb 761-supplemented or control diets for 5 months. The cerebral Aβ load after immunofluorescent staining (red) was significantly lower in EGb 761-treated APP mice than in control mice (A–B). Aβ concentrations in brain homogenates were measured by ELISA (C; *t*-test; *n* = 8 per group). (For interpretation of the references to colour in this figure legend, the reader is referred to the web version of this article.)

inhibits neuroinflammatory activation and improves cognitive function in TgCRND8 APP-transgenic mice.

Genome-wide association studies have identified the innate immune system as an important determinant of sporadic AD pathology (Lambert et al., 2010). Recently, the inflammasome containing NLRP3, ASC, and caspase 1 was observed to sense lysosomal instability induced by Aβ internalization (Halle et al., 2008). The NLRP3 inflammasome is known to process pro-IL-1 to mature and functional IL-1β (Schroder and Tschopp, 2010). Thus, the NLRP3 inflammasome is a key signaling pathway in Aβ-triggered microglial inflammatory activation (Heneka et al., 2014). Deletion of NLRP3 significantly attenuates neuroinflammation and improves AD-like pathology in APP-transgenic mice (Heneka et al., 2013). In our study, we observed colocalization of NLRP3 and LC3-positive cytoplasmic vesicles (probably autophagosomes or autolysosomes). EGb 761 administration enhanced autophagy, reduced NLRP3 concentrations, and decreased caspase 1 activity in microglia. Thus, EGb 761 could exert antiinflammatory effects by initiating an active cellular protective reaction (Chuang et al., 2013), a mechanism different from that of those antiinflammatory drugs that were tested in previous clinical trials aimed at preventing AD progression (Jaturapatpom et al., 2012).

It is known that the role of microglia in AD pathogenesis is that of a two-edged sword, with both detrimental neurotoxic inflammatory effects and beneficial Aβ-cleaning effects (Liu et al., 2005, 2014). Thus, we wondered whether antiinflammatory therapy could also attenuate microglial clearance of cerebral Aβ (Michaud

et al., 2013). In contrast, EGb 761 increased the expression of beclin1 and p62. Beclin1 promotes microglial phagocytosis of Aβ (Lucin et al., 2013), and autophagy is necessary for microglial Aβ degradation (Cho et al., 2014).

It is surprising that treatment with EGb 761 alone induces mild inflammatory activation; however, this activation could be necessary to enhance autophagy in microglia (Shi et al., 2012). EGb 761 contains flavonoids and terpene lactones. It has been reported that flavonoids derived from vegetables, fruits, tea, and wine can induce autophagy and inhibit the activation of NLRP3 inflammasomes (Chuang et al., 2014). The effects of terpene lactones on autophagy are unclear, although EGb 1212, another *Ginkgo* preparation containing more bilobalide and ginkgolide B than the preparation we used, inhibits autophagy in the ischemic brain (Yin et al., 2013). Thus, it is likely that EGb 761 contains both autophagy-enhancing and autophagy-inhibiting components. In the studies that administered EGb 761 at a concentration higher than one we used, its autophagy-inhibiting effect may have become relatively stronger than its autophagy-enhancing effect, although both effects were increased. As a result, the antiinflammatory effect of EGb 761 could have been lost.

In this study, we found that EGb 761 may attenuate Aβ pathology in AD mice. Immunological analysis demonstrated that the brains of APP-transgenic mice given EGb 761 for 5 months contained fewer Aβ deposits than did the brains of control mice, although this result was not confirmed by ELISA assays for Aβ40 and Aβ42. Long-term dietary supplementation with EGb 761



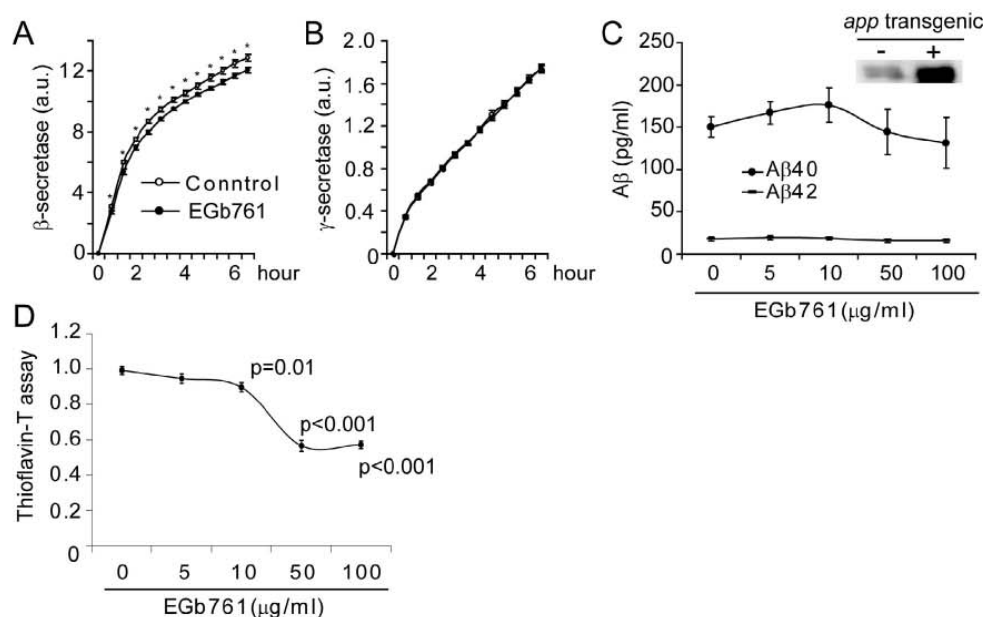


**Fig. 6.** EGb 761 treatment reduces  $\beta$ -secretase activity and A $\beta$  aggregation in APP-transgenic mouse brain. Two-month-old TgCRND8 APP-transgenic mice were fed with Ginkgo extract EGb 761-supplemented or control diets for 5 months. Membrane components were isolated from the brain, and  $\beta$ - and  $\gamma$ -secretase activity was measured by incubating membrane components with fluorogenic secretase substrates. EGb 761 treatment reduced  $\beta$ -secretase activity (A; two-way ANOVA,  $p < 0.05$ ;  $t$ -test comparing two groups at each time point,  $* < 0.05$ ;  $n = 7$  per group) but did not change  $\gamma$ -secretase activity (B; two-way ANOVA,  $p > 0.05$ ;  $n = 7$  per group). However, treatment with EGb 761 at various concentrations for 3 days did not change A $\beta$ 40 and A $\beta$ 42 release from SH-SY5Y cells that had been engineered to overexpress human APP695 (see insert) (C; one-way ANOVA,  $p > 0.05$ ;  $n = 4$  per group). Moreover, 25  $\mu$ M monomeric A $\beta$ 42 was incubated in PBS with EGb 761 at various concentrations (0, 5, 10, 50, and 100  $\mu$ g/ml) and allowed to aggregate at 37  $^{\circ}$ C for 96 h. Thereafter, the aggregation state was evaluated by thioflavin-T fluorescence assay (D; one-way ANOVA followed by Tukey HSD *post hoc* test;  $n = 17$  per group).

slightly but significantly suppressed  $\beta$ -secretase activity in APP-transgenic mouse brains, an outcome that most likely results from neuroinflammatory inhibition by EGb 761 (He et al., 2007; Xie et al., 2013), because EGb 761 did not directly alter A $\beta$  generation in APP-transgenic SH-SY5Y cells. We also found that EGb 761 interferes with A $\beta$  aggregation, a finding that confirms an earlier observation (Luo et al., 2002), but at a much lower concentration (10  $\mu$ g/ml) than the concentration used in Luo's experiments. This effect of EGb 761 on A $\beta$  aggregation could partially explain the inconsistency in the amounts of A $\beta$  detected by histologic and biochemical analyses, as discussed earlier. The interference with A $\beta$  aggregation benefits neuronal survival and inhibits neuroinflammation in AD mice, because A $\beta$  aggregation is a prerequisite for neurotoxicity and microglial activation (Dahlgren et al., 2002; Fassbender et al., 2004). Moreover, EGb 761 enhances autophagy and therefore may promote the degradation of C-terminal APP fragments (Tian et al., 2014). Indeed, long-term treatment with EGb 761 has been shown to decrease levels of APP in APP-transgenic mice (Augustin et al., 2009).

Apart from the anti-AD effects discussed above, EGb 761 treatment could have a direct effect on neuronal protection. EGb 761 enhances neurogenesis by phosphorylating cyclic-AMP response element binding protein (CREB) (Tchantchou et al., 2007, 2009). In our study, we also observed that 5 months of treatment with EGb 761 significantly stimulated the expression of BDNF in APP-transgenic mouse brains, a finding in accordance with those of a previous study of the antidepressant effects of EGb 761 (Hou et al., 2010).

The EGb 761 dose applied in our study (69 mg per kg body weight per day on average) is comparable to that used in other published *G. biloba* extract feeding experiments (Stackman et al.,

2003; Tchantchou et al., 2007) but lower than the frequently applied doses of 100–300 mg per kg body weight per day. Adequate dosing of EGb 761 in animal models has been a matter of debate (Lautenschlager et al., 2012). To ensure that dosing was comparable to human therapeutic exposure, we determined plasma levels of terpene lactones and compared them to human data. The plasma concentrations of EGb 761 in our animal models were in the same range as the levels in human plasma after daily intake of the therapeutic dose of 240 mg EGb 761 (Zadoyan et al., 2012), a finding suggesting that the anti-AD effects of EGb 761 observed in mice in this study would be similar in AD patients. Because we observed that higher concentrations of EGb 761 did not achieve stronger antiinflammatory effects in microglia, our study does not support the clinical use of dosages higher than 240 mg per day.

Indeed, the efficacy of EGb 761 in improving cognition, neuropsychiatric symptoms, and activities of daily living in patients with mild to moderate AD dementia has been demonstrated in numerous placebo-controlled trials (Weinmann et al., 2010; Ihl and Bachinskaya, 2011; Herrschaft et al., 2012; Tan et al., 2015), although other clinical trials did not find any preventive effects of *G. biloba* extract in dementia (Birks and Grimley Evans, 2009; Jiang et al., 2013). However, it should be noted that many clinical trials have recruited patients with various levels of cognitive ability, prescribed various *G. biloba* preparations, and used different study designs. Therefore, published meta-analyses based on different groups of studies have reported both positive and negative findings about the antidementia effects of *G. biloba* extract (Birks and Grimley Evans, 2009; Weinmann et al., 2010; Jiang et al., 2013; Tan et al., 2015). In the two trials with large numbers of participants, the GuidAge trial and the Ginkgo Evaluation of Memory

(GEM) trial, 5–6 years of treatment with EGb 761 was neither found nor not found to reduce the incidence of dementia; poor compliance rates, high drop-out rates, and low rates of the incidence of dementia complicated the interpretation of the data gathered in these trials (DeKosky et al., 2008; Kasper, 2012; Vellas and Coley, 2012). A 3-year randomized trial of *G. biloba* extract administered to 118 patients aged 85 years or older with no cognitive impairment at baseline found that the protective effect of *G. biloba* extract against cognitive decline was statistically significant when the analysis was controlled for drug adherence (Dodge et al., 2008). In our animal model we observed antiinflammatory and antideementia effects with long-term treatment, whereas the effects of short-term treatment were in the same direction but weak. This finding indicates that the anti-AD effects of EGb 761 require a sufficient duration of treatment.

In summary, we have for the first time demonstrated that long-term oral treatment with EGb 761 ameliorates AD pathogenesis by enhancing autophagy and inhibiting neuroinflammation. Together with other mechanisms, e.g., inhibiting A $\beta$  aggregation and promoting neuroprotection and neurogenesis, EGb 761 reduces synaptic loss and cognitive impairment in AD.

## Disclosure statement

Drs. M. Burkart and K. Schötz are employees of Dr. Willmar Schwabe GmbH & Co. KG. Other authors disclose no actual or potential conflicts of interest, including any financial, personal, or other relationships with other people or organizations during the 3-year period of this study that could inappropriately influence (bias) their work.

## Acknowledgments

This work was supported by Dr. Willmar Schwabe GmbH & Co. KG and the EU FP7 project LipiDiDiet, Grant Agreement No. 211696. However, the sponsors of this study played no role in designing the study; collecting, analyzing, or interpreting the data; or writing the report, except that the blood concentrations of EGb 761 components were measured in the laboratory of Willmar Schwabe GmbH. We thank Dr. D. Westaway (University of Toronto, Ontario, Canada) for providing TgCRND8 APP-transgenic mice; Dr. L. Fülöp (Albert Szent Györgyi Medical University, Hungary) for providing human A $\beta$ 42; and E. Gluding, K. Mohrbach, and R. Lancaster for their technical assistance.

## References

Akiyama, H., Barger, S., Barnum, S., Bradt, B., Bauer, J., Cole, G.M., Cooper, N.R., Eikelenboom, P., Emmerling, M., Fiebich, B.L., Finch, C.E., Frautschy, S., Griffin, W.S., Hampel, H., Hull, M., Landreth, G., Lue, L., Mrak, R., Mackenzie, I.R., McGeer, P.L., O'Banion, M.K., Pachter, J., Pasinetti, G., Plata-Salaman, C., Rogers, J., Rydel, R., Shen, Y., Streit, W., Strohmeyer, R., Tooyoma, I., Van Muiswinkel, F.L., Veerhuis, R., Walker, D., Webster, S., Wegrzyniak, B., Wenk, G., Wyss-Coray, T., 2000. Inflammation and Alzheimer's disease. *Neurobiol. Aging* 21, 383–421.

Augustin, S., Rimbach, G., Augustin, K., Schliebs, R., Wolfram, S., Cermak, R., 2009. Effect of a short- and long-term treatment with *Ginkgo biloba* extract on amyloid precursor protein levels in a transgenic mouse model relevant to Alzheimer's disease. *Arch. Biochem. Biophys.* 481, 177–182.

Bastianetto, S., Ramassamy, C., Doré, S., Christen, Y., Poirier, J., Quirion, R., 2000. The *Ginkgo biloba* extract (EGb 761) protects hippocampal neurons against cell death induced by beta-amyloid. *Eur. J. Neurosci.* 12, 1882–1890.

Biber, A., Koch, E., 1999. Bioavailability of ginkgolides and bilobalide from extracts of *Ginkgo biloba* using GC/MS. *Planta Med.* 65, 192–193.

Birks, J., Grimley Evans, J., 2009. *Ginkgo biloba* for cognitive impairment and dementia. *Cochrane Database Syst. Rev.* 1, CD003120.

Chishti, M.A., Yang, D.S., Janus, C., Phinney, A.L., Horne, P., Pearson, J., Strome, R., Zuker, N., Loukides, J., French, J., Turner, S., Lozza, G., Grilli, M., Kunicki, S., Morrisette, C., Paquette, J., Gervais, F., Bergeron, C., Fraser, P.E., Carlson, G.A., George-Hyslop, P.S., Westaway, D., 2001. Early-onset amyloid deposition and cognitive deficits in transgenic mice expressing a double mutant form of amyloid precursor protein 695. *J. Biol. Chem.* 276, 21562–21570.

Cho, M.H., Cho, K., Kang, H.J., Jeon, E.Y., Kim, H.S., Kwon, H.J., Kim, H.M., Kim, D.H., Yoon, S.Y., 2014. Autophagy in microglia degrades extracellular  $\beta$ -amyloid fibrils and regulates the NLRP3 inflammasome. *Autophagy* 10, 1761–1775.

Chuang, S.Y., Lin, C.H., Fang, J.Y., 2014. Natural compounds and aging: between autophagy and inflammasome. *Biomed. Res. Int.* 2014, 297293.

Chuang, S.Y., Yang, C.H., Chou, C.C., Chiang, Y.P., Chuang, T.H., Hsu, L.C., 2013. TLR-induced PAI-2 expression suppresses IL-1 $\beta$  processing via increasing autophagy and NLRP3 degradation. *Proc. Natl. Acad. Sci. U.S.A.* 110, 16079–16084.

Colciaghi, F., Borroni, B., Zimmermann, M., Bellone, C., Longhi, A., Padovani, A., Cattabeni, F., Christen, Y., Di Luca, M., 2004. Amyloid precursor protein metabolism is regulated toward alpha-secretase pathway by *Ginkgo biloba* extracts. *Neurobiol. Dis.* 16, 454–460.

Dahlgren, K.N., Manelli, A.M., Stine Jr., W.B., Baker, L.K., Krafft, G.A., LaDu, M.J., 2002. Oligomeric and fibrillar species of amyloid-beta peptides differentially affect neuronal viability. *J. Biol. Chem.* 277, 32046–32053.

DeFeudis, F.V., Drieu, K., 2000. *Ginkgo biloba* extract (EGb 761) and CNS functions: basic studies and clinical applications. *Curr. Drug Targets* 1, 25–58.

DeKosky, S.T., Williamson, J.D., Fitzpatrick, A.L., Kronmal, R.A., Ives, D.G., Saxton, J.A., Lopez, O.L., Burke, G., Carlson, M.C., Fried, L.P., Kuller, L.H., Robbins, J.A., Tracy, R.P., Woolard, N.F., Dunn, L., Snitz, B.E., Nahin, R.L., Furberg, C.D., 2008. Ginkgo evaluation of memory (GEM) study investigators. *Ginkgo biloba* for prevention of dementia: a randomized controlled trial. *JAMA* 300, 2253–2262.

Dodge, H.H., Zitzelberger, T., Oken, B.S., Howieson, D., Kaye, J., 2008. A randomized placebo-controlled trial of *Ginkgo biloba* for the prevention of cognitive decline. *Neurology* 70, 1809–1817.

Eckert, A., 2012. Mitochondrial effects of *Ginkgo biloba* extract. *Int. Psychogeriatr.* 24 (Suppl. 1), S18–S20.

Fassbender, K., Walter, S., Kühl, S., Landmann, R., Ishii, K., Bertsch, T., Stalder, A.K., Muehlhauser, F., Liu, Y., Ulmer, A.J., Rivest, S., Lentsch, A., Gulbins, E., Jucker, M., Staufenbiel, M., Brechtel, K., Walter, J., Multhaup, G., Penke, B., Adachi, Y., Hartmann, T., Beyreuther, K., 2004. The LPS receptor (CD14) links innate immunity with Alzheimer's disease. *FASEB J.* 18, 203–205.

Gundersen, H.J., Jensen, E.B., 1987. The efficiency of systematic sampling in stereology and its prediction. *J. Microsc.* 147, 229–263.

Haines, D.D., Varga, B., Bak, I., Juhasz, B., Mahmoud, F.F., Kalantari, H., Gesztelyi, R., Lekli, I., Czompa, A., Tosaki, A., 2011. Summative interaction between astaxanthin, *Ginkgo biloba* extract (EGb761) and vitamin C in suppression of respiratory inflammation: a comparison with ibuprofen. *Phytother. Res.* 25, 128–136.

Halle, A., Hornung, V., Petzold, G.C., Stewart, C.R., Monks, B.G., Reinheckel, T., Fitzgerald, K.A., Latz, E., Moore, K.J., Golenbock, D.T., 2008. The NALP3 inflammasome is involved in the innate immune response to amyloid-beta. *Nat. Immunol.* 9, 857–865.

Hao, W., Liu, Y., Liu, S., Walter, S., Grimm, M.O., Kiliaan, A.J., Penke, B., Hartmann, T., Rübke, C.E., Menger, M.D., Fassbender, K., 2011. Myeloid differentiation factor 88-deficient bone marrow cells improve Alzheimer's disease-related symptoms and pathology. *Brain* 134, 278–292.

He, P., Zhong, Z., Lindholm, K., Berning, L., Lee, W., Lemere, C., Staufenbiel, M., Li, R., Shen, Y., 2007. Deletion of tumor necrosis factor death receptor inhibits amyloid beta generation and prevents learning and memory deficits in Alzheimer's mice. *J. Cell Biol.* 178, 829–841.

Heneka, M.T., Kummer, M.P., Latz, E., 2014. Innate immune activation in neurodegenerative disease. *Nat. Rev. Immunol.* 14, 463–477.

Heneka, M.T., Kummer, M.P., Stutz, A., Delekate, A., Schwartz, S., Vieira-Saecker, A., Griep, A., Axt, D., Remus, A., Tzeng, T.C., Gelpi, E., Halle, A., Korte, M., Latz, E., Golenbock, D.T., 2013. NLRP3 is activated in Alzheimer's disease and contributes to pathology in APP/PS1 mice. *Nature* 493, 674–678.

Herrsch, H., Nacu, A., Likhachev, S., Sholomov, I., Hoerr, R., Schlaefke, S., 2012. *Ginkgo biloba* extract EGb 761® in dementia with neuropsychiatric features: a randomised, placebo-controlled trial to confirm the efficacy and safety of a daily dose of 240 mg. *J. Psychiatr. Res.* 46, 716–723.

Hou, Y., Aboukhatwa, M.A., Lei, D.L., Manaye, K., Khan, I., Luo, Y., 2010. Anti-depressant natural flavonols modulate BDNF and beta amyloid in neurons and hippocampus of double TgAD mice. *Neuropharmacology* 58, 911–920.

Huang, Y., Mucke, L., 2012. Alzheimer mechanisms and therapeutic strategies. *Cell* 148, 1204–1222.

Ihl, R., Bachinskaya, N., Korczyn, A.D., Vakhapova, V., Tribanek, M., Hoerr, R., Napryeyenko, O.GOTADAY Study Group, 2011. Efficacy and safety of a once-daily formulation of *Ginkgo biloba* extract EGb 761 in dementia with neuropsychiatric features: a randomized controlled trial. *Int. J. Geriatr. Psychiatry* 26, 1186–1194.

Jaturapatpom, D., Isaac, M.G., McCleery, J., Tabet, N., 2012. Aspirin, steroidal and non-steroidal anti-inflammatory drugs for the treatment of Alzheimer's disease. *Cochrane Database Syst. Rev.* 2, CD006378.

Jiang, L., Su, L., Cui, H., Ren, J., Li, C., 2013. *Ginkgo biloba* extract for dementia: a systematic review. *Shanghai Arch. Psychiatry* 25, 10–21.

Kasper, S., 2012. Clinical data in early intervention. *Int. Psychogeriatr.* 24 (Suppl. 1), S41–S45.

Klionsky, D.J. et al., 2008. Guidelines for the use and interpretation of assays for monitoring autophagy in higher eukaryotes. *Autophagy* 4, 151–175.

Kotakadi, V.S., Jin, Y., Hofseth, A.B., Ying, L., Cui, X., Volate, S., Chumanovich, A., Wood, P.A., Price, R.L., McNeal, A., Singh, U.P., Singh, N.P., Nagarkatti, M., Nagarkatti, P.S., Matesic, L.E., Audclair, K., Wargovich, M.J., Hofseth, L.J., 2008. *Ginkgo biloba* extract EGb 761 has anti-inflammatory properties and ameliorates colitis in mice by driving effector T cell apoptosis. *Carcinogenesis* 29, 1799–1806.



- Lambert, J.C., Grenier-Boley, B., Chouraki, V., Heath, S., Zelenika, D., Fievet, N., Hannequin, D., Pasquier, F., Hanon, O., Brice, A., Epelbaum, J., Berr, C., Dartigues, J.F., Tzourio, C., Campion, D., Lathrop, M., Amouyel, P., 2010. Implication of the immune system in Alzheimer's disease: evidence from genome-wide pathway analysis. *J. Alzheimers Dis.* 20, 1107–1118.
- Lautenschlager, N.T., Ihl, R., Müller, W.E., 2012. *Ginkgo biloba* extract Egb 761® in the context of current developments in the diagnosis and treatment of age-related cognitive decline and Alzheimer's disease: a research perspective. *Int. Psychogeriatr.* 24, S46–S50.
- Lee, Y.W., Lin, J.A., Chang, C.C., Chen, Y.H., Liu, P.L., Lee, A.W., Tsai, J.C., Li, C.Y., Tsai, C.S., Chen, T.L., Lin, F.Y., 2011. *Ginkgo biloba* extract suppresses endotoxin-mediated monocyte activation by inhibiting nitric oxide- and tristetraprolin-mediated toll-like receptor 4 expression. *J. Nutr. Biochem.* 22, 351–359.
- Liu, Y., Liu, X., Hao, W., Decker, Y., Schomburg, R., Fülöp, L., Pasparakis, M., Menger, M.D., Fassbender, K., 2014. IKK $\beta$  deficiency in myeloid cells ameliorates Alzheimer's disease-related symptoms and pathology. *J. Neurosci.* 34, 12982–12999.
- Liu, S., Liu, Y., Hao, W., Wolf, L., Kiliaan, A.J., Penke, B., Rübke, C.E., Walter, J., Heneka, M.T., Hartmann, T., Menger, M.D., Fassbender, K., 2012. TLR2 is a primary receptor for Alzheimer's amyloid  $\beta$  peptide to trigger neuroinflammatory activation. *J. Immunol.* 188, 1098–1107.
- Liu, Y., Walter, S., Stagi, M., Cherny, D., Letiembre, M., Schulz-Schaeffer, W., Heine, H., Penke, B., Neumann, H., Fassbender, K., 2005. LPS receptor (CD14): a receptor for phagocytosis of Alzheimer's amyloid peptide. *Brain* 128, 1778–1789.
- Lucin, K.M., O'Brien, C.E., Bieri, G., Czirr, E., Mosher, K.I., Abbey, R.J., Mastroeni, D.F., Rogers, J., Spencer, B., Masliah, E., Wyss-Coray, T., 2013. Microglial beclin 1 regulates retromer trafficking and phagocytosis and is impaired in Alzheimer's disease. *Neuron* 79, 873–886.
- Luo, Y., Smith, J.V., Paramasivam, V., Burdick, A., Curry, K.J., Buford, J.P., Khan, I., Netzer, W.J., Xu, H., Butko, P., 2002. Inhibition of amyloid-beta aggregation and caspase-3 activation by the *Ginkgo biloba* extract Egb761. *Proc. Natl. Acad. Sci. U.S.A.* 99, 12197–12202.
- Michaud, J.P., Hallé, M., Lampron, A., Thériault, P., Préfontaine, P., Filali, M., Tribout-Jover, P., Lantaigne, A.M., Jodoin, R., Cluff, C., Brichard, V., Palmantier, R., Pilorget, A., Larocque, D., Rivest, S., 2013. Toll-like receptor 4 stimulation with the detoxified ligand monophosphoryl lipid A improves Alzheimer's disease-related pathology. *Proc. Natl. Acad. Sci. U.S.A.* 110, 1941–1946.
- Schroder, K., Tschopp, J., 2010. The inflammasomes. *Cell* 140, 821–832.
- Selkoe, D.J., 2002. Alzheimer's disease is a synaptic failure. *Science* 298, 789–791.
- Shankar, G.M., Li, S., Mehta, T.H., Garcia-Munoz, A., Shepardson, N.E., Smith, I., Brett, F.M., Farrell, M.A., Rowan, M.J., Lemere, C.A., Regan, C.M., Walsh, D.M., Sabatini, B.L., Selkoe, D.J., 2008. Amyloid-beta protein dimers isolated directly from Alzheimer's brains impair synaptic plasticity and memory. *Nat. Med.* 14, 837–842.
- Shi, C.S., Shenderov, K., Huang, N.N., Kabat, J., Abu-Asab, M., Fitzgerald, K.A., Sher, A., Kehrl, J.H., 2012. Activation of autophagy by inflammatory signals limits IL-1 $\beta$  production by targeting ubiquitinated inflammasomes for destruction. *Nat. Immunol.* 13, 255–263.
- Smith, J.V., Luo, Y., 2003. Elevation of oxidative free radicals in Alzheimer's disease models can be attenuated by *Ginkgo biloba* extract Egb 761. *J. Alzheimers Dis.* 5, 287–300.
- Stackman, R.W., Eckenstein, F., Frei, B., Kulhanek, D., Nowlin, J., Quinn, J.F., 2003. Prevention of age-related spatial memory deficits in a transgenic mouse model of Alzheimer's disease by chronic *Ginkgo biloba* treatment. *Exp. Neurol.* 184, 510–520.
- Tan, M.S., Yu, J.T., Tan, C.C., Wang, H.F., Meng, X.F., Wang, C., Jiang, T., Zhu, X.C., Tan, L., 2015. Efficacy and adverse effects of *Ginkgo biloba* for cognitive impairment and dementia: a systematic review and meta-analysis. *J. Alzheimers Dis.* 43, 589–603.
- Tchantchou, F., Lacor, P.N., Cao, Z., Lao, L., Hou, Y., Cui, C., Klein, W.L., Luo, Y., 2009. Stimulation of neurogenesis and synaptogenesis by bilobalide and quercetin via common final pathway in hippocampal neurons. *J. Alzheimers Dis.* 18, 787–798.
- Tchantchou, F., Xu, Y., Wu, Y., Christen, Y., Luo, Y., 2007. Egb 761 enhances adult hippocampal neurogenesis and phosphorylation of CREB in transgenic mouse model of Alzheimer's disease. *FASEB J.* 21, 2400–2408.
- Tian, Y., Chang, J.C., Greengard, P., Flajolet, M., 2014. The convergence of endosomal and autophagosomal pathways: implications for APP-CTF degradation. *Autophagy* 10, 694–696.
- Ude, C., Schubert-Zsilavecz, M., Wurglics, M., 2013. *Ginkgo biloba* extracts: a review of the pharmacokinetics of the active ingredients. *Clin. Pharmacokinet.* 52, 727–749.
- Vassar, R., Citron, M., 2000. Abeta-generating enzymes: recent advances in beta- and gamma-secretase research. *Neuron* 27, 419–422.
- Vellas, B., Coley, N., Ousset, P.J., Berrut, G., Dartigues, J.F., Dubois, B., Grandjean, H., Pasquier, F., Piette, F., Robert, P., Touchon, J., Garnier, P., Mathiex-Fortunet, H., Andrieu, S., GuidAge Study Group, 2012. Long-term use of standardised *Ginkgo biloba* extract for the prevention of Alzheimer's disease (GuidAge): a randomised placebo-controlled trial. *Lancet Neurol.* 11, 851–859.
- Weinmann, S., Roll, S., Schwarzbach, C., Vauth, C., Willich, S.N., 2010. Effects of *Ginkgo biloba* in dementia: systematic review and meta-analysis. *BMC Geriatr.* 10, 14.
- Wyss-Coray, T., Rogers, J., 2012. Inflammation in Alzheimer disease – a brief review of the basic science and clinical literature. *Cold Spring Harb. Perspect. Med.* 2, a006346.
- Xie, K., Liu, Y., Hao, W., Walter, S., Penke, B., Hartmann, T., Schachner, M., Fassbender, K., 2013. Tenascin-C deficiency ameliorates Alzheimer's disease-related pathology in mice. *Neurobiol. Aging* 34, 2389–2398.
- Yao, Z.X., Han, Z., Drieu, K., Papadopoulos, V., 2004. *Ginkgo biloba* extract (Egb 761) inhibits beta-amyloid production by lowering free cholesterol levels. *J. Nutr. Biochem.* 15, 749–756.
- Yin, B., Liang, H., Chen, Y., Chu, K., Huang, L., Fang, L., Matro, E., Jiang, W., Luo, B., 2013. EGB1212 post-treatment ameliorates hippocampal CA1 neuronal death and memory impairment induced by transient global cerebral ischemia/reperfusion. *Am. J. Chin. Med.* 41, 1329–1341.
- Zadayan, G., Rokitta, D., Klement, S., Dienel, A., Hoerr, R., Gramatté, T., Fuhr, U., 2012. Effect of *Ginkgo biloba* special extract Egb 761® on human cytochrome P450 activity: a cocktail interaction study in healthy volunteers. *Eur. J. Clin. Pharmacol.* 68, 553–560.

---

## 9 REFERENCES

- Akama, K. T., Albanese, C., Pestell, R. G., and Van Eldik, L. J. (1998) Amyloid beta-peptide stimulates nitric oxide production in astrocytes through an NFkappaB-dependent mechanism. *Proceedings of the National Academy of Sciences of the United States of America* 95, 5795-5800
- Akiyama, H., Barger, S., Barnum, S., Bradt, B., Bauer, J., Cole, G. M., Cooper, N. R., Eikelenboom, P., Emmerling, M., Fiebich, B. L., Finch, C. E., Frautschy, S., Griffin, W. S., Hampel, H., Hull, M., Landreth, G., Lue, L., Mrak, R., Mackenzie, I. R., McGeer, P. L., O'Banion, M. K., Pachter, J., Pasinetti, G., Plata-Salaman, C., Rogers, J., Rydel, R., Shen, Y., Streit, W., Strohmeyer, R., Tooyoma, I., Van Muiswinkel, F. L., Veerhuis, R., Walker, D., Webster, S., Wegrzyniak, B., Wenk, G., and Wyss-Coray, T. (2000) Inflammation and Alzheimer's disease. *Neurobiology of aging* 21, 383-421
- Alzheimer, A., Stelzmann, R. A., Schnitzlein, H. N., and Murtagh, F. R. (1995) An English translation of Alzheimer's 1907 paper, "Über eine eigenartige Erkrankung der Hirnrinde". *Clinical anatomy* 8, 429-431
- Alzheimer A. (1911) "Über eigenartige Krankheitsfälle des späteren Alters." *Zeitschrift für die Gesamte Neurologie und Psychiatrie* 4: 356-385.
- Alzheimer's, Ass. (2014) 2014 Alzheimer's disease facts and figures. *Alzheimer's & dementia* 10, e47-92
- Arispe, N., Pollard, H. B., and Rojas, E. (1993) Giant multilevel cation channels formed by Alzheimer disease amyloid beta-protein [A beta P-(1-40)] in bilayer membranes. *Proceedings of the National Academy of Sciences of the United States of America* 90, 10573-10577
- Authier, F., Posner, B. I., and Bergeron, J. J. (1996) Insulin-degrading enzyme. *Clinical and investigative medicine. Medecine clinique et experimentale* 19, 149-160
- Avdulov, N. A., Chochina, S. V., Igbavboa, U., Warden, C. S., Vassiliev, A. V., and Wood, W. G. (1997) Lipid binding to amyloid beta-peptide aggregates: preferential binding of cholesterol as compared with phosphatidylcholine and fatty acids. *Journal of neurochemistry* 69, 1746-1752
- Avila-Munoz, E., and Arias, C. (2014) When astrocytes become harmful: Functional and inflammatory responses that contribute to Alzheimer's disease. *Ageing research reviews* 18C, 29-40
- Beinke, S., Robinson, M. J., Hugunin, M., and Ley, S. C. (2004) Lipopolysaccharide activation of the TPL-2/MEK/extracellular signal-regulated kinase mitogen-activated protein kinase cascade is regulated by IkappaB kinase-induced proteolysis of NF-kappaB1 p105. *Molecular and cellular biology* 24, 9658-9667
- Blonska, M., You, Y., Geleziunas, R., and Lin, X. (2004) Restoration of NF-kappaB activation by tumor necrosis factor alpha receptor complex-targeted MEKK3 in receptor-interacting protein-deficient cells. *Molecular and cellular biology* 24, 10757-10765

- Bolmont, T., Haiss, F., Eicke, D., Radde, R., Mathis, C. A., Klunk, W. E., Kohsaka, S., Jucker, M., and Calhoun, M. E. (2008) Dynamics of the microglial/amyloid interaction indicate a role in plaque maintenance. *The Journal of neuroscience* 28, 4283-4292
- Bradford, M. M. (1976) A rapid and sensitive method for the quantitation of microgram quantities of protein utilizing the principle of protein-dye binding. *Analytical biochemistry* 72, 248-254
- Browne, T. C., McQuillan, K., McManus, R. M., O'Reilly, J. A., Mills, K. H., and Lynch, M. A. (2013) IFN-gamma Production by amyloid beta-specific Th1 cells promotes microglial activation and increases plaque burden in a mouse model of Alzheimer's disease. *Journal of immunology* 190, 2241-2251
- Burg, V. K., Grimm, H. S., Rothhaar, T. L., Grosgen, S., Hundsdorfer, B., Haupenthal, V. J., Zimmer, V. C., Mett, J., Weingartner, O., Laufs, U., Broersen, L. M., Tanila, H., Vanmierlo, T., Lutjohann, D., Hartmann, T., and Grimm, M. O. (2013) Plant sterols the better cholesterol in Alzheimer's disease? A mechanistical study. *The Journal of neuroscience* 33, 16072-16087
- Butovsky, O., Koronyo-Hamaoui, M., Kunis, G., Ophir, E., Landa, G., Cohen, H., and Schwartz, M. (2006) Glatiramer acetate fights against Alzheimer's disease by inducing dendritic-like microglia expressing insulin-like growth factor 1. *Proceedings of the National Academy of Sciences of the United States of America* 103, 11784-11789
- Cagnin, A., Brooks, D. J., Kennedy, A. M., Gunn, R. N., Myers, R., Turkheimer, F. E., Jones, T., and Banati, R. B. (2001) In-vivo measurement of activated microglia in dementia. *Lancet* 358, 461-467
- Cameron, B., Tse, W., Lamb, R., Li, X., Lamb, B. T., and Landreth, G. E. (2012) Loss of interleukin receptor-associated kinase 4 signaling suppresses amyloid pathology and alters microglial phenotype in a mouse model of Alzheimer's disease. *The Journal of neuroscience* 32, 15112-15123
- Cao, Z., Henzel, W. J., and Gao, X. (1996) IRAK: a kinase associated with the interleukin-1 receptor. *Science* 271, 1128-1131
- Chakrabarty, P., Ceballos-Diaz, C., Beccard, A., Janus, C., Dickson, D., Golde, T. E., and Das, P. (2010) IFN-gamma promotes complement expression and attenuates amyloid plaque deposition in amyloid beta precursor protein transgenic mice. *Journal of immunology* 184, 5333-5343
- Chao, C. C., Hu, S., Ehrlich, L., and Peterson, P. K. (1995) Interleukin-1 and tumor necrosis factor-alpha synergistically mediate neurotoxicity: involvement of nitric oxide and of N-methyl-D-aspartate receptors. *Brain, behavior, and immunity* 9, 355-365
- Chen, J., Zhou, Y., Mueller-Steiner, S., Chen, L. F., Kwon, H., Yi, S., Mucke, L., and Gan, L. (2005) SIRT1 protects against microglia-dependent amyloid-beta toxicity through inhibiting NF-kappaB signaling. *The Journal of biological chemistry* 280, 40364-40374
- Chen, Z. J., Parent, L., and Maniatis, T. (1996) Site-specific phosphorylation of IkappaBalpha by a novel ubiquitination-dependent protein kinase activity. *Cell* 84, 853-862

- Cheng, X., Shen, Y., and Li, R. (2014) Targeting TNF: a therapeutic strategy for Alzheimer's disease. *Drug discovery today* 19, 1822-1827
- Chishti, M. A., Yang, D. S., Janus, C., Phinney, A. L., Horne, P., Pearson, J., Strome, R., Zuker, N., Loukides, J., French, J., Turner, S., Lozza, G., Grilli, M., Kunicki, S., Morissette, C., Paquette, J., Gervais, F., Bergeron, C., Fraser, P. E., Carlson, G. A., George-Hyslop, P. S., and Westaway, D. (2001) Early-onset amyloid deposition and cognitive deficits in transgenic mice expressing a double mutant form of amyloid precursor protein 695. *The Journal of biological chemistry* 276, 21562-21570
- Chung, H., Brazil, M. I., Soe, T. T., and Maxfield, F. R. (1999) Uptake, degradation, and release of fibrillar and soluble forms of Alzheimer's amyloid beta-peptide by microglial cells. *The Journal of biological chemistry* 274, 32301-32308
- Clausen, B. E., Burkhardt, C., Reith, W., Renkawitz, R., and Forster, I. (1999) Conditional gene targeting in macrophages and granulocytes using LysMcre mice. *Transgenic research* 8, 265-277
- Colton, C. A., Mott, R. T., Sharpe, H., Xu, Q., Van Nostrand, W. E., and Vitek, M. P. (2006) Expression profiles for macrophage alternative activation genes in AD and in mouse models of AD. *Journal of neuroinflammation* 3, 27
- Crews, L., Adame, A., Patrick, C., Delaney, A., Pham, E., Rockenstein, E., Hansen, L., and Masliah, E. (2010) Increased BMP6 levels in the brains of Alzheimer's disease patients and APP transgenic mice are accompanied by impaired neurogenesis. *The Journal of neuroscience* 30, 12252-12262
- Crews, L., Rockenstein, E., and Masliah, E. (2010) APP transgenic modeling of Alzheimer's disease: mechanisms of neurodegeneration and aberrant neurogenesis. *Brain structure & function* 214, 111-126
- Dahlgren, K. N., Manelli, A. M., Stine, W. B., Jr., Baker, L. K., Krafft, G. A., and LaDu, M. J. (2002) Oligomeric and fibrillar species of amyloid-beta peptides differentially affect neuronal viability. *The Journal of biological chemistry* 277, 32046-32053
- Davalos, D., Grutzendler, J., Yang, G., Kim, J. V., Zuo, Y., Jung, S., Littman, D. R., Dustin, M. L., and Gan, W. B. (2005) ATP mediates rapid microglial response to local brain injury in vivo. *Nature neuroscience* 8, 752-758
- De Strooper, B. (2010) Proteases and proteolysis in Alzheimer disease: a multifactorial view on the disease process. *Physiological reviews* 90, 465-494
- Deane, R., Du Yan, S., Subramanian, R. K., LaRue, B., Jovanovic, S., Hogg, E., Welch, D., Manness, L., Lin, C., Yu, J., Zhu, H., Ghiso, J., Frangione, B., Stern, A., Schmidt, A. M., Armstrong, D. L., Arnold, B., Liliensiek, B., Nawroth, P., Hofman, F., Kindy, M., Stern, D., and Zlokovic, B. (2003) RAGE mediates amyloid-beta peptide transport across the blood-brain barrier and accumulation in brain. *Nature medicine* 9, 907-913
- Deane, R., Wu, Z., Sagare, A., Davis, J., Du Yan, S., Hamm, K., Xu, F., Parisi, M., LaRue, B., Hu, H. W., Spijkers, P., Guo, H., Song, X., Lenting, P. J., Van Nostrand, W. E., and Zlokovic, B.



- 
- V. (2004) LRP/amyloid beta-peptide interaction mediates differential brain efflux of Abeta isoforms. *Neuron* 43, 333-344
- Decker, H., Lo, K. Y., Unger, S. M., Ferreira, S. T., and Silverman, M. A. (2010) Amyloid-beta peptide oligomers disrupt axonal transport through an NMDA receptor-dependent mechanism that is mediated by glycogen synthase kinase 3beta in primary cultured hippocampal neurons. *The Journal of neuroscience* 30, 9166-9171
- Decout, A., Labeur, C., Goethals, M., Brasseur, R., Vandekerckhove, J., and Rosseneu, M. (1998) Enhanced efficiency of a targeted fusogenic peptide. *Biochimica et biophysica acta* 1372, 102-116
- Demuro, A., Parker, I., and Stutzmann, G. E. (2010) Calcium signaling and amyloid toxicity in Alzheimer disease. *The Journal of biological chemistry* 285, 12463-12468
- DiDonato, J. A., Hayakawa, M., Rothwarf, D. M., Zandi, E., and Karin, M. (1997) A cytokine-responsive IkappaB kinase that activates the transcription factor NF-kappaB. *Nature* 388, 548-554
- Ea, C. K., Deng, L., Xia, Z. P., Pineda, G., and Chen, Z. J. (2006) Activation of IKK by TNFalpha requires site-specific ubiquitination of RIP1 and polyubiquitin binding by NEMO. *Molecular cell* 22, 245-257
- Eckman, E. A., Reed, D. K., and Eckman, C. B. (2001) Degradation of the Alzheimer's amyloid beta peptide by endothelin-converting enzyme. *The Journal of biological chemistry* 276, 24540-24548
- Edison, P., Archer, H. A., Gerhard, A., Hinz, R., Pavese, N., Turkheimer, F. E., Hammers, A., Tai, Y. F., Fox, N., Kennedy, A., Rossor, M., and Brooks, D. J. (2008) Microglia, amyloid, and cognition in Alzheimer's disease: An [11C](R)PK11195-PET and [11C]PIB-PET study. *Neurobiology of disease* 32, 412-419
- Eikelenboom, P., and Stam, F. C. (1982) Immunoglobulins and complement factors in senile plaques. An immunoperoxidase study. *Acta neuropathologica* 57, 239-242
- El Khoury, J., Toft, M., Hickman, S. E., Means, T. K., Terada, K., Geula, C., and Luster, A. D. (2007) Ccr2 deficiency impairs microglial accumulation and accelerates progression of Alzheimer-like disease. *Nature medicine* 13, 432-438
- El Khoury, J. B., Moore, K. J., Means, T. K., Leung, J., Terada, K., Toft, M., Freeman, M. W., and Luster, A. D. (2003) CD36 mediates the innate host response to beta-amyloid. *The Journal of experimental medicine* 197, 1657-1666
- Erickson, M. A., Hartvigson, P. E., Morofuji, Y., Owen, J. B., Butterfield, D. A., and Banks, W. A. (2012) Lipopolysaccharide impairs amyloid beta efflux from brain: altered vascular sequestration, cerebrospinal fluid reabsorption, peripheral clearance and transporter function at the blood-brain barrier. *Journal of neuroinflammation* 9, 150

- Exley, C., and Korchazhkina, O. V. (2001) Plasmin cleaves Abeta42 in vitro and prevents its aggregation into beta-pleated sheet structures. *Neuroreport* 12, 2967-2970
- Falkevall, A., Alikhani, N., Bhushan, S., Pavlov, P. F., Busch, K., Johnson, K. A., Eneqvist, T., Tjernberg, L., Ankarcrona, M., and Glaser, E. (2006) Degradation of the amyloid beta-protein by the novel mitochondrial peptidosome, PreP. *The Journal of biological chemistry* 281, 29096-29104
- Farris, W., Mansourian, S., Chang, Y., Lindsley, L., Eckman, E. A., Frosch, M. P., Eckman, C. B., Tanzi, R. E., Selkoe, D. J., and Guenette, S. (2003) Insulin-degrading enzyme regulates the levels of insulin, amyloid beta-protein, and the beta-amyloid precursor protein intracellular domain in vivo. *Proceedings of the National Academy of Sciences of the United States of America* 100, 4162-4167
- Fassbender, K., Walter, S., Kuhl, S., Landmann, R., Ishii, K., Bertsch, T., Stalder, A. K., Muehlhauser, F., Liu, Y., Ulmer, A. J., Rivest, S., Lentschat, A., Gulbins, E., Jucker, M., Staufenbiel, M., Brechtel, K., Walter, J., Multhaup, G., Penke, B., Adachi, Y., Hartmann, T., and Beyreuther, K. (2004) The LPS receptor (CD14) links innate immunity with Alzheimer's disease. *FASEB journal* 18, 203-205
- Ferri, C. P., Prince, M., Brayne, C., Brodaty, H., Fratiglioni, L., Ganguli, M., Hall, K., Hasegawa, K., Hendrie, H., Huang, Y., Jorm, A., Mathers, C., Menezes, P. R., Rimmer, E., Scazufca, M., and Alzheimer's Disease, I. (2005) Global prevalence of dementia: a Delphi consensus study. *Lancet* 366, 2112-2117
- Fetler, L., and Amigorena, S. (2005) Neuroscience. Brain under surveillance: the microglia patrol. *Science* 309, 392-393
- Fiala, M., Cribbs, D. H., Rosenthal, M., and Bernard, G. (2007) Phagocytosis of amyloid-beta and inflammation: two faces of innate immunity in Alzheimer's disease. *Journal of Alzheimer's disease* 11, 457-463
- Fiala, M., Lin, J., Ringman, J., Kermani-Arab, V., Tsao, G., Patel, A., Lossinsky, A. S., Graves, M. C., Gustavson, A., Sayre, J., Sofroni, E., Suarez, T., Chiappelli, F., and Bernard, G. (2005) Ineffective phagocytosis of amyloid-beta by macrophages of Alzheimer's disease patients. *Journal of Alzheimer's disease* 7, 221-232; discussion 255-262
- Frenkel, D., Maron, R., Burt, D. S., and Weiner, H. L. (2005) Nasal vaccination with a proteosome-based adjuvant and glatiramer acetate clears beta-amyloid in a mouse model of Alzheimer disease. *The Journal of clinical investigation* 115, 2423-2433
- Gao, Z., Hwang, D., Bataille, F., Lefevre, M., York, D., Quon, M. J., and Ye, J. (2002) Serine phosphorylation of insulin receptor substrate 1 by inhibitor kappa B kinase complex. *The Journal of biological chemistry* 277, 48115-48121
- Ghosh, A. K., Wei, J., Wu, M., and Varga, J. (2008) Constitutive Smad signaling and Smad-dependent collagen gene expression in mouse embryonic fibroblasts lacking peroxisome proliferator-activated receptor-gamma. *Biochemical and biophysical research communications* 374, 231-236

- Gilbert, B. J. (2013) The role of amyloid beta in the pathogenesis of Alzheimer's disease. *Journal of clinical pathology* 66, 362-366
- Glass, C. K., Saijo, K., Winner, B., Marchetto, M. C., and Gage, F. H. (2010) Mechanisms underlying inflammation in neurodegeneration. *Cell* 140, 918-934
- Goldmann, T., Wieghofer, P., Muller, P. F., Wolf, Y., Varol, D., Yona, S., Brendecke, S. M., Kierdorf, K., Staszewski, O., Datta, M., Luedde, T., Heikenwalder, M., Jung, S., and Prinz, M. (2013) A new type of microglia gene targeting shows TAK1 to be pivotal in CNS autoimmune inflammation. *Nature neuroscience* 16, 1618-1626
- Gong, C. Y., Zhou, A. L., Mao, J. H., Hu, Y. E., and Geng, J. S. (2014) The role of Toll-like receptor 4 on inflammation and A $\beta$  formation in cortex astrocytes. *Sheng li xue bao : [Acta physiologica Sinica]* 66, 631-638
- Grathwohl, S. A., Kalin, R. E., Bolmont, T., Prokop, S., Winkelmann, G., Kaeser, S. A., Odenthal, J., Radde, R., Eldh, T., Gandy, S., Aguzzi, A., Staufenbiel, M., Mathews, P. M., Wolburg, H., Heppner, F. L., and Jucker, M. (2009) Formation and maintenance of Alzheimer's disease beta-amyloid plaques in the absence of microglia. *Nature neuroscience* 12, 1361-1363
- Grimm, M. O., Mett, J., Stahlmann, C. P., Haupenthal, V. J., Zimmer, V. C., and Hartmann, T. (2013) Neprilysin and A $\beta$  Clearance: Impact of the APP Intracellular Domain in NEP Regulation and Implications in Alzheimer's Disease. *Frontiers in aging neuroscience* 5, 98
- Gringhuis, S. I., Garcia-Vallejo, J. J., van Het Hof, B., and van Dijk, W. (2005) Convergent actions of I kappa B kinase beta and protein kinase C delta modulate mRNA stability through phosphorylation of 14-3-3 beta complexed with tristetraprolin. *Molecular and cellular biology* 25, 6454-6463
- Gundersen, H. J., and Jensen, E. B. (1987) The efficiency of systematic sampling in stereology and its prediction. *Journal of microscopy* 147, 229-263
- Gutierrez, H., and Davies, A. M. (2011) Regulation of neural process growth, elaboration and structural plasticity by NF-kappaB. *Trends in neurosciences* 34, 316-325
- Halim, A., Brinkmalm, G., Ruetschi, U., Westman-Brinkmalm, A., Portelius, E., Zetterberg, H., Blennow, K., Larson, G., and Nilsson, J. (2011) Site-specific characterization of threonine, serine, and tyrosine glycosylations of amyloid precursor protein/amyloid beta-peptides in human cerebrospinal fluid. *Proceedings of the National Academy of Sciences of the United States of America* 108, 11848-11853
- Hall, A. M., and Roberson, E. D. (2012) Mouse models of Alzheimer's disease. *Brain research bulletin* 88, 3-12
- Hamley, I. W. (2012) The amyloid beta peptide: a chemist's perspective. Role in Alzheimer's and fibrillization. *Chemical reviews* 112, 5147-5192
- Hao, W., Liu, Y., Liu, S., Walter, S., Grimm, M. O., Kiliaan, A. J., Penke, B., Hartmann, T., Rube, C. E., Menger, M. D., and Fassbender, K. (2011) Myeloid differentiation factor 88-

---

deficient bone marrow cells improve Alzheimer's disease-related symptoms and pathology. *Brain* 134, 278-292

Haque, R., and Nazir, A. (2014) Insulin-degrading enzyme: a link between Alzheimer's and type 2 diabetes mellitus. *CNS & neurological disorders drug targets* 13, 259-264

Hawkes, C. A., and McLaurin, J. (2009) Selective targeting of perivascular macrophages for clearance of beta-amyloid in cerebral amyloid angiopathy. *Proceedings of the National Academy of Sciences of the United States of America* 106, 1261-1266

He, P., Zhong, Z., Lindholm, K., Berning, L., Lee, W., Lemere, C., Staufenbiel, M., Li, R., and Shen, Y. (2007) Deletion of tumor necrosis factor death receptor inhibits amyloid beta generation and prevents learning and memory deficits in Alzheimer's mice. *The Journal of cell biology* 178, 829-841

Hellstrom-Lindahl, E., Ravid, R., and Nordberg, A. (2008) Age-dependent decline of neprilysin in Alzheimer's disease and normal brain: inverse correlation with A beta levels. *Neurobiology of aging* 29, 210-221

Hemming, M. L., Selkoe, D. J., and Farris, W. (2007) Effects of prolonged angiotensin-converting enzyme inhibitor treatment on amyloid beta-protein metabolism in mouse models of Alzheimer disease. *Neurobiology of disease* 26, 273-281

Heneka, M. T., Kummer, M. P., Stutz, A., Delekate, A., Schwartz, S., Vieira-Saecker, A., Griep, A., Axt, D., Remus, A., Tzeng, T. C., Gelpi, E., Halle, A., Korte, M., Latz, E., and Golenbock, D. T. (2013) NLRP3 is activated in Alzheimer's disease and contributes to pathology in APP/PS1 mice. *Nature* 493, 674-678

Herndon, T. M., Shan, X. C., Tsokos, G. C., and Wange, R. L. (2001) ZAP-70 and SLP-76 regulate protein kinase C-theta and NF-kappa B activation in response to engagement of CD3 and CD28. *Journal of immunology* 166, 5654-5664

Hickman, S. E., Allison, E. K., and El Khoury, J. (2008) Microglial dysfunction and defective beta-amyloid clearance pathways in aging Alzheimer's disease mice. *The Journal of neuroscience* 28, 8354-8360

Hickman, S. E., and El Khoury, J. (2013) The neuroimmune system in Alzheimer's disease: the glass is half full. *Journal of Alzheimer's disease* 33 Suppl 1, S295-302

Hook, V. Y., Sei, C., Yasothornsrikul, S., Toneff, T., Kang, Y. H., Efthimiopoulos, S., Robakis, N. K., and Van Nostrand, W. (1999) The kunitz protease inhibitor form of the amyloid precursor protein (KPI/APP) inhibits the proneuropeptide processing enzyme prohormone thiol protease (PTP). Colocalization of KPI/APP and PTP in secretory vesicles. *The Journal of biological chemistry* 274, 3165-3172

Hsieh, H., Boehm, J., Sato, C., Iwatsubo, T., Tomita, T., Sisodia, S., and Malinow, R. (2006) AMPAR removal underlies Abeta-induced synaptic depression and dendritic spine loss. *Neuron* 52, 831-843

- Hu, J., Igarashi, A., Kamata, M., and Nakagawa, H. (2001) Angiotensin-converting enzyme degrades Alzheimer amyloid beta-peptide (A beta ); retards A beta aggregation, deposition, fibril formation; and inhibits cytotoxicity. *The Journal of biological chemistry* 276, 47863-47868
- Hu, M. C., Lee, D. F., Xia, W., Golfman, L. S., Ou-Yang, F., Yang, J. Y., Zou, Y., Bao, S., Hanada, N., Saso, H., Kobayashi, R., and Hung, M. C. (2004) IkappaB kinase promotes tumorigenesis through inhibition of forkhead FOXO3a. *Cell* 117, 225-237
- in 't Veld, B. A., Ruitenber, A., Hofman, A., Launer, L. J., van Duijn, C. M., Stijnen, T., Breteler, M. M., and Stricker, B. H. (2001) Nonsteroidal antiinflammatory drugs and the risk of Alzheimer's disease. *The New England journal of medicine* 345, 1515-1521
- Inoue, S. (2008) In situ Abeta pores in AD brain are cylindrical assembly of Abeta protofilaments. *Amyloid* 15, 223-233
- Ishii, K., Muelhauser, F., Liebl, U., Picard, M., Kuhl, S., Penke, B., Bayer, T., Wiessler, M., Hennerici, M., Beyreuther, K., Hartmann, T., and Fassbender, K. (2000) Subacute NO generation induced by Alzheimer's beta-amyloid in the living brain: reversal by inhibition of the inducible NO synthase. *FASEB journal* 14, 1485-1489
- Iwata, N., Tsubuki, S., Takaki, Y., Shirotani, K., Lu, B., Gerard, N. P., Gerard, C., Hama, E., Lee, H. J., and Saido, T. C. (2001) Metabolic regulation of brain Abeta by neprilysin. *Science* 292, 1550-1552
- James, B. D., Leurgans, S. E., Hebert, L. E., Scherr, P. A., Yaffe, K., and Bennett, D. A. (2014) Contribution of Alzheimer disease to mortality in the United States. *Neurology* 82, 1045-1050
- Jana, M., Palencia, C. A., and Pahan, K. (2008) Fibrillar amyloid-beta peptides activate microglia via TLR2: implications for Alzheimer's disease. *Journal of immunology* 181, 7254-7262
- Jantzen, P. T., Connor, K. E., DiCarlo, G., Wenk, G. L., Wallace, J. L., Rojiani, A. M., Coppola, D., Morgan, D., and Gordon, M. N. (2002) Microglial activation and beta -amyloid deposit reduction caused by a nitric oxide-releasing nonsteroidal anti-inflammatory drug in amyloid precursor protein plus presenilin-1 transgenic mice. *The Journal of neuroscience* 22, 2246-2254
- Jun, Z., Li, Z., Fang, W., Fengzhen, Y., Puyuan, W., Wenwen, L., Zhi, S., and Bondy, S. C. (2013) Melatonin decreases levels of S100beta and NFKappaB, increases levels of synaptophysin in a rat model of Alzheimer's disease. *Current aging science* 6, 142-149
- Kaltschmidt, B., and Kaltschmidt, C. (2009) NF-kappaB in the nervous system. *Cold Spring Harbor perspectives in biology* 1, a001271
- Kamenetz, F., Tomita, T., Hsieh, H., Seabrook, G., Borchelt, D., Iwatsubo, T., Sisodia, S., and Malinow, R. (2003) APP processing and synaptic function. *Neuron* 37, 925-937
- Kanayama, A., Seth, R. B., Sun, L., Ea, C. K., Hong, M., Shaito, A., Chiu, Y. H., Deng, L., and Chen, Z. J. (2004) TAB2 and TAB3 activate the NF-kappaB pathway through binding to polyubiquitin chains. *Molecular cell* 15, 535-548

- Kawai, T., and Akira, S. (2007) TLR signaling. *Seminars in immunology* 19, 24-32
- Kierdorf, K., Erny, D., Goldmann, T., Sander, V., Schulz, C., Perdiguero, E. G., Wieghofer, P., Heinrich, A., Riemke, P., Holscher, C., Muller, D. N., Luckow, B., Brocker, T., Debowski, K., Fritz, G., Opdenakker, G., Diefenbach, A., Biber, K., Heikenwalder, M., Geissmann, F., Rosenbauer, F., and Prinz, M. (2013) Microglia emerge from erythromyeloid precursors via Pu.1- and Irf8-dependent pathways. *Nature neuroscience* 16, 273-280
- Koenigsknecht-Talboo, J., and Landreth, G. E. (2005) Microglial phagocytosis induced by fibrillar beta-amyloid and IgGs are differentially regulated by proinflammatory cytokines. *The Journal of neuroscience* 25, 8240-8249
- Kopp, E., and Medzhitov, R. (2003) Recognition of microbial infection by Toll-like receptors. *Current opinion in immunology* 15, 396-401
- Kummer, M. P., Vogl, T., Axt, D., Griep, A., Vieira-Saecker, A., Jessen, F., Gelpi, E., Roth, J., and Heneka, M. T. (2012) Mrp14 deficiency ameliorates amyloid beta burden by increasing microglial phagocytosis and modulation of amyloid precursor protein processing. *The Journal of neuroscience* 32, 17824-17829
- Latta, C. H., Brothers, H. M., and Wilcock, D. M. (2014) Neuroinflammation in Alzheimer's disease; A source of heterogeneity and target for personalized therapy. *Neuroscience*
- Lawson, L. J., Perry, V. H., Dri, P., and Gordon, S. (1990) Heterogeneity in the distribution and morphology of microglia in the normal adult mouse brain. *Neuroscience* 39, 151-170
- Lee, D. F., Kuo, H. P., Chen, C. T., Hsu, J. M., Chou, C. K., Wei, Y., Sun, H. L., Li, L. Y., Ping, B., Huang, W. C., He, X., Hung, J. Y., Lai, C. C., Ding, Q., Su, J. L., Yang, J. Y., Sahin, A. A., Hortobagyi, G. N., Tsai, F. J., Tsai, C. H., and Hung, M. C. (2007) IKK beta suppression of TSC1 links inflammation and tumor angiogenesis via the mTOR pathway. *Cell* 130, 440-455
- Lee, K. Y., D'Acquisto, F., Hayden, M. S., Shim, J. H., and Ghosh, S. (2005) PDK1 nucleates T cell receptor-induced signaling complex for NF-kappaB activation. *Science* 308, 114-118
- Lee, S., Andrieu, C., Saltel, F., Destaing, O., Auclair, J., Pouchkine, V., Michelon, J., Salaun, B., Kobayashi, R., Jurdic, P., Kieff, E. D., and Sylla, B. S. (2004) IkappaB kinase beta phosphorylates Dok1 serines in response to TNF, IL-1, or gamma radiation. *Proceedings of the National Academy of Sciences of the United States of America* 101, 17416-17421
- Leissring, M. A., Farris, W., Chang, A. Y., Walsh, D. M., Wu, X., Sun, X., Frosch, M. P., and Selkoe, D. J. (2003) Enhanced proteolysis of beta-amyloid in APP transgenic mice prevents plaque formation, secondary pathology, and premature death. *Neuron* 40, 1087-1093
- Leissring, M. A., Farris, W., Wu, X., Christodoulou, D. C., Haigis, M. C., Guarente, L., and Selkoe, D. J. (2004) Alternative translation initiation generates a novel isoform of insulin-degrading enzyme targeted to mitochondria. *The Biochemical journal* 383, 439-446

- Li, Q., Estepa, G., Memet, S., Israel, A., and Verma, I. M. (2000) Complete lack of NF-kappaB activity in IKK1 and IKK2 double-deficient mice: additional defect in neurulation. *Genes & development* 14, 1729-1733
- Li, Q., and Verma, I. M. (2002) NF-kappaB regulation in the immune system. *Nature reviews. Immunology* 2, 725-734
- Li, S., Hong, S., Shepardson, N. E., Walsh, D. M., Shankar, G. M., and Selkoe, D. (2009) Soluble oligomers of amyloid Beta protein facilitate hippocampal long-term depression by disrupting neuronal glutamate uptake. *Neuron* 62, 788-801
- Li, S., Jin, M., Koeglsperger, T., Shepardson, N. E., Shankar, G. M., and Selkoe, D. J. (2011) Soluble Abeta oligomers inhibit long-term potentiation through a mechanism involving excessive activation of extrasynaptic NR2B-containing NMDA receptors. *The Journal of neuroscience* 31, 6627-6638
- Liao, M. C., and Van Nostrand, W. E. (2010) Degradation of soluble and fibrillar amyloid beta-protein by matrix metalloproteinase (MT1-MMP) in vitro. *Biochemistry* 49, 1127-1136
- Lim, J. E., Kou, J., Song, M., Pattanayak, A., Jin, J., Lalonde, R., and Fukuchi, K. (2011) MyD88 deficiency ameliorates beta-amyloidosis in an animal model of Alzheimer's disease. *The American journal of pathology* 179, 1095-1103
- Liu, L., Wong, T. P., Pozza, M. F., Lingenhoehl, K., Wang, Y., Sheng, M., Auberson, Y. P., and Wang, Y. T. (2004) Role of NMDA receptor subtypes in governing the direction of hippocampal synaptic plasticity. *Science* 304, 1021-1024
- Liu, S., Liu, Y., Hao, W., Wolf, L., Kiliaan, A. J., Penke, B., Rube, C. E., Walter, J., Heneka, M. T., Hartmann, T., Menger, M. D., and Fassbender, K. (2012) TLR2 is a primary receptor for Alzheimer's amyloid beta peptide to trigger neuroinflammatory activation. *Journal of immunology* 188, 1098-1107
- Liu, Y., Hao, W., Letiembre, M., Walter, S., Kulanga, M., Neumann, H., and Fassbender, K. (2006) Suppression of microglial inflammatory activity by myelin phagocytosis: role of p47-PHOX-mediated generation of reactive oxygen species. *The Journal of neuroscience* 26, 12904-12913
- Liu, Y., Liu, X., Hao, W., Decker, Y., Schomburg, R., Fulop, L., Pasparakis, M., Menger, M. D., and Fassbender, K. (2014) IKKbeta deficiency in myeloid cells ameliorates Alzheimer's disease-related symptoms and pathology. *The Journal of neuroscience* 34, 12982-12999
- Liu, Y., Walter, S., Stagi, M., Cherny, D., Letiembre, M., Schulz-Schaeffer, W., Heine, H., Penke, B., Neumann, H., and Fassbender, K. (2005) LPS receptor (CD14): a receptor for phagocytosis of Alzheimer's amyloid peptide. *Brain* 128, 1778-1789
- Liu, Y., Zhang, M., Hao, W., Mihaljevic, I., Liu, X., Xie, K., Walter, S., and Fassbender, K. (2013) Matrix metalloproteinase-12 contributes to neuroinflammation in the aged brain. *Neurobiology of aging* 34, 1231-1239

- Lorenzo, A., and Yankner, B. A. (1994) Beta-amyloid neurotoxicity requires fibril formation and is inhibited by congo red. *Proceedings of the National Academy of Sciences of the United States of America* 91, 12243-12247
- Lucey, B. P., and Bateman, R. J. (2014) Amyloid-beta diurnal pattern: possible role of sleep in Alzheimer's disease pathogenesis. *Neurobiology of aging* 35 Suppl 2, S29-34
- Ma, T. C., Campana, A., Lange, P. S., Lee, H. H., Banerjee, K., Bryson, J. B., Mahishi, L., Alam, S., Giger, R. J., Barnes, S., Morris, S. M., Jr., Willis, D. E., Twiss, J. L., Filbin, M. T., and Ratan, R. R. (2010) A large-scale chemical screen for regulators of the arginase 1 promoter identifies the soy isoflavone daidzein as a clinically approved small molecule that can promote neuronal protection or regeneration via a cAMP-independent pathway. *The Journal of neuroscience* 30, 739-748
- Martinez, F. O., Helming, L., and Gordon, S. (2009) Alternative activation of macrophages: an immunologic functional perspective. *Annual review of immunology* 27, 451-483
- Matsumura, A., Suzuki, S., Iwahara, N., Hisahara, S., Kawamata, J., Suzuki, H., Yamauchi, A., Takata, K., Kitamura, Y., and Shimohama, S. (2014) Temporal Changes of CD68 and alpha7 Nicotinic Acetylcholine Receptor Expression in Microglia in Alzheimer's Disease-Like Mouse Models. *Journal of Alzheimer's disease* 44, 409-23
- McGeer, P. L., Itagaki, S., Boyes, B. E., and McGeer, E. G. (1988) Reactive microglia are positive for HLA-DR in the substantia nigra of Parkinson's and Alzheimer's disease brains. *Neurology* 38, 1285-1291
- McLaurin, J., Franklin, T., Fraser, P. E., and Chakrabartty, A. (1998) Structural transitions associated with the interaction of Alzheimer beta-amyloid peptides with gangliosides. *The Journal of biological chemistry* 273, 4506-4515
- Medeiros, R., Prediger, R. D., Passos, G. F., Pandolfo, P., Duarte, F. S., Franco, J. L., Dafre, A. L., Di Giunta, G., Figueiredo, C. P., Takahashi, R. N., Campos, M. M., and Calixto, J. B. (2007) Connecting TNF-alpha signaling pathways to iNOS expression in a mouse model of Alzheimer's disease: relevance for the behavioral and synaptic deficits induced by amyloid beta protein. *The Journal of neuroscience* 27, 5394-5404
- Meunier, J., Borjini, N., Gillis, C., Villard, V., and Maurice, T. (2014) Brain Toxicity and Inflammation Induced In Vivo in Mice by the Amyloid-beta Forty-Two Inducer Aftin-4, a Roscovitine Derivative. *Journal of Alzheimer's disease* 44, 507-24
- Meyer-Luehmann, M., Spires-Jones, T. L., Prada, C., Garcia-Alloza, M., de Calignon, A., Rozkalne, A., Koenigsknecht-Talboo, J., Holtzman, D. M., Bacskai, B. J., and Hyman, B. T. (2008) Rapid appearance and local toxicity of amyloid-beta plaques in a mouse model of Alzheimer's disease. *Nature* 451, 720-724
- Michaud, J. P., Halle, M., Lampron, A., Theriault, P., Prefontaine, P., Filali, M., Tribout-Jover, P., Lanteigne, A. M., Jodoin, R., Cluff, C., Brichard, V., Palmantier, R., Pilorget, A., Larocque, D., and Rivest, S. (2013) Toll-like receptor 4 stimulation with the detoxified ligand



- monophosphoryl lipid A improves Alzheimer's disease-related pathology. *Proceedings of the National Academy of Sciences of the United States of America* 110, 1941-1946
- Michaud, J. P., Richard, K. L., and Rivest, S. (2011) MyD88-adaptor protein acts as a preventive mechanism for memory deficits in a mouse model of Alzheimer's disease. *Molecular neurodegeneration* 6, 5
- Michaud, J. P., Richard, K. L., and Rivest, S. (2012) Hematopoietic MyD88-adaptor protein acts as a natural defense mechanism for cognitive deficits in Alzheimer's disease. *Stem cell reviews* 8, 898-904
- Michaud, M., Balardy, L., Moulis, G., Gaudin, C., Peyrot, C., Vellas, B., Cesari, M., and Nourhashemi, F. (2013) Proinflammatory cytokines, aging, and age-related diseases. *Journal of the American Medical Directors Association* 14, 877-882
- Mildner, A., Schlevogt, B., Kierdorf, K., Bottcher, C., Erny, D., Kummer, M. P., Quinn, M., Bruck, W., Bechmann, I., Heneka, M. T., Priller, J., and Prinz, M. (2011) Distinct and non-redundant roles of microglia and myeloid subsets in mouse models of Alzheimer's disease. *The Journal of neuroscience* 31, 11159-11171
- Mildner, A., Schmidt, H., Nitsche, M., Merkler, D., Hanisch, U. K., Mack, M., Heikenwalder, M., Bruck, W., Priller, J., and Prinz, M. (2007) Microglia in the adult brain arise from Ly-6ChiCCR2+ monocytes only under defined host conditions. *Nature neuroscience* 10, 1544-1553
- Miners, J. S., Baig, S., Palmer, J., Palmer, L. E., Kehoe, P. G., and Love, S. (2008) Abeta-degrading enzymes in Alzheimer's disease. *Brain pathology* 18, 240-252
- Mizutani, M., Pino, P. A., Saederup, N., Charo, I. F., Ransohoff, R. M., and Cardona, A. E. (2012) The fractalkine receptor but not CCR2 is present on microglia from embryonic development throughout adulthood. *Journal of immunology* 188, 29-36
- Moore, A. H., Wu, M., Shaftel, S. S., Graham, K. A., and O'Banion, M. K. (2009) Sustained expression of interleukin-1beta in mouse hippocampus impairs spatial memory. *Neuroscience* 164, 1484-1495
- Mucke, L., and Selkoe, D. J. (2012) Neurotoxicity of amyloid beta-protein: synaptic and network dysfunction. *Cold Spring Harbor perspectives in medicine* 2, a006338
- Muzumdar, M. D., Tasic, B., Miyamichi, K., Li, L., and Luo, L. (2007) A global double-fluorescent Cre reporter mouse. *Genesis* 45, 593-605
- Nguyen, M. D., Julien, J. P., and Rivest, S. (2002) Innate immunity: the missing link in neuroprotection and neurodegeneration? *Nature reviews. Neuroscience* 3, 216-227
- Nimmerjahn, A., Kirchhoff, F., and Helmchen, F. (2005) Resting microglial cells are highly dynamic surveillants of brain parenchyma in vivo. *Science* 308, 1314-1318
- O'Brien, C. (1996) Auguste D. and Alzheimer's disease. *Science* 273, 28

- 
- Park, J. M., Greten, F. R., Wong, A., Westrick, R. J., Arthur, J. S., Otsu, K., Hoffmann, A., Montminy, M., and Karin, M. (2005) Signaling pathways and genes that inhibit pathogen-induced macrophage apoptosis--CREB and NF-kappaB as key regulators. *Immunity* 23, 319-329
- Pasparakis, M., Luedde, T., and Schmidt-Supprian, M. (2006) Dissection of the NF-kappaB signalling cascade in transgenic and knockout mice. *Cell death and differentiation* 13, 861-872
- Patterson, S. (2014) Immune dysregulation and cognitive vulnerability in the aging brain: Interactions of microglia, IL-1beta, BDNF and synaptic plasticity. *Neuropharmacology*
- Perkins, N. D. (2007) Integrating cell-signalling pathways with NF-kappaB and IKK function. *Nature reviews. Molecular cell biology* 8, 49-62
- Piani, D., Spranger, M., Frei, K., Schaffner, A., and Fontana, A. (1992) Macrophage-induced cytotoxicity of N-methyl-D-aspartate receptor positive neurons involves excitatory amino acids rather than reactive oxygen intermediates and cytokines. *European journal of immunology* 22, 2429-2436
- Priller, J., Prinz, M., Heikenwalder, M., Zeller, N., Schwarz, P., Heppner, F. L., and Aguzzi, A. (2006) Early and rapid engraftment of bone marrow-derived microglia in scrapie. *The Journal of neuroscience* 26, 11753-11762
- Prokop, S., Miller, K. R., and Heppner, F. L. (2013) Microglia actions in Alzheimer's disease. *Acta neuropathologica* 126, 461-77
- Qian, L., Block, M. L., Wei, S. J., Lin, C. F., Reece, J., Pang, H., Wilson, B., Hong, J. S., and Flood, P. M. (2006) Interleukin-10 protects lipopolysaccharide-induced neurotoxicity in primary midbrain cultures by inhibiting the function of NADPH oxidase. *The Journal of pharmacology and experimental therapeutics* 319, 44-52
- Qian, Y., Commene, M., Ninomiya-Tsuji, J., Matsumoto, K., and Li, X. (2001) IRAK-mediated translocation of TRAF6 and TAB2 in the interleukin-1-induced activation of NFkappa B. *The Journal of biological chemistry* 276, 41661-41667
- Qiu, W. Q., Walsh, D. M., Ye, Z., Vekrellis, K., Zhang, J., Podlisny, M. B., Rosner, M. R., Safavi, A., Hersh, L. B., and Selkoe, D. J. (1998) Insulin-degrading enzyme regulates extracellular levels of amyloid beta-protein by degradation. *The Journal of biological chemistry* 273, 32730-32738
- Querfurth, H. W., and LaFerla, F. M. (2010) Alzheimer's disease. *The New England journal of medicine* 362, 329-344
- Quist, A., Doudevski, I., Lin, H., Azimova, R., Ng, D., Frangione, B., Kagan, B., Ghiso, J., and Lal, R. (2005) Amyloid ion channels: a common structural link for protein-misfolding disease. *Proceedings of the National Academy of Sciences of the United States of America* 102, 10427-10432

- Reed-Geaghan, E. G., Reed, Q. W., Cramer, P. E., and Landreth, G. E. (2010) Deletion of CD14 attenuates Alzheimer's disease pathology by influencing the brain's inflammatory milieu. *The Journal of neuroscience* 30, 15369-15373
- Reed-Geaghan, E. G., Savage, J. C., Hise, A. G., and Landreth, G. E. (2009) CD14 and toll-like receptors 2 and 4 are required for fibrillar A $\beta$ -stimulated microglial activation. *The Journal of neuroscience* 29, 11982-11992
- Rezaie, P., and Male, D. (2002) Mesoglia & microglia--a historical review of the concept of mononuclear phagocytes within the central nervous system. *Journal of the history of the neurosciences* 11, 325-374
- Ribes, S., Ebert, S., Czesnik, D., Regen, T., Zeug, A., Bukowski, S., Mildner, A., Eiffert, H., Hanisch, U. K., Hammerschmidt, S., and Nau, R. (2009) Toll-like receptor prestimulation increases phagocytosis of *Escherichia coli* DH5 $\alpha$  and *Escherichia coli* K1 strains by murine microglial cells. *Infection and immunity* 77, 557-564
- Richard, K., Pierce, S. K., and Song, W. (2008) The agonists of TLR4 and 9 are sufficient to activate memory B cells to differentiate into plasma cells in vitro but not in vivo. *Journal of immunology* 181, 1746-1752
- Roher, A. E., Kasunic, T. C., Woods, A. S., Cotter, R. J., Ball, M. J., and Fridman, R. (1994) Proteolysis of A  $\beta$  peptide from Alzheimer disease brain by gelatinase A. *Biochemical and biophysical research communications* 205, 1755-1761
- Rothwarf, D. M., and Karin, M. (1999) The NF-kappa B activation pathway: a paradigm in information transfer from membrane to nucleus. *Science's STKE* 1999, RE1
- Rudolph, D., Yeh, W. C., Wakeham, A., Rudolph, B., Nallainathan, D., Potter, J., Elia, A. J., and Mak, T. W. (2000) Severe liver degeneration and lack of NF-kappaB activation in NEMO/IKKgamma-deficient mice. *Genes & development* 14, 854-862
- Saederup, N., Cardona, A. E., Croft, K., Mizutani, M., Cotleur, A. C., Tsou, C. L., Ransohoff, R. M., and Charo, I. F. (2010) Selective chemokine receptor usage by central nervous system myeloid cells in CCR2-red fluorescent protein knock-in mice. *PloS one* 5, e13693
- Saijo, K., and Glass, C. K. (2011) Microglial cell origin and phenotypes in health and disease. *Nature reviews. Immunology* 11, 775-787
- Schubert, D., Soucek, T., and Blouw, B. (2009) The induction of HIF-1 reduces astrocyte activation by amyloid beta peptide. *The European journal of neuroscience* 29, 1323-1334
- Schulze-Luehrmann, J., and Ghosh, S. (2006) Antigen-receptor signaling to nuclear factor kappa B. *Immunity* 25, 701-715
- Schwalm, M. T., Pasquali, M., Miguel, S. P., Dos Santos, J. P., Vuolo, F., Comim, C. M., Petronilho, F., Quevedo, J., Gelain, D. P., Moreira, J. C., Ritter, C., and Dal-Pizzol, F. (2014) Acute brain inflammation and oxidative damage are related to long-term cognitive deficits and markers of neurodegeneration in sepsis-survivor rats. *Molecular neurobiology* 49, 380-385

- 
- Selkoe, D. J. (2008) Biochemistry and molecular biology of amyloid beta-protein and the mechanism of Alzheimer's disease. *Handbook of clinical neurology* 89, 245-260
- Shaftel, S. S., Kyrkanides, S., Olschowka, J. A., Miller, J. N., Johnson, R. E., and O'Banion, M. K. (2007) Sustained hippocampal IL-1 beta overexpression mediates chronic neuroinflammation and ameliorates Alzheimer plaque pathology. *The Journal of clinical investigation* 117, 1595-1604
- Shankar, G. M., Bloodgood, B. L., Townsend, M., Walsh, D. M., Selkoe, D. J., and Sabatini, B. L. (2007) Natural oligomers of the Alzheimer amyloid-beta protein induce reversible synapse loss by modulating an NMDA-type glutamate receptor-dependent signaling pathway. *The Journal of neuroscience* 27, 2866-2875
- Shankar, G. M., Li, S., Mehta, T. H., Garcia-Munoz, A., Shepardson, N. E., Smith, I., Brett, F. M., Farrell, M. A., Rowan, M. J., Lemere, C. A., Regan, C. M., Walsh, D. M., Sabatini, B. L., and Selkoe, D. J. (2008) Amyloid-beta protein dimers isolated directly from Alzheimer's brains impair synaptic plasticity and memory. *Nature medicine* 14, 837-842
- Sharma, S., Yang, B., Xi, X., Grotta, J. C., Aronowski, J., and Savitz, S. I. (2011) IL-10 directly protects cortical neurons by activating PI-3 kinase and STAT-3 pathways. *Brain research* 1373, 189-194
- Sheng, J. G., Bora, S. H., Xu, G., Borchelt, D. R., Price, D. L., and Koliatsos, V. E. (2003) Lipopolysaccharide-induced-neuroinflammation increases intracellular accumulation of amyloid precursor protein and amyloid beta peptide in APPswe transgenic mice. *Neurobiology of disease* 14, 133-145
- Simard, A. R., and Rivest, S. (2006) Neuroprotective properties of the innate immune system and bone marrow stem cells in Alzheimer's disease. *Molecular psychiatry* 11, 327-335
- Simard, A. R., Soulet, D., Gowing, G., Julien, J. P., and Rivest, S. (2006) Bone marrow-derived microglia play a critical role in restricting senile plaque formation in Alzheimer's disease. *Neuron* 49, 489-502
- Snyder, E. M., Nong, Y., Almeida, C. G., Paul, S., Moran, T., Choi, E. Y., Nairn, A. C., Salter, M. W., Lombroso, P. J., Gouras, G. K., and Greengard, P. (2005) Regulation of NMDA receptor trafficking by amyloid-beta. *Nature neuroscience* 8, 1051-1058
- Song, M., Jin, J., Lim, J. E., Kou, J., Pattanayak, A., Rehman, J. A., Kim, H. D., Tahara, K., Lalonde, R., and Fukuchi, K. (2011) TLR4 mutation reduces microglial activation, increases Abeta deposits and exacerbates cognitive deficits in a mouse model of Alzheimer's disease. *Journal of neuroinflammation* 8, 92
- Stepanichev, M. Y., Zdobnova, I. M., Yakovlev, A. A., Onufriev, M. V., Lazareva, N. A., Zarubenko, II, and Gulyaeva, N. V. (2003) Effects of tumor necrosis factor-alpha central administration on hippocampal damage in rat induced by amyloid beta-peptide (25-35). *Journal of neuroscience research* 71, 110-120

- Szekely, C. A., Breitner, J. C., Fitzpatrick, A. L., Rea, T. D., Psaty, B. M., Kuller, L. H., and Zandi, P. P. (2008) NSAID use and dementia risk in the Cardiovascular Health Study: role of APOE and NSAID type. *Neurology* 70, 17-24
- Tahara, K., Kim, H. D., Jin, J. J., Maxwell, J. A., Li, L., and Fukuchi, K. (2006) Role of toll-like receptor signalling in Abeta uptake and clearance. *Brain* 129, 3006-3019
- Takaesu, G., Kishida, S., Hiyama, A., Yamaguchi, K., Shibuya, H., Irie, K., Ninomiya-Tsuji, J., and Matsumoto, K. (2000) TAB2, a novel adaptor protein, mediates activation of TAK1 MAPKKK by linking TAK1 to TRAF6 in the IL-1 signal transduction pathway. *Molecular cell* 5, 649-658
- Takahashi, K., Rochford, C. D., and Neumann, H. (2005) Clearance of apoptotic neurons without inflammation by microglial triggering receptor expressed on myeloid cells-2. *The Journal of experimental medicine* 201, 647-657
- Takatsuna, H., Kato, H., Gohda, J., Akiyama, T., Moriya, A., Okamoto, Y., Yamagata, Y., Otsuka, M., Umezawa, K., Semba, K., and Inoue, J. (2003) Identification of TIFA as an adapter protein that links tumor necrosis factor receptor-associated factor 6 (TRAF6) to interleukin-1 (IL-1) receptor-associated kinase-1 (IRAK-1) in IL-1 receptor signaling. *The Journal of biological chemistry* 278, 12144-12150
- Tan, J., Town, T., Crawford, F., Mori, T., DelleDonne, A., Crescentini, R., Obregon, D., Flavell, R. A., and Mullan, M. J. (2002) Role of CD40 ligand in amyloidosis in transgenic Alzheimer's mice. *Nature neuroscience* 5, 1288-1293
- Tan, J., Town, T., Paris, D., Mori, T., Suo, Z., Crawford, F., Mattson, M. P., Flavell, R. A., and Mullan, M. (1999) Microglial activation resulting from CD40-CD40L interaction after beta-amyloid stimulation. *Science* 286, 2352-2355
- Terzi, E., Holzemann, G., and Seelig, J. (1995) Self-association of beta-amyloid peptide (1-40) in solution and binding to lipid membranes. *Journal of molecular biology* 252, 633-642
- Tong, L., Yuan, Y., and Wu, S. (2015) Therapeutic microRNAs targeting the NF-kappa B signaling circuits of cancers. *Advanced drug delivery reviews* 81C, 1-15
- Town, T., Laouar, Y., Pittenger, C., Mori, T., Szekely, C. A., Tan, J., Duman, R. S., and Flavell, R. A. (2008) Blocking TGF-beta-Smad2/3 innate immune signaling mitigates Alzheimer-like pathology. *Nature medicine* 14, 681-687
- Townsend, K. P., Town, T., Mori, T., Lue, L. F., Shytle, D., Sanberg, P. R., Morgan, D., Fernandez, F., Flavell, R. A., and Tan, J. (2005) CD40 signaling regulates innate and adaptive activation of microglia in response to amyloid beta-peptide. *European journal of immunology* 35, 901-910
- Tracey, K. J., and Cerami, A. (1994) Tumor necrosis factor: a pleiotropic cytokine and therapeutic target. *Annual review of medicine* 45, 491-503

- Tsubuki, S., Takaki, Y., and Saido, T. C. (2003) Dutch, Flemish, Italian, and Arctic mutations of APP and resistance of A $\beta$  to physiologically relevant proteolytic degradation. *Lancet* 361, 1957-1958
- Tucker, H. M., Kihiko, M., Caldwell, J. N., Wright, S., Kawarabayashi, T., Price, D., Walker, D., Scheff, S., McGillis, J. P., Rydel, R. E., and Estus, S. (2000) The plasmin system is induced by and degrades amyloid-beta aggregates. *The Journal of neuroscience* 20, 3937-3946
- Turner, A. J., Isaac, R. E., and Coates, D. (2001) The neprilysin (NEP) family of zinc metalloendopeptidases: genomics and function. *BioEssays* 23, 261-269
- Vallabhapurapu, S., and Karin, M. (2009) Regulation and function of NF-kappaB transcription factors in the immune system. *Annual review of immunology* 27, 693-733
- Varvel, N. H., Grathwohl, S. A., Baumann, F., Liebig, C., Bosch, A., Brawek, B., Thal, D. R., Charo, I. F., Heppner, F. L., Aguzzi, A., Garaschuk, O., Ransohoff, R. M., and Jucker, M. (2012) Microglial repopulation model reveals a robust homeostatic process for replacing CNS myeloid cells. *Proceedings of the National Academy of Sciences of the United States of America* 109, 18150-18155
- Vekrellis, K., Ye, Z., Qiu, W. Q., Walsh, D., Hartley, D., Chesneau, V., Rosner, M. R., and Selkoe, D. J. (2000) Neurons regulate extracellular levels of amyloid beta-protein via proteolysis by insulin-degrading enzyme. *The Journal of neuroscience* 20, 1657-1665
- Villalba, M., Bi, K., Hu, J., Altman, Y., Bushway, P., Reits, E., Neefjes, J., Baier, G., Abraham, R. T., and Altman, A. (2002) Translocation of PKC[theta] in T cells is mediated by a nonconventional, PI3-K- and Vav-dependent pathway, but does not absolutely require phospholipase C. *The Journal of cell biology* 157, 253-263
- Walter, L., and Neumann, H. (2009) Role of microglia in neuronal degeneration and regeneration. *Seminars in immunopathology* 31, 513-525
- Walter, S., Letiembre, M., Liu, Y., Heine, H., Penke, B., Hao, W., Bode, B., Manietta, N., Walter, J., Schulz-Schuffer, W., and Fassbender, K. (2007) Role of the toll-like receptor 4 in neuroinflammation in Alzheimer's disease. *Cellular physiology and biochemistry* 20, 947-956
- Wang, C., Deng, L., Hong, M., Akkaraju, G. R., Inoue, J., and Chen, Z. J. (2001) TAK1 is a ubiquitin-dependent kinase of MKK and IKK. *Nature* 412, 346-351
- Wang, W., Wang, X., Chun, J., Vilaysane, A., Clark, S., French, G., Bracey, N. A., Trpkov, K., Bonni, S., Duff, H. J., Beck, P. L., and Muruve, D. A. (2013) Inflammasome-independent NLRP3 augments TGF-beta signaling in kidney epithelium. *Journal of immunology* 190, 1239-1249
- Wegener, E., Oeckinghaus, A., Papadopoulou, N., Lavitas, L., Schmidt-Supprian, M., Ferch, U., Mak, T. W., Ruland, J., Heissmeyer, V., and Krappmann, D. (2006) Essential role for IkappaB kinase beta in remodeling Carma1-Bcl10-Malt1 complexes upon T cell activation. *Molecular cell* 23, 13-23

- Weggen, S., Eriksen, J. L., Das, P., Sagi, S. A., Wang, R., Pietrzik, C. U., Findlay, K. A., Smith, T. E., Murphy, M. P., Bulter, T., Kang, D. E., Marquez-Sterling, N., Golde, T. E., and Koo, E. H. (2001) A subset of NSAIDs lower amyloidogenic Abeta42 independently of cyclooxygenase activity. *Nature* 414, 212-216
- Weil, R., and Israel, A. (2006) Deciphering the pathway from the TCR to NF-kappaB. *Cell death and differentiation* 13, 826-833
- Wilcock, D. M., Gordon, M. N., and Morgan, D. (2006) Quantification of cerebral amyloid angiopathy and parenchymal amyloid plaques with Congo red histochemical stain. *Nature protocols* 1, 1591-1595
- Wimo, A., Jonsson, L., Bond, J., Prince, M., Winblad, B., and Alzheimer Disease, I. (2013) The worldwide economic impact of dementia 2010. *Alzheimer's & dementia* 9, 1-11.e13
- Wu, C. J., Conze, D. B., Li, T., Srinivasula, S. M., and Ashwell, J. D. (2006) Sensing of Lys 63-linked polyubiquitination by NEMO is a key event in NF-kappaB activation [corrected]. *Nature cell biology* 8, 398-406
- Wyss-Coray, T., and Rogers, J. (2012) Inflammation in Alzheimer disease-a brief review of the basic science and clinical literature. *Cold Spring Harbor perspectives in medicine* 2, a006346
- Xia, Z. P., Sun, L., Chen, X., Pineda, G., Jiang, X., Adhikari, A., Zeng, W., and Chen, Z. J. (2009) Direct activation of protein kinases by unanchored polyubiquitin chains. *Nature* 461, 114-119
- Xie, J., Brayne, C., Matthews, F. E., Medical Research Council Cognitive, F., and Ageing Study, c. (2008) Survival times in people with dementia: analysis from population based cohort study with 14 year follow-up. *Bmj* 336, 258-262
- Xie, K., Liu, Y., Hao, W., Walter, S., Penke, B., Hartmann, T., Schachner, M., and Fassbender, K. (2013) Tenascin-C deficiency ameliorates Alzheimer's disease-related pathology in mice. *Neurobiology of aging* 34, 2389-2398
- Yamamoto, M., Kiyota, T., Walsh, S. M., Liu, J., Kipnis, J., and Ikezu, T. (2008) Cytokine-mediated inhibition of fibrillar amyloid-beta peptide degradation by human mononuclear phagocytes. *Journal of immunology* 181, 3877-3886
- Yamamoto, Y., and Gaynor, R. B. (2001) Therapeutic potential of inhibition of the NF-kappaB pathway in the treatment of inflammation and cancer. *The Journal of clinical investigation* 107, 135-142
- Yamanaka, M., Ishikawa, T., Griep, A., Axt, D., Kummer, M. P., and Heneka, M. T. (2012) PPARgamma/RXRalpha-induced and CD36-mediated microglial amyloid-beta phagocytosis results in cognitive improvement in amyloid precursor protein/presenilin 1 mice. *The Journal of neuroscience* 32, 17321-17331

- 
- Yamaoka, S., Courtois, G., Bessia, C., Whiteside, S. T., Weil, R., Agou, F., Kirk, H. E., Kay, R. J., and Israel, A. (1998) Complementation cloning of NEMO, a component of the IkappaB kinase complex essential for NF-kappaB activation. *Cell* 93, 1231-1240
- Yan, P., Hu, X., Song, H., Yin, K., Bateman, R. J., Cirrito, J. R., Xiao, Q., Hsu, F. F., Turk, J. W., Xu, J., Hsu, C. Y., Holtzman, D. M., and Lee, J. M. (2006) Matrix metalloproteinase-9 degrades amyloid-beta fibrils in vitro and compact plaques in situ. *The Journal of biological chemistry* 281, 24566-24574
- Yin, K. J., Cirrito, J. R., Yan, P., Hu, X., Xiao, Q., Pan, X., Bateman, R., Song, H., Hsu, F. F., Turk, J., Xu, J., Hsu, C. Y., Mills, J. C., Holtzman, D. M., and Lee, J. M. (2006) Matrix metalloproteinases expressed by astrocytes mediate extracellular amyloid-beta peptide catabolism. *The Journal of neuroscience* 26, 10939-10948
- Zelcer, N., Khanlou, N., Clare, R., Jiang, Q., Reed-Geaghan, E. G., Landreth, G. E., Vinters, H. V., and Tontonoz, P. (2007) Attenuation of neuroinflammation and Alzheimer's disease pathology by liver x receptors. *Proceedings of the National Academy of Sciences of the United States of America* 104, 10601-10606
- Zhang, X. M., Zheng, X. Y., Sharkawi, S. S., Ruan, Y., Amir, N., Azimullah, S., Hasan, M. Y., Zhu, J., and Adem, A. (2013) Possible protecting role of TNF-alpha in kainic acid-induced neurotoxicity via down-regulation of NFkappaB signaling pathway. *Current Alzheimer research* 10, 660-669



## 10 LIST OF FIGURES AND COOPERATIONS

Figure 1.1	<b>History of Alzheimer's disease.</b> From: “Über eigenartige Krankheitsfälle des späteren Alters „ Alois Alzheimer, 1911
Figure 1.2	<b>Projected number of people aged 65 years and older (total and by age group) in the U.S. population with Alzheimer's disease, 2010 to 2050.</b> From: Alzheimer's association, Alzheimer's & dementia, 2014
Figure 1.3	<b>APP processing and APP mutations.</b> From: Hall and Roberson, Brain Res Bull, 2012
Figure 1.4	<b>IKKs-NF-<math>\kappa</math>B activation pathways.</b> From: Li and Verma, Nat Rev Immunol, 2002
Figure 1.5	<b>The consequences of IKK<math>\beta</math> activation.</b> From: Perkin, Nat Rev Mol Cell Biol, 2007
Figure 3.1	<b>Schematic figure of brain sample sections preparation.</b> Picture from: Shirong Liu
Figure 4.1	<b>LysM-Cre efficiently excises the floxed <i>ikkb</i> gene in microglia and brain macrophages.</b> Immunofluorescence: Xu Liu and Wenlin Hao; Western blot and Real time PCR: Xu Liu
Figure 4.2	<b>LysM-Cre efficiently excises the floxed <i>ikkb</i> gene in bone marrow derived macrophages and peripheral monocytes.</b> Western blot and analysis: Xu Liu
Figure 4.3	<b>LysM-Cre does not affect IKK<math>\beta</math> expression in neurons and astrocytes.</b> Tissue collection and cutting: Xu Liu; Immunofluorescence: Wenlin Hao
Figure 4.4	<b>Infiltration of CD45<sup>+</sup> or CCR2<sup>+</sup> cells in APP-transgenic mouse brain.</b> Immunohistochemistry, FACS and Immunofluorescence: Xu Liu; Data analysis: Alex Liu
Figure 4.5	<b>IKK<math>\beta</math> ablation inhibits NF-<math>\kappa</math>B activation in primary cultured microglia.</b> Western blot and analysis: Xu Liu
Figure 4.6	<b>Deficiency in IKK<math>\beta</math> in myeloid cells improves cognitive function in APP-transgenic mice.</b> Barnes maze: Xu Liu; Data analysis: Xu Liu and Alex Liu
Figure 4.7	<b>Deficiency in IKK<math>\beta</math> in myeloid cells attenuated synaptic protein loss in APP-transgenic mice.</b> Western blot and analysis: Xu Liu
Figure 4.8	<b>Deficiency of IKK<math>\beta</math> in myeloid cells reduces the number of microglia in APP-transgenic mice.</b> Immunohistochemistry and analysis: Xu Liu
Figure 4.9	<b>Deficiency of IKK<math>\beta</math> in myeloid cells decreased TNF-<math>\alpha</math> protein level in the brain.</b> ELISA: Xu Liu
Figure 4.10	<b>Myeloid IKK<math>\beta</math> deficiency reduces proinflammatory gene transcription in AD mouse brain.</b> Real time PCR: Xu Liu
Figure 4.11	<b>Deficiency of IKK<math>\beta</math> in myeloid cells relieved A<math>\beta</math> load in AD mouse brain.</b> Tissue collection and homogenization: Xu Liu; ELISA: Alex Liu
Figure 4.12	<b>Myeloid IKK<math>\beta</math> deficiency reduces A<math>\beta</math> plaque in APP-transgenic mouse brain.</b> Immunohistochemistry: Xu Liu; Congo red staining: Yann Decker; Data analysis: Xu Liu and Yann Decker

## LIST OF FIGURES AND COOPERATIONS

Figure 4.13	<b>IKK<math>\beta</math> deficiency increases microglial/brain macrophage recruitment toward A<math>\beta</math> deposits in APP-transgenic mouse brain.</b> Immunofluorescence: Xu Liu and Alex Liu; 3D imaging and analysis: Xu Liu
Figure 4.14	<b>IKK<math>\beta</math> deficiency enhances cerebral expressin of A<math>\beta</math>-interacting receptors.</b> Real time PCR: Xu Liu
Figure 4.15	<b>IKK<math>\beta</math> deficiency enhances internalization of oligomeric A<math>\beta</math>42 in microglia.</b> Western blot and FACS: Xu Liu
Figure 4.16	<b>IKK<math>\beta</math> deficiency neither changes proinflammatory gene transcription nor alters A<math>\beta</math> load in 3-month-old mice.</b> Real time PCR : Xu Liu; ELISA: Alex Liu
Figure 4.17	<b>IKK<math>\beta</math> deficiency reduces oligomeric A<math>\beta</math>-induced inflammatory genes expression in microglia.</b> Real time PCR: Xu Liu
Figure 4.18	<b>IKK<math>\beta</math> deficiency blocks TGF-<math>\beta</math>-SMAD2/3 signal pathway.</b> Real time PCR: Xu Liu and Alex Liu; Western blot and analysis: Xu Liu
Figure 4.19	<b>Blockade of TGF-<math>\beta</math>-SMAD2/3 signal increases A<math>\beta</math> internalization in microglia.</b> Western blot and analysis: Xu Liu; FACS: Xu Liu and Alex Liu
Figure 4.20	<b>Deficiency of IKK<math>\beta</math> in myeloid cells does not increase A<math>\beta</math> clearance through brain-to-blood transportation.</b> Immunofluorescence and analysis: Yann Decker; Real time PCR: Xu Liu; ELISA: Alex Liu
Figure 4.21	<b>Deficiency of microglial IKK<math>\beta</math> does not affect <math>\beta</math>- and <math>\gamma</math>-secretase activity in APP-transgenic mouse brain.</b> Secretase activity assay: Xu Liu
Figure 4.22	<b>Deficiency of microglial IKK<math>\beta</math> does not change gene transcriptions of A<math>\beta</math>-degrading enzymes in APP-transgenic mouse brain.</b> Real time PCR: Xu Liu

## 11 PUBLICATIONS AND PRESENTATIONS

### 11.1 Publications

1. **Liu X**, Hao WL, Qin YR, Decker Y, Burkart M, Menger MD, Fassbender K, Liu Y. Long-term treatment with ginkgo biloba extract EGb 761 improves Alzheimer's disease-related symptoms and pathology. *Brain Behav Immun*, 2015, <http://doi:10.1016/j.bbi.2015.01.011>.
2. Liu Y, **Liu X**<sup>(Co-first authorship)</sup>, Hao WL, Decker Y, Schomburg R, Fülöp L, Pasparakis M, Menger MD, Fassbender K. IKK $\beta$  Deficiency in Myeloid Cells Ameliorates Alzheimer's Disease-Related Symptoms and Pathology. *J Neurosci*, 2014 Sep 24;34(39):12982–12999.
3. Liu Y, Zhang M, Hao W, Mihaljevic I, **Liu X**, Xie K, Walter S, Fassbender K. Matrixmetalloproteinase-12 contributes to neuroinflammation in the aged brain. *Neurobiol Aging*, 2013 Oct;34(10):2389-98.
4. Zhao L, **Liu X**, Liang J, Han S, Wang Y, Yin Y, Luo Y, Li J. Phosphorylation of p38 MAPK mediates hypoxic preconditioning-induced neuroprotection against cerebral ischemic injury via mitochondria translocation of Bcl-xL in mice. *Brain Res*, 2013 Mar 29;1503:78-88.
5. Li Z, Li J, Bu X, **Liu X**, Tankersley CG, Wang C, Huang K. Age-induced augmentation of p38 MAPK phosphorylation in mouse lung. *Exp Gerontol*, 2011 Aug; 46(8):694-702.
6. Zhang Y, Su P, Liang P, Liu T, **Liu X**, Liu XY, Zhang B, Han T, Zhu YB, Yin DM, Li J, Zhou Z, Wang KW, Wang Y. The DREAM protein negatively regulates the NMDA receptor through interaction with the NR1 subunit. *J Neurosci*, 2010 Jun 2; 30(22):7575-86.

### 11.2 Poster presentations

1. **Liu X**, Hao WL, Fassbender K and Liu Y. IKK $\beta$  Deficiency in myeloid cells improves Alzheimer's Disease-Related Symptoms and Pathology. 9<sup>th</sup> FENS Forum of Neuroscience 2014. Milan, Italy, 2014, 07.
2. **Liu X**, Hao WL, Fassbender K and Liu Y. IKK $\beta$  Deficiency in Microglia attenuated Alzheimer's Disease-Related Symptoms and Pathology. AD/PD<sup>TM</sup> 2013. Florence, Italy, 2013, 03.

## 12 ACKNOWLEDGEMENTS

Foremost, I would like to express my sincere gratitude and respect to my advisors Dr. Yang Liu, Prof. Dr. Klaus Fassbender and Prof. Tobia Hartmann for the continuous support and outstanding guidance in accomplishing these works. I am heartily thankful to them, who supervised the project with their enthusiasm and immense knowledge. I am grateful to them for their motivation, patience and valuable discussions throughout the work. Without their guidance and persistent help, this dissertation would not have been possible.

I would like to credit my friendly and cheerful colleagues in AG Fassbender for making a joy experience in the last four years. Special thanks must go to Dr. Wenlin Hao, who introduced me into this lab and assisted me in my thesis works. Dr. Yann Decker provided daily supportive guidance with his knowledge and experience. Ms. Andrea Schottek and Ms. Rebecca Lancaster provided the skillful technical support for the progress of the projects. Ms. Laura Schnoeder, Mr. Yiren Qin, Mr. Marwan Chami and Ms. Anikó Kasztner were my best neighbors in the office and offered me their supportive discussions and suggestions. I express my thanks to all my lab mates.

I would like to appreciate Prof. Dr. David Westaway (University of Toronto), who provided TgCRND8 APP transgenic mice; Prof. Dr. Manolis Pasparakis (University of Cologne), who provided *Ikbkb<sup>fl/fl</sup>* mice; Prof. Dr. Livia Fülöp (Albert Szent Gyorgyi Medical University), who provided high-quality Aβ.

I want to gratefully acknowledge the sufficient financial support on my thesis projects from Alzheimer Forschung Initiative e.V., Fritz Thyssen Stiftung, Dr. Willmar Schwabe GmbH & Co. KG, Medical Faculty of University of the Saarland through HOMFOR2013, Forschungspreis 2011 der Freunde des Universitätsklinikums des Saarlandes and the EU FP7 project LipiDiDiet.

Furthermore, I offer my regards to my wife for her love, kindness and support. Lastly, and most importantly, I owe my deepest gratitude to my parents for giving birth to me at the first place and supporting me spiritually throughout my life. To them I dedicate this dissertation.